UNIVERSITY of CALIFORNIA
Santa Barbara

Discrete Inverse Scattering

A Dissertation submitted in partial satisfaction of the
requirements for the degree

Doctor of Philosophy
in
Electrical and Computer Engineering

by

Kaviyesh Doshi

Committee in charge:

Professor Shiv Chandrasekaran, Chair
Professor Forrest Brewer
Professor Ming Gu
Professor Roy Smith

June 2008

The dissertation of Kaviyesh Doshi is approved.

Professor Forrest Brewer

Professor Ming Gu

Professor Roy Smith

Professor Shiv Chandrasekaran, Committee Chair

March 2008

Discrete Inverse Scattering

by

Kaviyesh Doshi

Contents

List of Figures

Chapter 1

Introduction

The field of inverse problems is broad and diverse. The inverse problem is to determine some coefficient(s) of the equation given some information about the solutions. Analysis of such problems brings together diverse areas of mathematics such as complex analysis, differential geometry, harmonic analysis, integral geometry, numerical analysis, optimization, partial differential equations, probability, statistics etc. [1]. One of the critical components of inverse problems is the problem of inverse scattering.

Inverse scattering problem arises when we illuminate a medium with (acoustic, electromagnetic, elastic) energy, observe the scattered field, and from these observations, infer the contents of the medium. Figure (1.1) demonstrates a setup for an inverse scattering problem. The region denoted by X corresponds to the unknown inhomogeneous medium. The waves (in blue) on the lower left corner represent the incident energy. These waves travel in the homogeneous medium until it encounters the inhomogeneity, X. This causes the waves to scatter (shown in red). It is assumed that the interaction mechanisms of the wave field with the target are qualitatively known, i.e. we know the mechanism of wave travel in

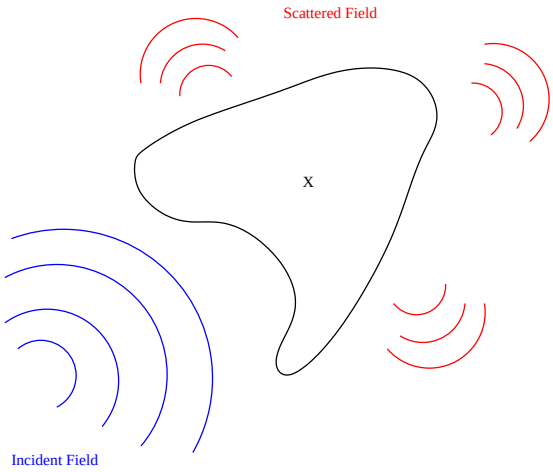

Figure 1.1. Inverse Scattering

the homogeneous medium, and we know how the wave field will behave upon reaching the scatterer. The inverse scattering problem is to observe the scattered energy, and estimate the properties of the medium, X.

1.1 Applications of Inverse Scattering

There are various applications of the inverse scattering problem ([2],[3]), some of which are listed below:

1. Radar Imaging: radio waves are emitted and reflected signal is observed. Based on the received signal a decision is made on the nature of the reflecting body (figure (1.2)).

2. Non-destructive testing: an object to be tested is bombarded with acoustic waves [5]. The waves scattered by the object are observed, and based on the scattered signal, a decision is made on the wellness of the object (figure(1.3)).

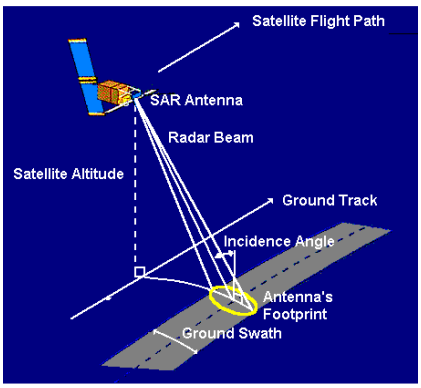

Figure 1.2. Inverse scattering application: Radar Imaging [4]

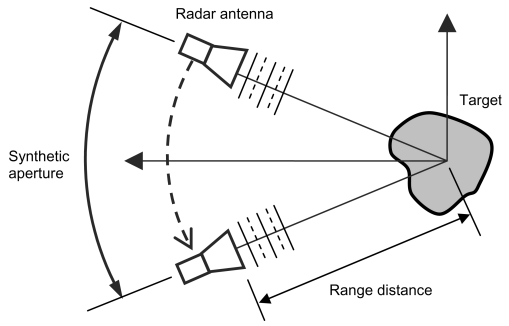

Figure 1.3. Inverse scattering application: Non Destructive Testing [6]

3. For imaging earth's interior, huge trucks are made to oscillate on the earth's surface, causing the energy to propagate below. The scattered field is observed on the surface, and characteristics like density, or bulk modulus of earth's interior, are estimated.

4. Fault detection: Cables do occasionally fail, for a variety of reasons and in many different ways. Lightening strikes, overloads or surges, installation problems, shovel and rodent damage are some of the common causes of damage that can lead to cable failure. Concepts of inverse scattering are widely implemented in various tools and technologies to detect such faults along a transmission line or along underwater cables

1.2 Problem Statement

In 1955 Gel'fand and Levitan [7] reduced the solution to the Schrodinger inverse scattering problem to the solution of a parameterized set of linear integral equations [8], [9]. Since then, different approaches have been proposed to solve the problem. It was in 1992, when Chen and Rokhlin [10] proposed a numerically stable algorithm to solve a version of the one dimensional inverse scattering problem. The problem setup in [10] was different in comparison to all the works that had been done in this field till then. The authors consider a string of infinite length. For a fixed section along the length ($x \in [0, 1]$), the mass per unit length of the string is an unknown function $q(x)$ (shown in red in figure (1.4)). The rest of the string is homogeneous, with a known constant mass per unit length.

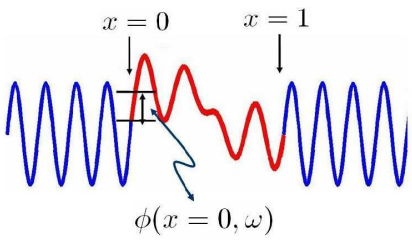

Figure 1.4. Infinite string: Inverse scattering problem for the Helmholtz equation in one dimension

Energy is incident from the left ($x < 0$), and the scattered data (amplitude $\phi(0, \omega)$) is measured at the boundary $x = 0$. The CR algorithm stably recovers $q(x)$ from $\phi(0, \omega)$ by solving a system of integro-differential equations. This system of equations is obtained due to the characteristic behavior of the infinite sections at the boundary. A solution that can provide the same characteristic behavior of an infinite transmission line in real world problems based on Chen

and Rokhlin's method demands exploration and research.

This dissertation proposes an equivalent problem in a discrete setting, and extends the Chen and Rokhlin's method to provide insights into actual implementation of inverse scattering problem. The problem has now been explained in further details in the following section.

The dissertation also takes an initiative to explore an alternative algorithm proposed by Sylvester *et. al.* [11],[12],and [13]. The authors consider the inverse scattering problem for a semi-infinite transmission line, and propose a completely different approach as compared to the Chen-Rokhlin algorithm.

1.3 Problem Setup

To describe the inverse scattering problem in one dimension, we consider an infinite length transmission line. (The equations governing the wave propagation are the same for the string and the transmission line.) Figure (1.5) shows a transmission line, which is a medium used to transfer energy (mainly electromagnetic) from one point to another [14]. Due to the magnetic field around the

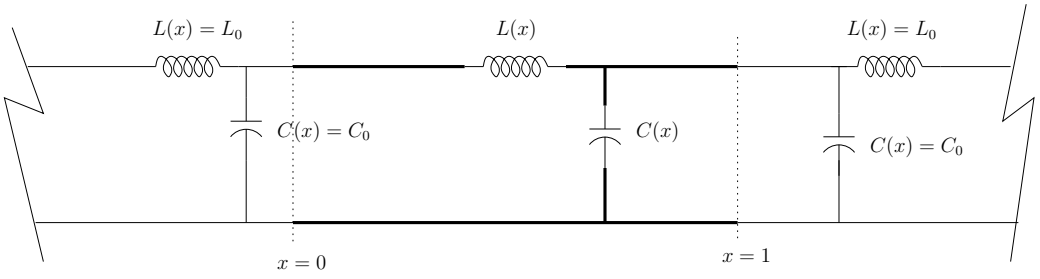

Figure 1.5. Transmission Line

wires, there is an inductance $L(x)$ at any point x. Also, at any point x, there

is a capacitive effect, $C(x)$, between the two conductors. We consider an ideal, loss less transmission line, with no series resistance or shunt conductance. Note that, although the figure (1.5) shows only one inductor for $x \in [0,1]$, there is an inductance at each point on the line, and is a function of depth x. Also, for most part of the line ($x \notin [0,1]$), the inductance and capacitance are constants, L_0 and C_0 respectively. The voltage, $V(x,t)$ and current, $I(x,t)$, on such a line are functions of distance, x and time, t, and are given by Telegrapher's equation [15].

$$\begin{aligned} \frac{\partial V(x,t)}{\partial x} &= -L(x)\frac{\partial I(x,t)}{\partial t}, \\ \frac{\partial I(x,t)}{\partial x} &= -C(x)\frac{\partial V(x,t)}{\partial t}. \end{aligned}$$

Consider the case when $x < 0$. Since the inductance and capacitance are constant in this part of the transmission line, the telegrapher's equation boils down to wave equation for both, current and voltage [9].

$$\frac{\partial^2 I(x,t)}{\partial t^2} = c_0^2 \frac{\partial^2 I(x,t)}{\partial x^2}. \tag{1.1}$$

where $c_0^2 = \frac{1}{L_0 C_0}$ is the velocity of the wave. The solution of such an equation is given as

$$I(x,t) = f(x - c_0 t) + g(x + c_0 t),$$

for some functions $f(.)$ and $g(.)$, which depend on the initial condition. Assuming a source function at $x = x_0$, f represents a wave traveling to the right of x_0, and g represents a wave traveling to the left of x_0. If the values of L and C remain constant throughout, then the two waves will travel in opposite directions, without any interruption. The amount of time taken to travel distance d, depends on the velocity of the wave, c_0.

In the case under consideration, $L(x)$ and $C(x)$ change at $x = 0$. As a result, when f reaches the boundary at $x = 0$, it is split into two: part of the wave keeps

on moving to the right, call it f_t, for transmitted wave and other part is reflected back, call it f_r, for the reflected wave. The transmitted wave f_t, as it penetrates in $x \in [0, 1]$, it becomes the source wave and is further divided into left and right going waves. This happens because the inductance and capacitance are functions of depth inside the region.

The one dimensional inverse problem can now be stated as :

> ***Inverse Scattering for continuous transmission line:*** *Observe the reflected energy at $x = 0$, and estimate the values of $L(x)$ and $C(x)$ for $x \in [0, 1]$.*

It turns out that under this problem setting, one cannot recover both L and C separately. It is the product that appears as the velocity, and that is what we can recover. Or we can consider constant capacitance and unknown inductance (as in this dissertation),or constant inductance and unknown capacitance, or we can consider both the capacitance and the inductance to be the unknown, but both taking the same value (as done in [8]).

Bruckstein and Kailath in [8] consider a special case for the inductance (figure 1.6). In the region, where the inductance is a constant, we have left and right going waves. On the boundary of such a region, the mismatch in the value of the inductance divides the wave into reflected and transmitted wave. The authors use the principle of causality to recover the values of L_k's. For example, the first reflected wave to be observed, would be due to the mismatch in L_0 and L_1. Assuming that L_0 is known, this reflection data is used to recover L_1. The same L_1 is used to recover the reflection data in the interior, and the process is repeated. Although unstable, their algorithm is general enough to include the discrete version of the previously known solutions by Gel'fand and Levitan [7], Gopinath and Sondhi [16], and Krein [17].

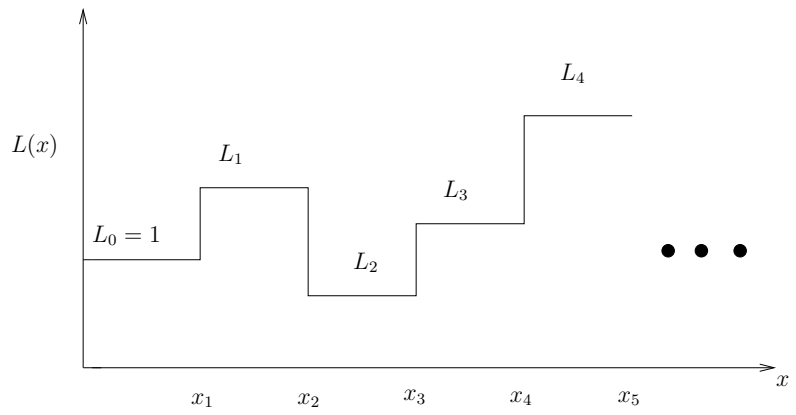

Figure 1.6. Step profile for inductance

Although the problem is described in terms of transmission line, it is quite general in the sense that it applies to examples where the energy propagation can be described using wave equation. For example, acoustic PDE model for imaging earth, acoustic PDE model for medical imaging etc.

To setup the problem in discrete domain, we first analyze the Chen-Rokhlin problem (CRP) in chapter 2. In CRP, the authors consider the Helmholtz equation, which is frequency transformed version of the wave equation.

$$\frac{\partial^2 \hat{I}(x,\omega)}{\partial x^2} - \frac{\omega^2}{c^2(x)}\hat{I}(x,\omega) = 0 \tag{1.2}$$

where $\hat{I}(x,\omega)$ is the Fourier transform of $I(x,t)$, and is given by

$$\hat{I}(x,\omega) = \int_{-\infty}^{\infty} I(x,t)e^{-j\omega t}dt$$

The Helmholtz equation is discretized, and a lumped parameter model, which is a discrete approximation of the continuous transmission line (figure 1.7) is obtained. Here each L_k is the unknown inductance value, C_0 is the known capacitance, $I_k(\omega)$ is the current in the k-th loop, $V(\omega)$ is the supply voltage, and $Y(\omega) = \frac{I_1(\omega)}{V(\omega)}$ is the input admittance. The currents, voltage and the admittance are each functions of frequency ω. The z in the first and the last loop corresponds to a component with

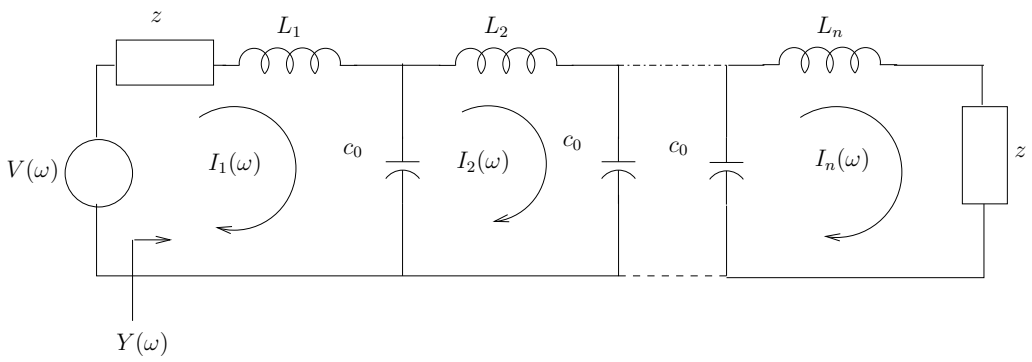

Figure 1.7. LC ladder network

a known negative impedance. The presence of z is crucial in the development of the discrete algorithm. All the approaches used before, did not consider such component in their problem definition. Intuitively, the negative impedance can be viewed as an amplifier, which pumps the energy back in the system, thereby illuminating the scatterer. In chapter 3 it is proved that, the presence of this negative impedance, guarantees that the poles of the scattered data are trapped in the lower half plane. This observation paves the way for the discrete algorithm.

Thus the inverse problem in this discrete setting can be stated as:

> ***Discrete Inverse Scattering Problem:*** *Observe the admittance $Y(\omega)$, at different frequencies, and obtain the values of L_k's.*

A physical problem that motivated the study of the discrete inverse scattering problem was that of sensor networks. Sensors are devices which measure a certain physical quantity (e.g. temperature) and convert them into an electrical signal (e.g. voltage). The idea of a sensor network is to deploy many such sensors in a field, and through local measurements from each sensor, decipher global information about the whole field. Tiny size and limited capability makes it possible to gather information in a cost effective way, from places where it was

not possible before. The measurements from each of the sensors are collected and sent to a base station, where the local information is assimilated.

Consider a logically one dimensional, network of sensors as shown in figure (1.8).

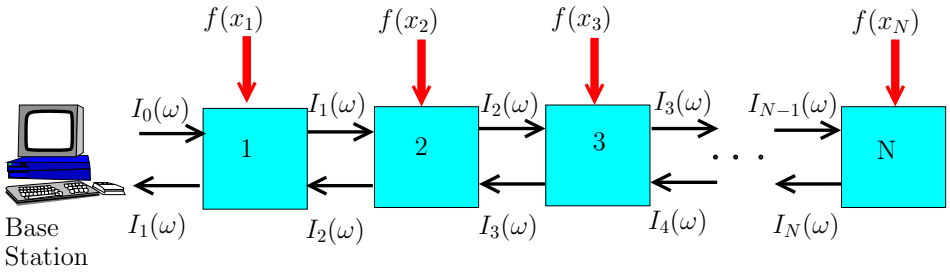

Figure 1.8. Schematic diagram of the proposed sensor network model

Here rectangular box j represents a sensor, which takes in the physical parameter $f(x_j)$ and converts it into an appropriate electrical signal. Each sensor in turn is capable of transmitting this electrical signal to its adjacent neighbors. Also, it can receive signals from its two adjacent neighbors. $I_k(\omega)$ is the signal transmitted by sensor k, and received by its neighbors $k-1$ and $k+1$. The k-th sensor receives the signal $I_{k-1}(\omega)$, from sensor $k-1$, and signal $I_{k+1}(\omega)$, from sensor $k+1$. The base station, by sending some input signal $I_0(\omega)$, communicates with the first sensor at the boundary and makes some independent measurements $I_1(\omega)$. The goal of the base station is to figure out the unknowns $f(x_j)$'s from these measurements.

The remaining of the chapters now address the aforementioned problem.

Chapter 2 investigates Chen and Rokhlin's inverse scattering algorithm for the Helmholtz equation for the continuous transmission line [10]. The Helmholtz equation is discretized to obtain a circuit equivalent of the sensor network problem. It is shown that for a specific approximation, the continuous algorithm

provides a viable solution, which is stable with respect to scaling of sensors and resistive noise. Simulation results for the sensor network problem are provided.

In chapter 3, a discrete inverse scattering algorithm is proposed to alleviate the limitations of CR algorithm in solving a discrete problem. Theorems characterizing the nature of reflection data are proved, and the CR algorithm is extended in discrete domain.

In chapter 4 alternative approaches are analyzed. An inverse scattering algorithm by Sylvester *et. al.* is explored. Derivations along with intuitive explanation is provided. A connection between circuit synthesis problem and inverse spectral method is also demonstrated.

Results and open problems are discussed in chapter 5.

Chapter 2

LC ladder network and Chen-Rokhlin algorithm

In this chapter, Chen-Rokhlin's ([10]) inverse scattering algorithm for the Helmholtz equation in one dimension is investigated. Detailed derivation and the underlying physical intuition is provided. An equivalent discrete problem, which provides insights into actual implementation of the continuous problem, is set up.

2.1 Problem Setup

We consider an infinite length transmission line (figure (2.1)) Due to the magnetic field around the wires, there is an inductance $L(x)$ at any point x. Also, at any point x, there is a capacitive effect, $C(x)$, between the two conductors. We consider an ideal, lossless transmission line, with no resistance or conductance and a constant capacitance, i.e. $C(x) = C_0$ for all x. As shown in the figure (2.1), the inductance is a constant for most part of the line i.e. $L(x) = L_0$ for $x \notin [0, 1]$. The voltage, $V(x, t)$ and current, $I(x, t)$, on such a line are functions of distance,

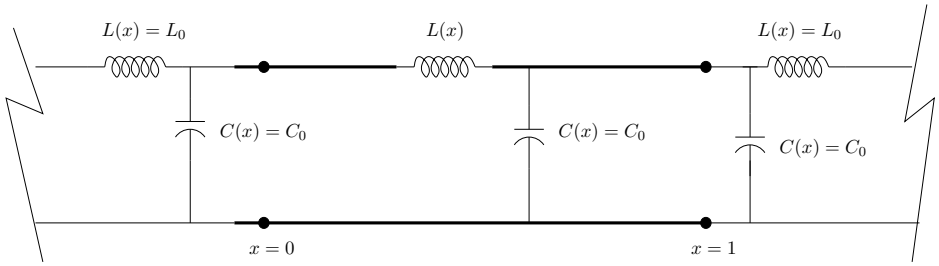

Figure 2.1. Transmission Line

x and time, t, and are given by Telegrapher's equation [15].

$$\frac{\partial V(x,t)}{\partial x} = -L(x)\frac{\partial I(x,t)}{\partial t}, \tag{2.1}$$

$$\frac{\partial I(x,t)}{\partial x} = -C_0\frac{\partial V(x,t)}{\partial t}. \tag{2.2}$$

Differentiating equation (2.1) with respect to t and equation (2.2) with respect to x we obtain

$$\frac{\partial^2 V(x,t)}{\partial x \partial t} = -L(x)\frac{\partial^2 I(x,t)}{\partial t^2}, \tag{2.3}$$

$$\frac{\partial^2 V(x,t)}{\partial x \partial t} = -\frac{1}{C_0}\frac{\partial^2 I(x,t)}{\partial x^2}. \tag{2.4}$$

Comparing equations (2.3) and (2.4) we obtain the wave equation

$$L(x)\frac{\partial^2 I(x,t)}{\partial t^2} = \frac{1}{C_0}\frac{\partial^2 I(x,t)}{\partial x^2}. \tag{2.5}$$

To obtain an equation similar to that used by Chen-Rokhlin, substitute $L(x)C_0 = 1+q(x)$ in the above equation. Also, for $x \notin [0,1]$, $L(x) = L_0$ is chosen such that $L(x)C_0 = 1$, i.e. $q(x) = 0$ in this region.

$$\frac{\partial^2 I(x,t)}{\partial x^2} - (1+q(x))\frac{\partial^2 I(x,t)}{\partial t^2} = 0. \tag{2.6}$$

Define Fourier Transform of a function as

$$\hat{f}(\omega) = \int_{-\infty}^{\infty} f(t)e^{-i\omega t}dt$$

$$f(t) = \frac{1}{2\pi}\int_{-\infty}^{\infty} \hat{f}(\omega)e^{i\omega t}d\omega.$$

Applying Fourier transform to equation (2.6), we obtain the Helmholtz equation.

$$\frac{\partial^2 \hat{I}(x,\omega)}{\partial x^2} + \omega^2(1+q(x))\hat{I}(x,\omega) = 0, \tag{2.7}$$

where, $\hat{I}(x,\omega)$ is the transform of $I(x,t)$. The authors consider solutions of the Helmholtz equation $\hat{I}_+(x,\omega)$ and $\hat{I}_-(x,\omega)$ which have the form

$$\hat{I}_+(x,\omega) = \hat{I}_{inc+}(x,\omega) + \hat{I}_{scat+}(x,\omega), \tag{2.8}$$

$$\hat{I}_-(x,\omega) = \hat{I}_{inc-}(x,\omega) + \hat{I}_{scat-}(x,\omega), \tag{2.9}$$

with

$$\hat{I}_{inc+}(x,\omega) = e^{i\omega x}, \tag{2.10}$$

$$\hat{I}_{inc-}(x,\omega) = e^{-i\omega x}. \tag{2.11}$$

Here $\hat{I}_{inc+}$ and $\hat{I}_{inc-}$ are the right-going and left-going incident fields, respectively, and $\hat{I}_{scat+}$ and $\hat{I}_{scat-}$ are the scattered fields corresponding to the excitations $\hat{I}_{inc+}$ and $\hat{I}_{inc-}$. The sum of incident and the corresponding reflected field is called the total field (2.8,2.9). Both $\hat{I}_{scat+}$, $\hat{I}_{scat-}$ satisfy the outgoing radiation boundary conditions

$$\hat{I}'_{scat}(0,\omega) + i\omega\hat{I}_{scat}(0,\omega) = 0, \tag{2.12}$$

$$\hat{I}'_{scat}(1,\omega) - i\omega\hat{I}_{scat}(1,\omega) = 0, \tag{2.13}$$

where prime denotes the derivative with respect to x. Equation (2.12) implies that once the scattered field has reached $x = 0$ it simply keeps on moving to the left without any further reflections. Similarly equation (2.13) implies the scattered field moving to the right on reaching $x = 1$.

Hence $\hat{I}_{scat}$ is of the form

$$\hat{I}_{scat} = \mu_+(\omega)e^{-i\omega x} \text{ for } x \leq 0, \tag{2.14}$$

$$\hat{I}_{scat} = \mu_-(\omega)e^{i\omega x} \text{ for } x \geq 1, \tag{2.15}$$

for some $\mu_+(\omega)$ and $\mu_-(\omega)$.

Using equations (2.8,2.10, and 2.12) and equations (2.9,2.11, and 2.13) we get

$$\hat{I}_+ = \begin{cases} e^{i\omega x} + \mu_+(\omega)e^{-i\omega x} & \text{if } x \leq 0 \qquad \text{incident + scattered} \\ \alpha e^{i\omega x} & \text{if } x \geq 1 \qquad\qquad \text{transmitted} \end{cases} \tag{2.16}$$

Equation (2.16) corresponds to the data collection experiment at $x = 0$. A right going input signal is applied at $x = 0$. This wave is reflected and transmitted. The reflected waves moves in the opposite direction ($x < 0$), while the transmitted waves moves along and comes out at $x = 1$.

$$\hat{I}_- = \begin{cases} e^{-i\omega x} + \mu_-(\omega)e^{i\omega x} & \text{if } x \geq 1 \qquad \text{incident + scattered} \\ \beta e^{-i\omega x} & \text{if } x \leq 0 \qquad\qquad \text{transmitted} \end{cases} \tag{2.17}$$

Equation (2.17) corresponds to the data collection experiment at $x = 1$. A left going input signal is applied at $x = 1$. This wave is reflected and transmitted. The reflected waves moves in the opposite direction ($x > 1$), while the transmitted waves moves along and comes out at $x = 0$. Using equation (2.16) ,we have the boundary conditions for the total field

$$\hat{I}'_+(0,\omega) + i\omega\hat{I}_+(0,\omega) = i2\omega \tag{2.18}$$

$$\hat{I}'_+(1,\omega) - i\omega\hat{I}_+(1,\omega) = 0 \tag{2.19}$$

Let C^+ is the complex upper half plane so that

$$C^+ = \{\omega \in C | \Im(\omega) \geq 0\}.$$

For any $\omega \in C^+$, the reflection data $p_+(x,\omega)$, and $p_-(x,\omega)$ associated with $\hat{I}_+(x,\omega)$ and $\hat{I}_-(x,\omega)$, respectively, are defined as

$$p_+(x,\omega) = \frac{\hat{I}'_+(x,\omega)}{i\omega\hat{I}_+(x,\omega)}, \tag{2.20}$$

$$p_-(x,\omega) = \frac{\hat{I}'_-(x,\omega)}{-i\omega\hat{I}_-(x,\omega)}, \tag{2.21}$$

Using the telegrapher's equation, equations (2.20) and (2.21) can be simplified to

$$p_+(x,\omega) = \frac{C_0\hat{V}_+(x,\omega)}{\hat{I}_+(x,\omega)},, \tag{2.22}$$

$$p_-(x,\omega) = \frac{C_0\hat{V}_-(x,\omega)}{\hat{I}_-(x,\omega)},. \tag{2.23}$$

Here $p_+(x,\omega)$ corresponds to the scaled impedance of the line by looking from the terminal at $x = 0$, and $p_-(x,\omega)$ is the impedance of the line as seen from $x = 1$ toward $x = 0$ (figure 2.2). The Chen-Rokhlin inverse scattering problem

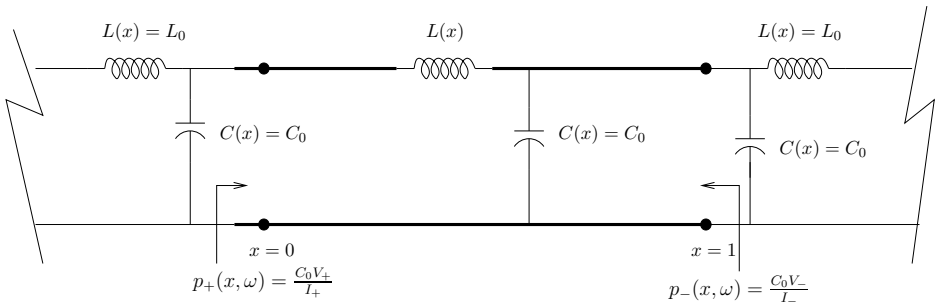

Figure 2.2. Reflection data: impedance $p_+(x,\omega)$ and $p_-(x,\omega)$

can now be defined as:

> ***Inverse Scattering Problem for the Helmholtz equation in one dimension:*** *suppose that the impedance function $p_+(0,\omega)$ is given for finite frequencies ω_k. Reconstruct the inductor profile $L(x)$ in the interval $[0,1]$.*

2.2 Chen-Rokhlin Algorithm

The inverse algorithm consists of the following steps:

1. Measure the reflection data at $x = 0$ (figure (2.3)).
2. From the reflection data, recover the unknown $L(x)$ for $x \in [0,\delta]$ (figure (2.4)).

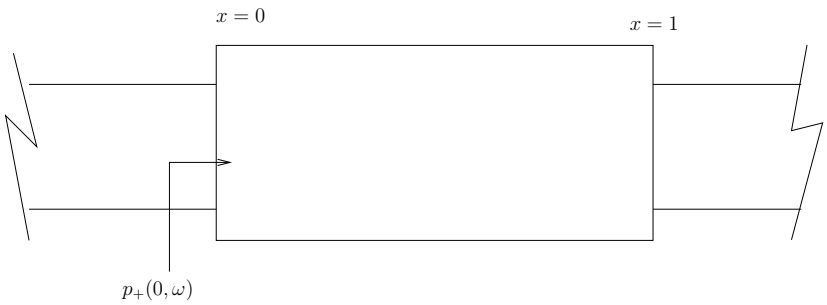

Figure 2.3. Observe reflection data: impedance $p_+(0, \omega)$

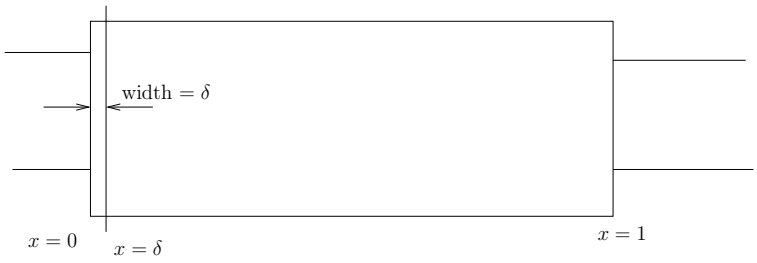

Figure 2.4. Recover $L(x)$ for $x \in [0, \delta]$

3. "Peel" the line, to obtain the reflection data at $x = \delta$ (figure (2.5)).

4. With the new data go back to step 2.

2.2.1 Algorithm Details

- As the first step [18] proves that the reflection data $p_+(x, \omega)$ is analytic and bounded ("well behaved") for all x and $\omega \in C^+$. Also, the reflection data

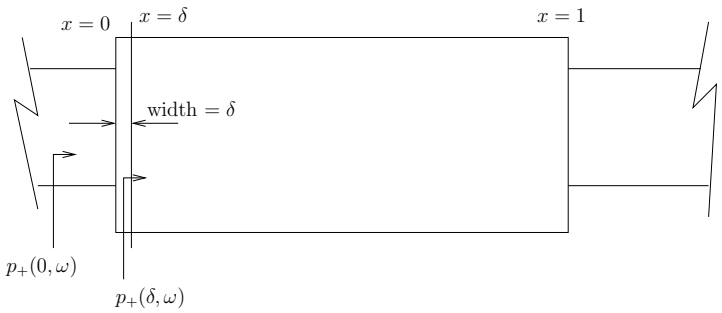

Figure 2.5. Obtain reflection data at $x = \delta$.

is simplified by substituting the value of I_+ from equation (2.16)

$$\begin{aligned} p_+(x,\omega) &= \frac{e^{i\omega x} - \mu_+(\omega)e^{-\omega x}}{e^{i\omega x} + \mu_+(\omega)e^{-\omega x}} \\ &= \frac{2e^{i\omega x} - e^{i\omega x} - \mu_+(\omega)e^{-\omega x}}{e^{i\omega x} + \mu_+(\omega)e^{-\omega x}} \\ &= \frac{2e^{i\omega x}}{e^{i\omega x} + \mu_+(\omega)e^{-\omega x}} - 1 \\ \therefore p_+(0,\omega) &= \frac{2}{1 + \mu_+(\omega)} - 1 \\ \Rightarrow p_+(0,\omega) &= \frac{2}{\hat{I}_+(0,\omega)} - 1 \end{aligned}$$

- The initial condition for $p_-(0,\omega)$ can be obtained by calculating the impedance of the semi-infinite transmission line (figure (2.6)).

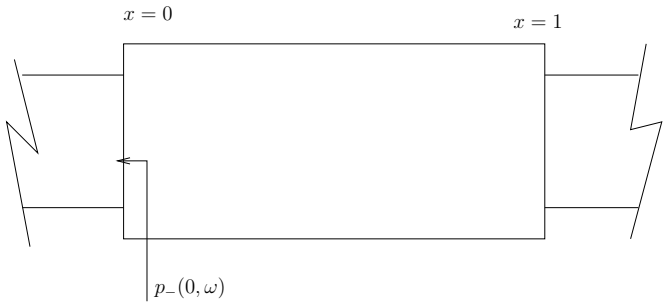

Figure 2.6. Initial condition for $p_-(0,\omega)$.

From equation (2.17), for $x \leq 0$,

$$\begin{aligned} p_-(x,\omega) &= \frac{-i\omega\beta e^{-i\omega x}}{-i\omega\beta e^{-i\omega x}} \\ \therefore p_-(0,\omega) &= 1 \end{aligned}$$

- The inversion formula is derived by first deriving the layer peeling Riccati equation for the reflection data. This layer peeling equation is a differential equation in x, which gives a way to find the reflection data inside the line, given the data at the boundary.

$$\begin{aligned} p_+(x,\omega) &= -C\frac{V(x,\omega)}{I(x,\omega)} \\ p'_+(x,\omega) &= -C\frac{I(x,\omega)V'(x,\omega) - I'(x,\omega)V(x,\omega)}{I^2(x,\omega)} \end{aligned}$$

using Telegrapher's equation,

$$\begin{aligned} p'_+(x,\omega) &= -C\frac{I(x,\omega)(-i\omega L(x)I(x,\omega)) - (-i\omega CV(x,\omega))V(x,\omega)}{I^2(x,\omega)} \\ p'_+(x,\omega) &= i\omega(1+q(x)) + \frac{(-i\omega C^2V^2(x,\omega))}{I^2(x,\omega)} \\ p'_+(x,\omega) &= i\omega(1+q(x)) - i\omega p_+^2(x,\omega) \\ p'_+(x,\omega) &= -i\omega(p_+^2(x,\omega) - (1+q(x))) \end{aligned}$$

Similarly, for $p_-(x,\omega)$ we have,

$$p'_-(x,\omega) = i\omega(p_-^2(x,\omega) - (1+q(x)))$$

Note that no experiments are performed to obtain the data $p_(0,\omega)$. It can be considered as a thought experiment. The Riccati equation for $p_(x,\omega)$ gives the value of the impedance function for this dummy experiment, and it performs a crucial role in recovering the scattering potential $q(x)$.

- Asymptotic formula for the reflection data: find $a_k(x)$ such that the impedance can be written as

$$p_+(x,\omega) = a_0(x) + \frac{a_1(x)}{i\omega} + O(\omega^{-2})$$

We compare the Riccati equation with the evolution of the above approximation to find the unknown coefficients a_k.

$$\begin{aligned} p'_+(x,\omega) &= a'_0(x) + \frac{a'_1(x)}{i\omega} + O(\omega^{-2}) \\ \Rightarrow -i\omega\left(a_0^2(x) + \frac{a_1^2(x) + 2a_0(x)a_2(x)}{(i\omega)^2} + \frac{2a_0(x)a_1(x)}{i\omega} - ((1+q(x)) + O(\omega^{-3}))\right) & \\ = a'_0(x) + \frac{a'_1(x)}{i\omega} + O(\omega^{-2}) & \end{aligned}$$

Comparing the coefficients of $i\omega$ we have

$$\begin{aligned} a_0^2 - (1+q(x)) &= 0 \\ \Rightarrow a_0 &= \sqrt{(1+q(x))} \end{aligned}$$

Comparing the coefficients for the terms independent of ω

$$\begin{aligned} -2a_0(x)a_1(x) &= a'_0 \\ \Rightarrow a_1(x) = \frac{-a'_0}{2a_0} &= \frac{-q'(x)}{4(1+q(x))} \end{aligned}$$

$$\therefore p_+(x,\omega) = \sqrt{(1+q(x))} - \frac{q'(x)}{4(1+q(x))i\omega} + O(\omega^{-2}) \tag{2.24}$$

Similarly for p_- we have,

$$p_-(x,,\omega) = \sqrt{(1+q(x))} + \frac{q'(x)}{4(1+q(x))i\omega} + O(\omega^{-2})$$

- Consider a closed contour in the upper half plane (figure(2.7)). Gamma is the curve in the upper half plane with clockwise orientation. Since $p_+ - p_-$ is analytic in the upper half plane, Cauchy's theorem guarantees that

$$\begin{aligned} \oint p_+(x,\omega) - p_-(x,\omega)d\omega &= 0 \\ \int_{-R}^{R} p_+(x,\omega) - p_-(x,\omega)d\omega &= \int_\Gamma p_+(x,\omega) - p_-(x,\omega)d\omega \end{aligned}$$

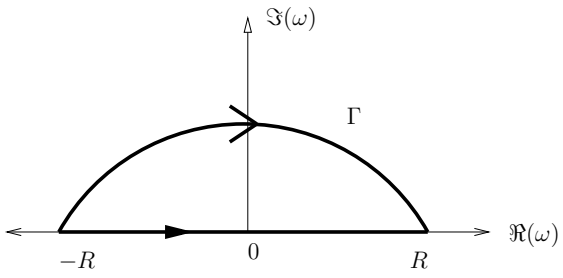

Figure 2.7. Closed contour in the upper half plane

Substituting the asymptotic expansion in the right hand integral,

$$\begin{aligned}
\int_{-R}^{R} p_+(x,\omega) - p_-(x,\omega)d\omega &= \frac{-q'(x)}{2(1+q(x))}\int_\Gamma \frac{1}{i\omega}d\omega + \int_\Gamma O(\omega^{-2}) \\
\text{Let } Re^{j\theta} &= \omega \\
\Rightarrow jRe^{j\theta}d\theta &= d\omega \\
\Rightarrow j\omega d\theta &= d\omega \\
\Rightarrow d\theta &= \frac{d\omega}{j\omega} \\
\int_{-R}^{R} p_+(x,\omega) - p_-(x,\omega)d\omega &= \frac{-q'(x)}{2(1+q(x))}\int_\pi^0 d\theta + \int_\Gamma O(\omega^{-2} \\
\therefore q'(x) &= \frac{2}{\pi}(1+q(x))\int_{-R}^{R} p_+(x,\omega) - p_-(x,\omega)d\omega + O(\omega^{-1}) \\
\Rightarrow q'(x) &= \frac{2}{\pi}(1+q(x))\int_{-\infty}^{\infty} p_+(x,\omega) - p_-(x,\omega)d\omega
\end{aligned}$$

In practice the integral needs to be truncated at some finite frequency. If $\omega_{\max}$ is the maximum frequency, then

$$\begin{aligned}
q'(x) &= \frac{2}{\pi}(1+q(x))\int_{-\omega_{\max}}^{\omega_{\max}} p_+(x,\omega) - p_-(x,\omega)d\omega + I(\omega_{\max}) \\
\text{where } I(\omega_{\max}) &= \frac{2}{\pi}(1+q(x))\left(\int_{-\infty}^{-\omega_{\max}} + \int_{\omega_{\max}}^{\infty}\right)(p_+(x,\omega) - p_-(x,\omega))d\omega.
\end{aligned}$$

From [18], if $q(x) \in c^m([0,1])$ for $m \geq 2$, then there exists a constant α such that

$$|I(\omega_{\max})| \leq \frac{\alpha}{|\omega|^{(m-1)}}$$

Thus, the "trace formula" to obtain the unknown $q(x)$ is given as

$$q'(x) = \frac{2}{\pi}(1+q(x))\int_{-a}^{a}(p_+(x,\omega)-p_-(x,\omega))d\omega + O(a^{-(m-1)})$$

where m is the smoothness of the scatterer $q(x)$.

Thus, to obtain $q(x)$ from the scattered data, Chen and Rokhlin solve the following non-linear system of differential equations

$$\begin{aligned} p'_+(x,\omega) &= -i\omega(p_+^2(x,\omega)-(1+q(x))), && (2.25)\\ p'_-(x,\omega) &= i\omega(p_-^2(x,\omega)-(1+q(x))), && (2.26)\\ q'(x) &= \frac{2}{\pi}(1+q(x))\int_{-\omega_{\max}}^{\omega_{\max}}(p_+(x,\omega)-p_-(x,\omega))d\omega, && (2.27) \end{aligned}$$

with the initial conditions

$$\begin{aligned} p_+(0,\omega) &= \frac{2}{\hat{I}(0,\omega)}-1, && (2.28)\\ p_-(0,\omega) &= 1, && (2.29)\\ q(0) &= 0, && (2.30) \end{aligned}$$

2.3 Discrete Helmholtz Equation and Sensor Networks

Having explained the Chen Rokhlin problem, the first question that arises is, how to physically setup the problem? How to simulate or connect an infinite transmission line section? In transmission line theory, the semi-infinite transmission line is approximated by its characteristic impedance [19]. It turns out, that the role performed by this characteristic impedance is not the same as that demanded by the outgoing boundary conditions. In order to develop the algorithm

in discrete domain, the Helmholtz equation (2.7) is discretized using a finite difference scheme. In doing so, a LC ladder circuit- a discrete approximation of the transmission line, is identified. This discrete LC circuit is used to model the network of sensors.

Discretizing the Helmholtz equation (2.7) using the centered difference formula

$$\hat{I}''(x_i,\omega) \approx \frac{\hat{I}(x_i-h,\omega)-2\hat{I}(x_i,\omega)+\hat{I}(x_i+h,\omega)}{h^2},$$

we get

$$\begin{aligned}\frac{\hat{I}(x_i-h,\omega)-2\hat{I}(x_i,\omega)+\hat{I}(x_i+h,\omega)}{h^2}+&\\ \omega^2(1+q(x_i))\hat{I}(x_i,\omega) &= 0. \end{aligned} \tag{2.31}$$

At the boundaries, we discretize the outgoing radiation conditions (2.18) and combine it with the discrete Helmholtz equation at the boundary. At $x=0$ we get

$$\begin{aligned}\frac{\hat{I}(h,\omega)-\hat{I}(-h,\omega)}{2h}+i\omega\hat{I}(0,\omega) &= 2i\omega,\\ \frac{\hat{I}(-h,\omega)-2\hat{I}(0,\omega)+\hat{I}(h,\omega)}{h^2}+&\\ \omega^2(1+q(0))\hat{I}(0,\omega) &= 0.\end{aligned}$$

Eliminating $\hat{I}(-h,\omega)$ from the above two equations, we get

$$(-2+i2h\omega+\omega^2h^2(1+q(0)))\hat{I}(0,\omega)+2\hat{I}(h,\omega)=i4h\omega. \tag{2.32}$$

Similarly at $x=1$ we get,

$$\begin{aligned}\frac{\hat{I}(1+h,\omega)-\hat{I}(1-h,\omega)}{2h}-i\omega\hat{I}(1,\omega) &= 0,\\ \frac{\hat{I}(1-h,\omega)-2\hat{I}(1,\omega)+\hat{I}(1+h,\omega)}{h^2}+&\\ \omega^2(1+q(1))\hat{I}(1,\omega) &= 0.\end{aligned}$$

Eliminating $\hat{I}(1+h,\omega)$ from the above two equations, we get

$$-2\hat{I}(1-h,\omega)+(2-i2h\omega-\omega^2h^2(1+q(1)))\hat{I}(1,\omega)=0. \tag{2.33}$$

After some algebraic manipulation, equations (2.31), (2.32) and (2.33) can be rewritten as

$$(\frac{2}{i\omega h}-2+i\omega h(1+q(0)))\hat{I}(0,\omega)-\frac{2}{i\omega h}\hat{I}(h,\omega)=-4, \tag{2.34}$$

$$-\frac{2}{i\omega h}\hat{I}(x_j-h,\omega)+(\frac{4}{i\omega h}+i\omega 2h(1+q(x_j)))\hat{I}(x_j,\omega) \quad - \\ \frac{2}{i\omega h}\hat{I}(x_j+h,\omega)=0 \qquad , \tag{2.35}$$

$$-\frac{2}{i\omega h}\hat{I}(1-h,\omega)+(\frac{2}{i\omega h}-2+i\omega h(1+q(1)))\hat{I}(1,\omega)=0. \tag{2.36}$$

Equations (2.34), (2.35), (2.36) are the Kirchhoff's Voltage law (KVL) equations for the first, jth and the last loop respectively. LC ladder circuit obeying the KVL can now be formed (figure (2.8)).

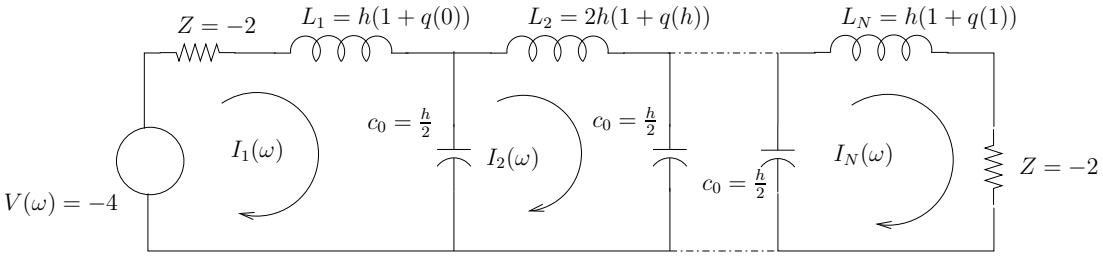

Figure 2.8. Electrical Circuit Realization of the 1D sensor Network Model

We now adapt the circuit for our sensor network by identifying each inductor with a sensor, and make the special requirement that the sensed field value determines the inductor's inductance. In particular, the jth inductor with a sensed value of $q(x_j)$ has inductance $2h(1+q(x_j))$. Such inductors can be realized using active RC circuits ([20]). To operate the sensor network, we need to make certain measurements. We supply input signals $V_s(\omega)$ (constant voltage source in

frequency domain) for different frequencies, and measure the current in the first loop, $I_1(\omega)$. Then the function $p(\omega)$ ("impedance") is calculated as

$$p(\omega) = \frac{2}{I_1(\omega)} - 1. \tag{2.37}$$

To find the unknown field values $q(x_j)$, we need to find the unknown inductances from the $p(\omega)$ obtained at different frequencies. For this we can follow Chen and Rokhlin algorithm and solve equations (2.25)-(2.30).

Note the presence of negative impedances, z, at the two ends of the circuit. These components come into play while discretizing the outgoing boundary conditions. Thus, we can say that these components play the role of the semi-infinite sections at the two ends. Physically they represent amplifiers, which pump the energy into the system. More about this negative impedances will be discussed in chapter 3.

2.4 Implementation Details

The circuit shown in figure (2.8) is simulated in MATLAB [21]. For the forward problem, different profiles for $q(x)$ are chose. An input voltage signal, which is an impulse in time (and hence a constant in frequency), is applied to the circuit, and the current ($I_1(\omega)$) in the first loop is measured. It is equivalent to solving a linear system of equations obtained by writing the KVL equations. To add noise, we simply put a resistor in each loop. The value of the resistor is a uniform random number in $[0, .1]$, which is of the order of (or greater than) the product of $LC(= h^2)$. Once we have $I_1(\omega)$, we form the "impedance" function, and solve the system of ODE's (2.25) - (2.30), to obtain $q(x)$.

To implement the algorithm, we follow [10]'s approach, and approximate the

integral using trapezoidal sum

$$\int_{-\omega_{\max}}^{\omega_{\max}} (p_+(x,\omega) - p_-(x,\omega))d\omega = h\left(\sum_{j=-M+1}^{M-1} p_+(x,\omega_j) - p_-(x,\omega_j)\right) + \frac{h}{2}\left((p_+(x,-\omega_{\max}) - p_-(x,-\omega_{\max})) + (p_+(x,\omega_{\max}) - p_-(x,\omega_{\max}))\right)$$

with $h = \frac{\omega_{\max}}{M}$, $\omega_j = jh, j = -M, -M+1, \ldots, M$. The system of equations now become:

$$\begin{aligned}
p'_+(x,\omega_j) &= -i\omega_j(p_+^2(x,\omega_j) - (1+q(x))), && (2.38)\\
p'_-(x,\omega_j) &= i\omega_j(p_-^2(x,\omega_j) - (1+q(x))), && (2.39)\\
q'(x) &= \frac{4h}{\pi}(1+q(x))\left(\sum_{j=1}^{M-1} \Re(p_+(x,\omega_j) - p_-(x,\omega_j)) + \right.\\
&\quad \left.\frac{1}{2}\left[\Re(p_+(x,0) - p_-(x,0)) + \right.\right.\\
&\quad \left.\left.\Re(p_+(x,\omega_{\max}) - p_-(x,\omega_{\max}))\right]\right), && (2.40)
\end{aligned}$$

with the initial conditions

$$\begin{aligned}
p_+(0,\omega_j) &= \frac{2}{\hat{I}_1(\omega_j)} - 1, && (2.41)\\
p_-(0,\omega_j) &= 1, && (2.42)\\
q(0) &= 0, && (2.43)
\end{aligned}$$

We use MATLAB's ode23s solver for solving the system of differential equations. The solver is based on a modified Rosenbrock formula of order 2 [22].

Once we have the reconstructed profile $\hat{q}(x)$, we calculate the error as

$$e(x) = q(x) - \hat{q}(x).$$

In the captions of each figure, we show two different norms of errors:

- $||e(x)||_\infty = \max_i e(x_i)$, which is the maximum reconstruction error made by a sensor.

- $||e(x)||_2 = \left(\frac{1}{\sqrt{N}}\right) \sqrt{(\sum_i e(x_i)^2)}$, which is the root mean squared reconstruction error.

Note: Vales of L, c_0, Z, ω, V, I, $\omega_{\max}$, and resistance, R are scaled by some constant. To obtain practical values they need to be rescaled by appropriate amount [23].

2.5 Results

Our goal is to show that it is possible to recover the unknown sensed profile by making measurements at the boundary. According to [10], the inverse algorithm works the best when the unknown profile is smooth, and the error tends to zero as one takes samples at higher frequencies. The following observations are verified through plots:

- The reconstruction error decreases up to a point as we increase the maximum frequency (ω_{max}). Beyond that the error persists, which is due to the fact that we have used different models for the forward and inverse problem.
- The algorithm scales quite well with the number of sensors, and the error does not blow up with the increase in the number of sensors.
- The reconstruction algorithm is able to resolve two peaks separated by some distance.
- Although [10] does not have proof for detecting non-smooth profiles, the algorithm does a good job reconstructing it. We show this by using profiles, which are piecewise smooth, and piecewise non-smooth.

For all the plots shown below, the x-axis represents the spatial axis along which the sensors are aligned, and the y-axis is the sensed field value, as well as the absolute value of the reconstructed potential.

2.5.1 Smooth Profile

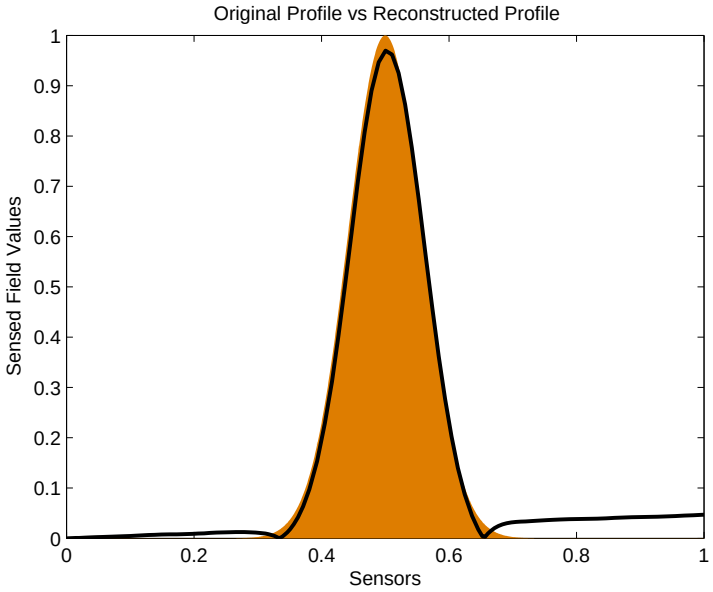

Figure 2.9. Smooth $q(x)$: 1,000 sensors, $\omega_{max} = 30$. Noisy resistor is uniformly chosen from the interval [0,0.1]. $||error||_2 = 0.0295$, $||error||_\infty = 0.0552$. The solid line corresponds to the reconstructed profile and the area plot corresponds to the original profile.

Here we show that if the L_i's (the spatially distributed sensed value) vary smoothly then it is possible to recover them to a high degree of accuracy. We show experimental results for different ω_{max} and show that the recovered profile follows the original profile closely as we increase ω_{max}. We choose $q(x)$ as

$$q(x_i) = exp\left(-\left(\frac{x_i - .5}{\sigma}\right)^2\right)$$

where $\sigma = \frac{1}{8}\sqrt{\log_{10}(e)}$ and $L(x_i)$ is obtained from $q(x_i)$ as shown in figure (2.8). In most practical situation, one would expect high correlation between adjacent sensed values and hence the smoothness requirement would be satisfied most of the time. As can be seen in figure (2.9), the inverse algorithm is successful in

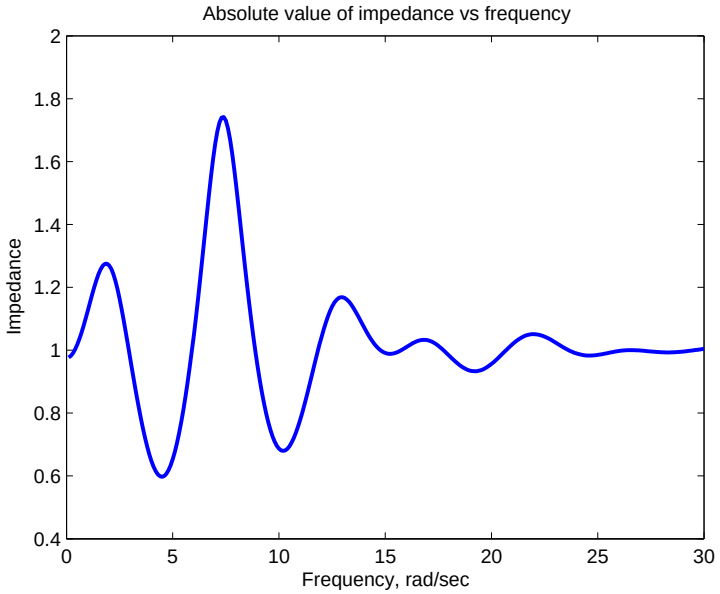

Figure 2.10. Impedance profile for figure (2.9). 1,000 sensors, $\omega_{max} = 30$.

reconstructing the $q(x)$; i.e. it follows the original profile quite closely. Figure (2.10) shows the plot of impedance (as a function of frequency), which is supplied to inverse algorithm (equation (2.37)).

We don't see significant improvement when the frequency is raised from 30 to 60 (figures (2.9) and (2.11)). This is due to the fact that, the forward problem (i.e. collecting the data $I_1(\omega)$) is in discrete domain (i.e. obtained through a lumped parameter model), whereas the reconstruction algorithm (the inverse problem - equations (2.25), (2.26), and (2.27)) is in continuous domain.

On other hand figure (2.12) indicates that if we decrease the maximum frequency of experiments, the performance of the inverse algorithm deteriorates.

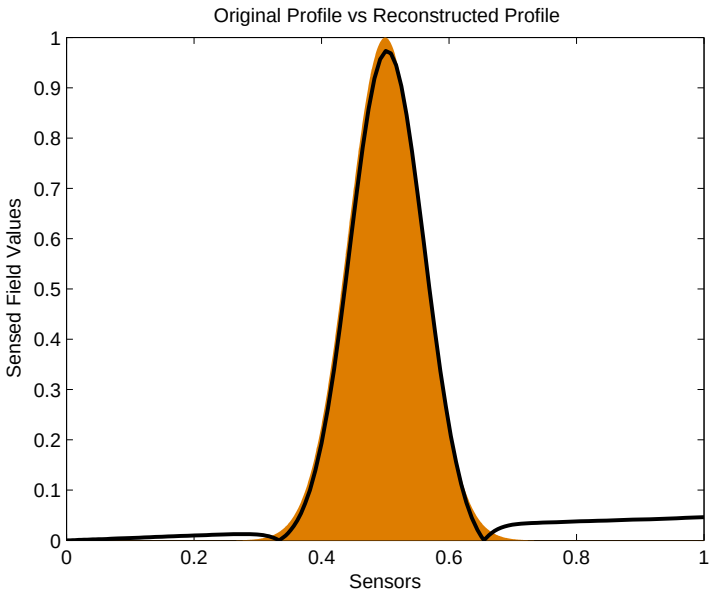

Figure 2.11. Smooth $q(x)$: 1,000 sensors, $\omega_{max} = 60$. Noise is a uniform random number between [0,0.1]. $||error||_2 = 0.0291$, $||error||_\infty = .0543$. The solid line corresponds to the reconstructed profile and the area plot corresponds to the original profile.

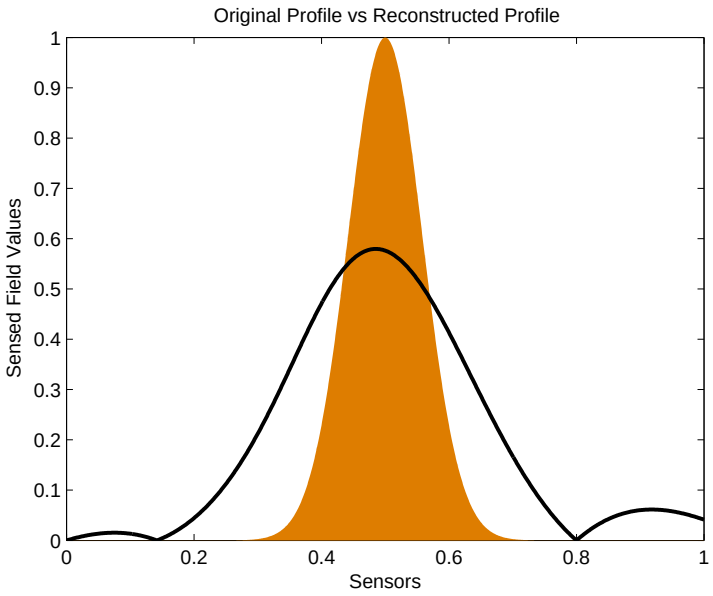

Figure 2.12. Smooth $q(x)$: 1,000 sensors, $\omega_{max} = 5$. Noise is a uniform random number between [0,.1]. $||error||_2 = 0.1695$, $||error||_\infty = .4242$. The solid line corresponds to the reconstructed profile and the area plot corresponds to the original profile.

2.5.2 Recovery using Noisy data

Here we add noise to the scattered data $I_1(\omega)$. Noise here is a uniform random number in $[0, .0001]$. Thus the scattered data is accurate for only three digits, and still the CR algorithm manages to recover the profile (figure (2.13))

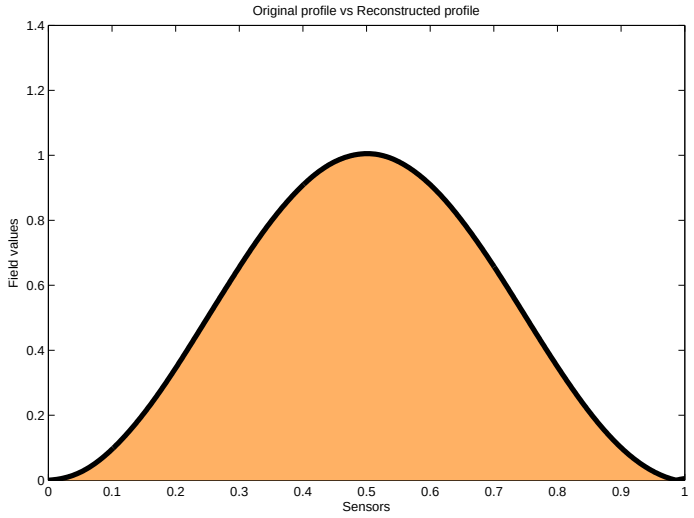

Figure 2.13. Recovery using Noisy data: 1000 sensors, $\omega_{max} = 25$. Noise, n is a uniform random number between $[0, .0001]$, i.e. $\hat{I}_1(\omega) = I_1(\omega) + n$. The solid line corresponds to the reconstructed profile and the area plot corresponds to the original profile.

2.5.3 Step profile

In practice, step profile would correspond to a case, where the sensed value is among a few quantized levels. Although Chen-Rokhlin algorithm requires smooth potential, it is able to reconstruct a piecewise smooth profile to great accuracy. Figure (2.14) corresponds to the case where the number of quantization level is more than two, whereas figure (2.15) corresponds to the case where only one bit

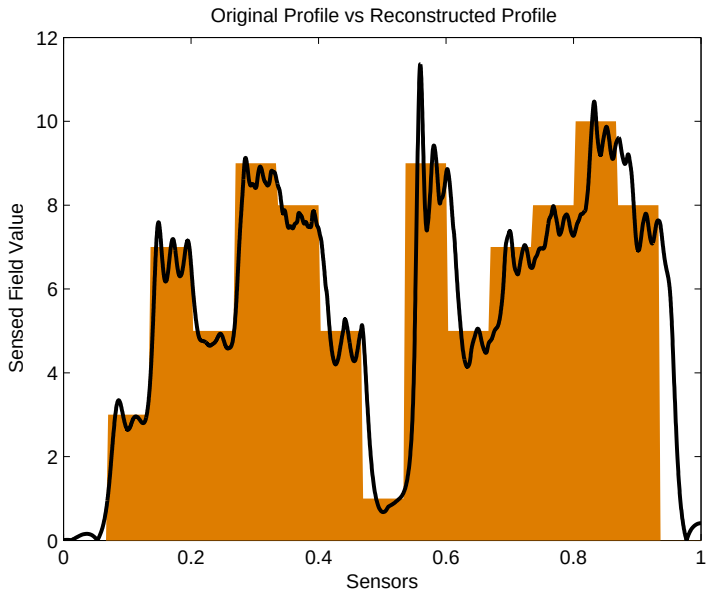

Figure 2.14. Step profile: 300 sensors, $\omega_{max} = 50$. Noise is a uniform random number between [0,.1]. $||error||_2 = 1.6127$, $||error||_\infty = 7.7227$. The solid line corresponds to the reconstructed profile and the area plot corresponds to the original profile.

of information (either 0 or 1) is transmitted. The reconstructed profile for both the cases give a reasonable picture of the quantized field values. As shown in figure (2.16), when the maximum frequency is increased to 75 , we see that the error in reconstruction further decreases.

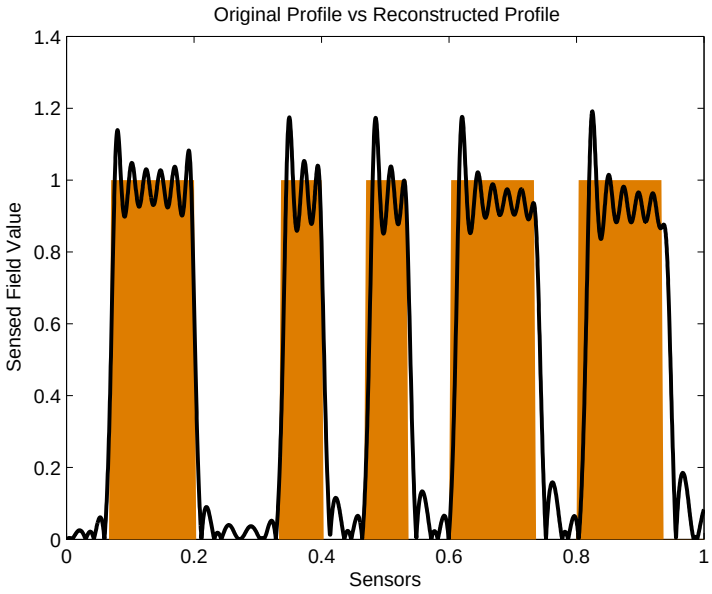

Figure 2.15. Step profile: 300 sensors, $\omega_{max} = 100$. Noise is a uniform random number between [0,.1]. $||error||_2 = .2118$, $||error||_\infty = 1.0033$. The solid line corresponds to the reconstructed profile and the area plot corresponds to the original profile.

2.5.4 Resolution

To test the inverse algorithm for its resolution ability we considered two cases. Figure (2.17) indicates successful resolution of two peaks separated by some distance, and the inverse algorithm works quite well even when the distance between the two peaks is reduced (figure (2.18).

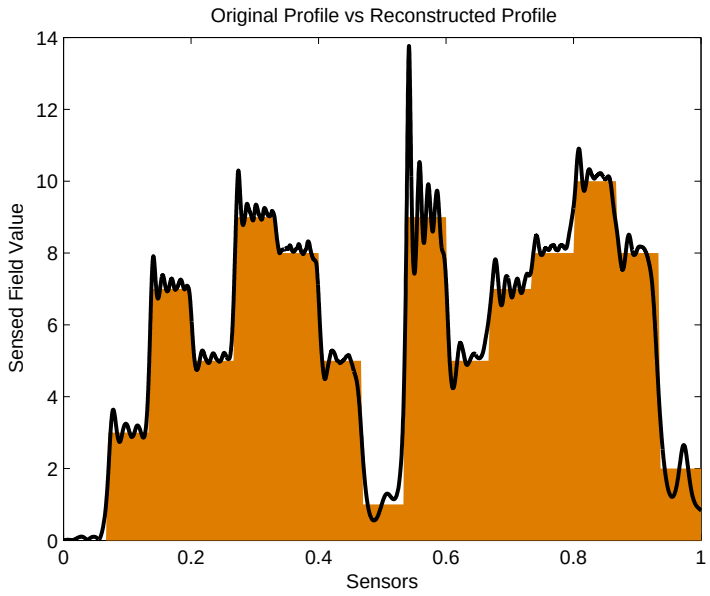

Figure 2.16. Step profile: 300 sensors, $\omega_{max} = 75$. Noise is a uniform random number between [0,.1]. $||error||_2 = .6508$, $||error||_\infty = 3.9715$. The solid line corresponds to the reconstructed profile and the area plot corresponds to the original profile.

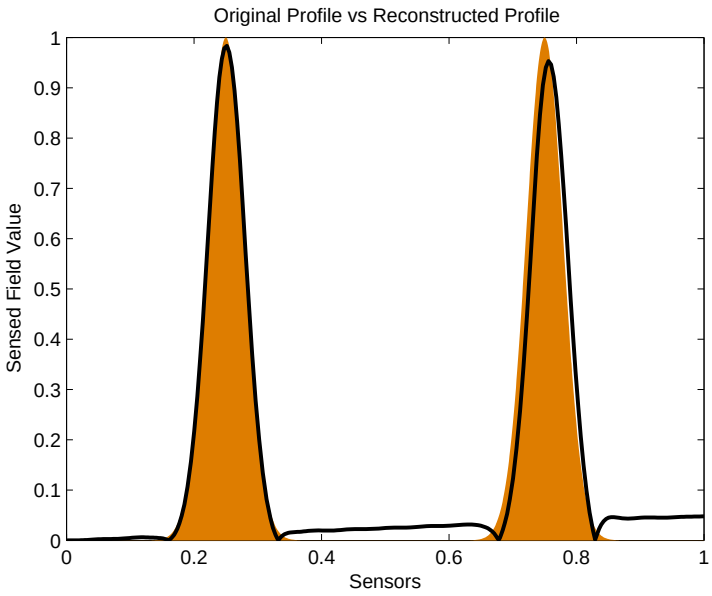

Figure 2.17. Resolution: 1,000 sensors, $\omega_{max} = 50$. Noise is a uniform random number between [0,.1], $||error||_2 = 0.0487$, $||error||_\infty = 0.1913$. The solid line corresponds to the reconstructed profile and the area plot corresponds to the original profile.

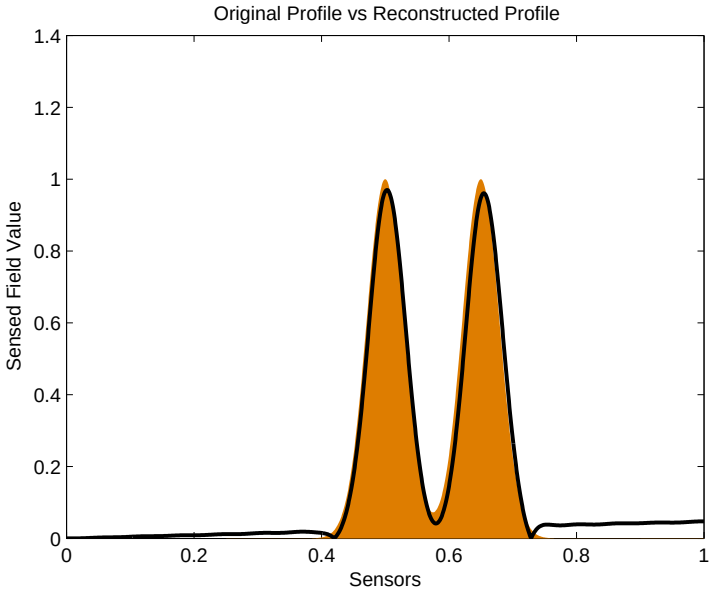

Figure 2.18. Resolution: 1,000 sensors, $\omega_{max} = 50$. Noise is a uniform random number between [0,.1], $||error||_2 = 0.0426$, $||error||_\infty = 0.1393$. The solid line corresponds to the reconstructed profile and the area plot corresponds to the original profile.

Figure (2.19) indicates successful resolution of a highly localized peak.

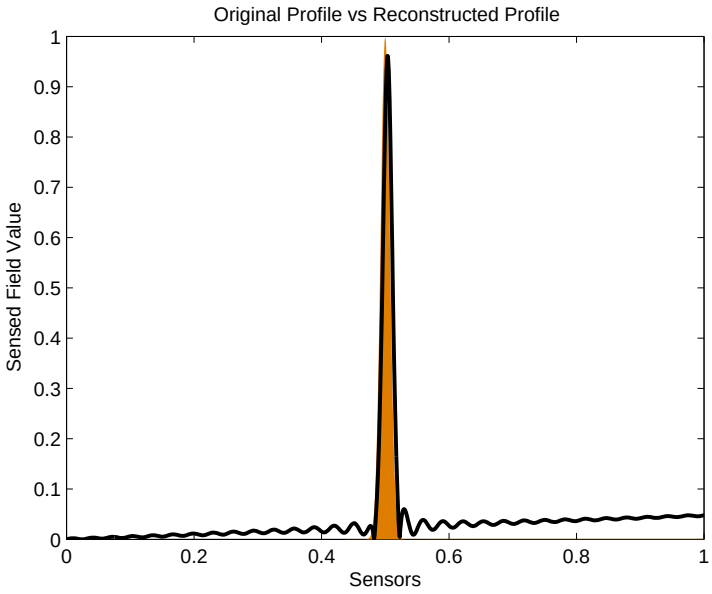

Figure 2.19. Resolution: 1,000 sensors, $\omega_{max} = 100$. Noise is a uniform random number between [0,.1]. $||error||_2 = 0.0481$, $||error||_\infty = 0.32$. The solid line corresponds to the reconstructed profile and the area plot corresponds to the original profile.

2.5.5 Scalability

The number of sensors is increased to 10,000 now. As shown in figures (2.20) and (2.21), the inverse algorithm was able to detect the profile successfully, thereby indicating the scalability of the algorithm. Also, the noise level for figure (2.21) is reduced by an order of magnitude resulting in a better reconstruction.

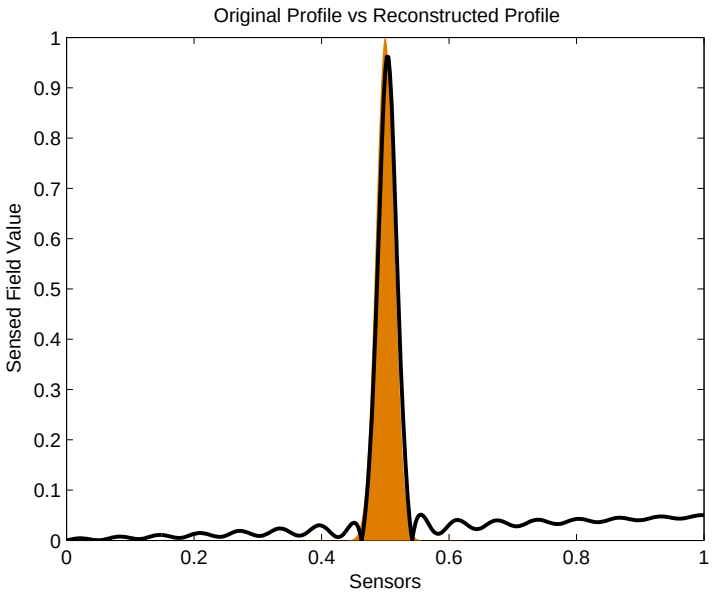

Figure 2.20. Scalability: 10,000 sensors, $\omega_{max} = 50$. Noise is a uniform random number between [0,.1]. $||error||_2 = 0.0395$, $||error||_\infty = 0.178$. The solid line corresponds to the reconstructed profile and the area plot corresponds to the original profile.

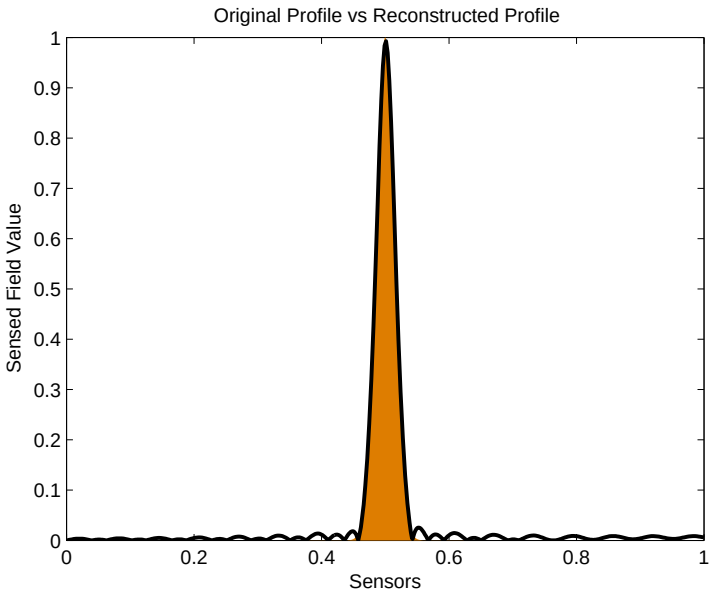

Figure 2.21. Scalability: 10,000 sensors, $\omega_{max} = 50$. Noise is a uniform random number between [0,.01], $||error||_2 = 0.0101$, $||error||_\infty = 0.0497$. The solid line corresponds to the reconstructed profile and the area plot corresponds to the original profile.

2.5.6 Non-smooth profiles

Although for most practical cases, the sensed profile will be smooth, we would like to see if the inverse algorithm is able to reconstruct non-smooth profiles. We used the function

$$q(x_i) = |0.5(\sin(2k\pi x_i))^{.25}|$$

which has infinite derivative (and hence not piecewise smooth) for finite values of x. The parameter k controls the number of lobes. As shown in figure (2.22),

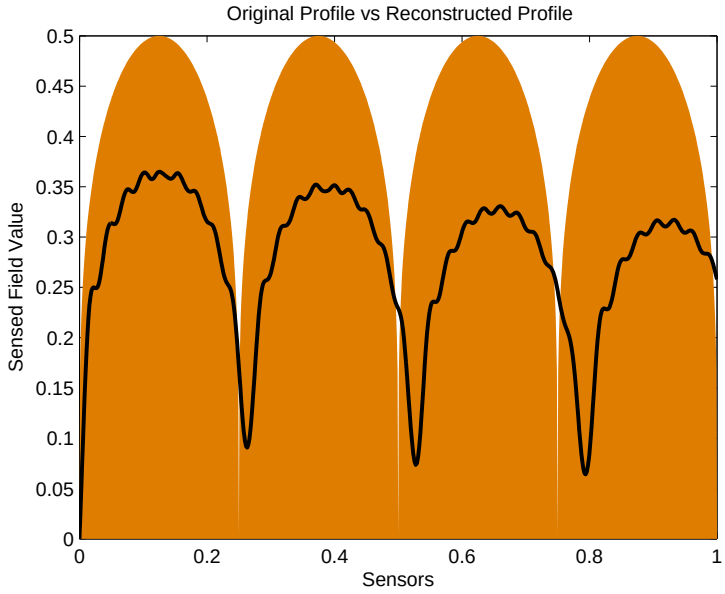

Figure 2.22. Piecewise non-smooth: $q(x_i) = |0.5(\sin(4\pi x_i))^{.25}|$, 1,000 Sensors, $\omega_{max} = 100$. Noise is a uniform random number between [0,.1]. $||error||_2 = .1643$, $||error||_\infty = .3629$. The solid line corresponds to the reconstructed profile and the area plot corresponds to the original profile.

Chen-Rokhlin algorithm is able to detect the shape of the potential along with number of lobes.

2.6 Comments on the Results

Using a continuous inverse scattering algorithm, it was possible to recover the unknown field values at discrete locations. The simulation results indicate a stable recovery of different profiles and a high degree of scalability. The algorithm is stable in the sense that the error does not blow up either due to increasing the number of sensors or due to noise in the network.

There are certain issues with this approach, which are listed below:

- The finite difference scheme is not a good approximation at higher frequencies. Equation (2.24) suggests that the $p_+(0,\omega) - p_-(0,\omega)$, which is proportional to the inverse of the current, $I_1(\omega)$, apart from the dc term, decays like $\frac{1}{\omega}$. But in chapter 3 it will be shown that $I_1(\omega)$ decays like $\frac{1}{\omega}$, implying that the p_+ is not bounded. Figure (2.23) shows the unbounded nature of the scattered data for high frequencies.

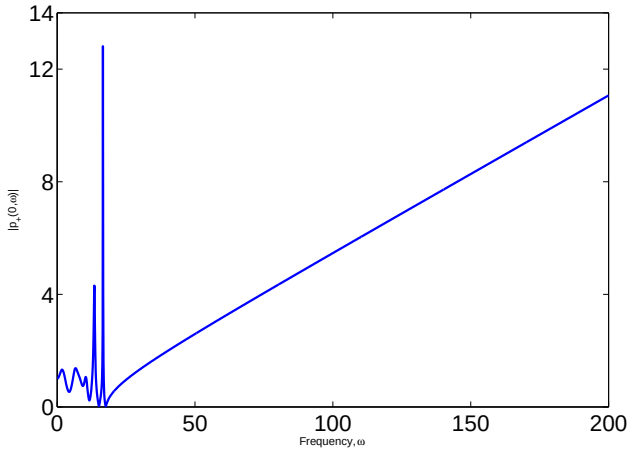

Figure 2.23. Absolute value of the scattered data vs frequency.

- The plots for the case of smooth field values show a presence of a finite error between the actual field values and the recovered field values. The

error does not decrease by taking samples of impedance at higher frequencies as predicted by the inverse scattering algorithm [10]. It is due to the discrepancy in the two (forward and inverse) models, i.e. (in the forward model) impedance is calculated using a discrete circuit, while (in the inverse model) the impedance data is supplied to a continuous inverse scattering algorithm.

- Since the circuit has been obtained through discretizing the continuous equations, the values of V, C, and Z cannot be chosen arbitrarily.

- Again, the finite difference discretization puts a lower bound on the number of sensors. The continuous equations won't give good results if the number of sensors are less than this bound. For example, the continuous algorithm won't be able to recover the values if there are only hundred sensors on the field (figure (2.24). The reflection data for the scattering profile shown in

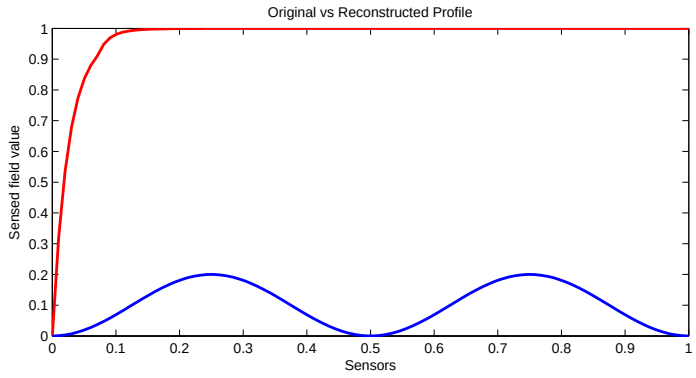

Figure 2.24. Failure of Chen-Rokhlin algorithm due to small number of sensors. Blue curve is the actual $q(x)$ and the red curve is the recovered $q(x)$.

figure (2.24) is shown in figure (2.25). Note the highly oscillatory behavior, which was absent for the cases shown before.

To address the above mentioned issues, in the next chapter, we extend the

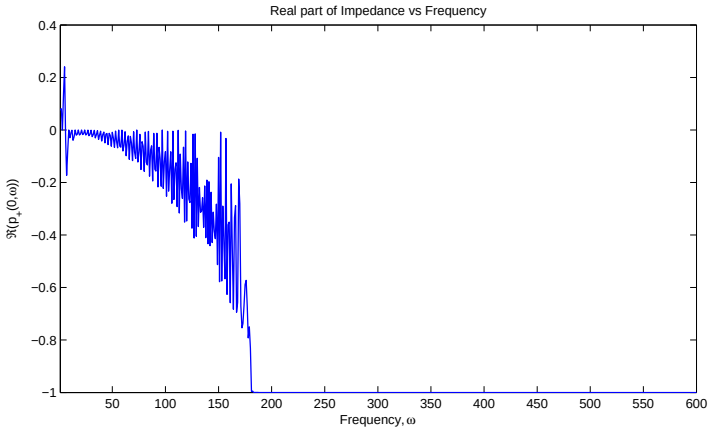

Figure 2.25. Real part of the scattered data for the $q(x)$ shown in figure (2.24).

Chen-Rokhlin algorithm for a discrete setting. We present discrete analogs of the Riccati equation and the trace formula, along with some simulation results.

Chapter 3

Discrete Inverse Scattering Algorithm

In the last chapter, we noted the disconnect between the discrete forward model and the continuous inverse algorithm. In this chapter, we extend the Chen-Rokhlin algorithm to discrete domain. We develop analogs of differential equations to peel the network, and to recover the unknown inductances.

3.1 Problem Setup

The discrete inverse scattering problem is now described for an LC ladder network shown in the figure (3.1). In the circuit, the inductors L_i's are the unknowns. Each capacitor takes the known value c_0. Negative impedance z, is also known. The input voltage $V(\omega)$ is applied to the circuit, and current $I_1(\omega)$ is measured. The problem can be defined as:

> ***Inverse Scattering for the discrete LC ladder network:*** *Given the admittacne,* $Y(\omega) = \frac{I_1(\omega)}{V(\omega)}$ *for different* ω*, obtain* L_1*,* L_2*, ...,* L_N*.*

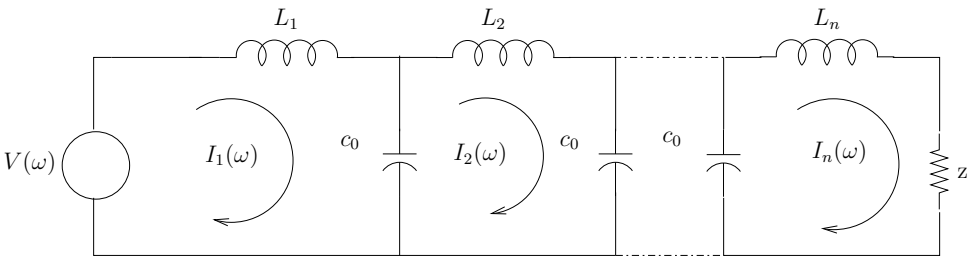

Figure 3.1. LC Ladder Network

Writing Kirchhoff's voltage loop (KVL) equations for the first, j-th, and the last loop, we have

$$(\frac{1}{i\omega c_0} + i\omega L_1)I_1(\omega) - \frac{1}{i\omega c_0}I_2(\omega) = V(\omega), \tag{3.1}$$

$$-\frac{1}{i\omega c_0}I_{j-1}(\omega) + (\frac{2}{i\omega c_0} + i\omega L_j)I_j(\omega) - \frac{1}{i\omega c_0}I_{j+1}(\omega) = 0, \tag{3.2}$$

$$-\frac{1}{i\omega c_0}I_{N-1}(\omega) + (\frac{1}{i\omega c_0} - z + i\omega L_N)I_N(\omega) = 0. \tag{3.3}$$

Writing the above equations in matrix-vector form

$$(\frac{1}{j\omega c_0}T + j\omega L + ze_n e_n^T)I(\omega) = V(\omega)e_1, \tag{3.4}$$

where,

$$
\begin{aligned}
T &= \begin{pmatrix}
1 & -1 & & & & & \\
-1 & 2 & -1 & & & & \\
 & \ddots & \ddots & \ddots & & & \\
 & & & -1 & 2 & -1 & \\
 & & & & -1 & 1 &
\end{pmatrix} \\
L &= diag(L_1, L_2, \cdots, L_N) \\
e_n &= \begin{pmatrix} 0 & 0 & \cdots & 0 & 1 \end{pmatrix}^T \text{ the nth basis vector} \\
&\quad \text{Similarly } e_1 \text{ is the first basis vector} \\
I &= \begin{pmatrix} I_1(\omega) & I_2(\omega) & \cdots & I_N(\omega) \end{pmatrix}^T \\
V &= \begin{pmatrix} V_s(\omega) & 0 & \cdots & 0 & 0 \end{pmatrix}^T \\
z &< 0
\end{aligned}
$$

Comparing the above circuit with discrete approximation of the helmholtz equation, we note the following differences.

- The values of L's, c_0, and z are no longer constrained to be some specific values.

- In the discrete approximation (chapter 2), z appears at both ends of the circuit. The outgoing boundary condition implied the presence of this negative impedance. For the finite LC ladder network, the negative impedance implies an amplifier, which pumps the energy synchronously, into the system from the other end of the network. In the next few sections, we show that the presence of z, makes the scattered data well behaved for real ω, and its presence makes the recovery of L's possible.

3.2 Characterize forward data

For our experiment, admittance $Y_1(\omega)$ or the current $I_1(\omega)$ (with input voltage constant) constitute forward data. We determine the behaviour of $Y_1(\omega)$ as a function of ω and as a function of the inductor values.

3.2.1 Poles of the admittance $Y_1(\omega)$ of the network

In this section we show that in the domain of operation ($\omega \in R$), the admittance is bounded and well defined, i.e. we find some constraints on the poles of $Y_1(\omega)$.

Theorem 1. *$Y_1(\omega) = \frac{I_1(\omega)}{V_s(\omega)}$ has no real poles if $z \neq 0$.*

Proof. Using equation (3.4), the admittance is given as

$$Y_1(\omega) = j\omega c_0(T - \omega^2 Lc_0 + j\omega z c_0 e_n e_n^T)^{-1}_{11} = j\omega c_0 \frac{\det(T - \omega^2 L\hat{c_0} + j\omega z c_0 e_n e_n^T)}{\det(T - \omega^2 Lc_0 + j\omega z c_0 e_n e_n^T)}$$

where the hat implies the matrix with first row and column removed. Thus, ω constitute a pole of $Y_1(\omega)$ if

$$\det(T - \omega^2 Lc_0 + j\omega z c_0 e_n e_n^T) = 0$$

The pole at $\omega = 0$ is canceled by the zero. Let $x + jy$ be in the null space of the matrix.

$$\begin{aligned} (T - \omega^2 Lc_0 + j\omega z c_0 e_n e_n^T)(x + jy) &= 0 \qquad (3.5) \\ \Rightarrow \begin{pmatrix} T - \omega^2 Lc_0 & -\omega z c_0 e_n e_n^T \\ \omega z c_0 e_n e_n^T & T - \omega^2 Lc_0 \end{pmatrix} \begin{pmatrix} x \\ y \end{pmatrix} &= \begin{pmatrix} 0 \\ 0 \end{pmatrix} \end{aligned}$$

Case 1: $\omega^2 \neq \lambda_i(T)_{Lc_0}$ From the first block equation we have

$$\begin{aligned} x &= (T - \omega^2 Lc_0)^{-1}(-\omega c_0 z e_n e_n^T y) \\ x &= (-\omega c_0 z e_n^T y)(T - \omega^2 Lc_0)^{-1} e_n) \end{aligned}$$

$\Rightarrow x = \alpha$ last column of $(T - \omega^2 Lc_0)^{-1}$

$$\begin{aligned} \Rightarrow x \approx y \approx & \quad \text{last column of } (T - \omega^2 Lc_0)^{-1} \\ \Rightarrow x + jy &\approx \underbrace{x}_{real}(\alpha + j\beta) \end{aligned}$$

Substituting the above value in equation (3.5),

$$\begin{aligned} (T - \omega^2 Lc_0 + j\omega z c_0 e_n e_n^T)x &= 0 \\ \Rightarrow (T - \omega^2 Lc_0)x &= -j\omega z c_0 e_n e_n^T x \end{aligned}$$

Let ω (the pole frequency) be real.

$$\begin{aligned} \Rightarrow (T - \omega^2 Lc_0)x &\in R^n \\ \text{but } -j\omega z c_0 e_n e_n^T)x &\notin R^n \\ \Rightarrow \omega &\notin R \end{aligned}$$

$\Rightarrow$ No real poles.

Case 2: $\omega^2 = \lambda_i(T)_{Lc_0}$

$$
\begin{aligned}
\Rightarrow (T - \omega^2 Lc_0)x &= (\omega z c_0 e_n^T y) e_n \\
\Rightarrow e_n &\in R(T - \omega^2 Lc_0) \\
\therefore (T - \omega^2 Lc_0)x = 0 &\Rightarrow x^T e_n = 0 \\
\Rightarrow x_n &= 0 \\
(T - \omega^2 Lc_0) \begin{pmatrix} x_1 \\ x_2 \\ \vdots \\ x_{n-1} \\ 0 \end{pmatrix} &= 0 \\
\Rightarrow x_{n-1} &= 0 \\
&\vdots \\
x_1 &= 0 \\
\Rightarrow x &= 0
\end{aligned}
$$

Thus the only null space possible is the trivial null space, which is not true. Hence $\omega^2 \neq \lambda_i(T)_{Lc_0}$. Thus the poles of the admittance are not real. □

Next we prove that the poles are trapped in one of the half planes (lower or upper) depending on the value of z.

Theorem 2. *If $z < 0$, the poles are trapped in the lower half plane.*

Proof. Consider the case where all Ls are the same, i.e. $L = lI$. As mentioned earlier, the poles of $I_1(\omega)$ or the admittance $(\frac{I_1(\omega)}{V(\omega)})$ are given by the zeros of the

$\det(T - \omega^2 l c_0 I + j\omega c_0 z e_n e_n^T)$, i.e. ω such that

$$\begin{aligned} \det(T - \omega^2 l c_0 I + j\omega c_0 z e_n e_n^T) &= 0 \\ \Rightarrow \det(T - \omega^2 l c_0 I)\det(I + (T - \omega^2 l c_0 I)^{-1} j\omega z c_0 e_n e_n^T) &= 0 \\ \Rightarrow \det(I + (T - \omega^2 l c_0 I)^{-1} j\omega z c_0 e_n e_n^T) &= 0 \end{aligned}$$

(the first determinant is not zero because we consider $\omega \notin R$ and T is a symmetric matrix with real eigenvalues.)

$$\begin{aligned} \Rightarrow (1 + j\omega z c_0 e_n^T (T - \omega^2 l c_0 I)^{-1} e_n) &= 0 \\ \Rightarrow 1 + j\omega z c_0 e_n^T Q(\Lambda - \omega^2 l c_0 I)^{-1} Q^H e_n &= 0 \\ \Rightarrow 1 + j\omega z c_0 \sum_i \frac{|v_{ni}|^2}{\lambda_i - \omega^2 l c_0} &= 0 \end{aligned}$$

For $\omega = \omega_R + j\omega_I$

$$
\begin{aligned}
0 &= 1 + (j\omega_R - \omega_I) z c_0 \sum_i \frac{|v_{ni}|^2}{\lambda_i - (\omega_R^2 - \omega_I^2 + j2\omega_R\omega_I) l c_0} \\
0 &= 1 + (j\omega_R - \omega_I) z c_0 \sum_i \frac{|v_{ni}|^2(\lambda_i - (\omega_R^2 - \omega_I^2) l c_0 + j2\omega_R\omega_I l c_0)}{(\lambda_i - (\omega_R^2 - \omega_I^2) l c_0)^2 + 4\omega_R^2\omega_I^2 l^2 c_0^2} \qquad (3.6)
\end{aligned}
$$

Taking real parts

$$
\begin{aligned}
0 &= 1 - \omega_I z c_0 \sum_i \frac{|v_{ni}|^2(\lambda_i - (\omega_R^2 - \omega_I^2) l c_0)}{(\lambda_i - (\omega_R^2 - \omega_I^2) l c_0)^2 + 4\omega_R^2\omega_I^2 l^2 c_0^2} - \\
&\quad \omega_R z c_0 \sum_i \frac{|v_{ni}|^2(2\omega_R\omega_I l c_0)}{(\lambda_i - (\omega_R^2 - \omega_I^2) l c_0)^2 + 4\omega_R^2\omega_I^2 l^2 c_0^2} \\
0 &= 1 + z c_0 \sum_i \frac{|v_{ni}|^2(-\omega_I\lambda_i + \omega_I(\omega_R^2 - \omega_I^2) l c_0)}{(\lambda_i - (\omega_R^2 - \omega_I^2) l c_0)^2 + 4\omega_R^2\omega_I^2 l^2 c_0^2} + \\
&\quad z c_0 \sum_i \frac{|v_{ni}|^2(-2\omega_R^2\omega_I l c_0)}{(\lambda_i - (\omega_R^2 - \omega_I^2) l c_0)^2 + 4\omega_R^2\omega_I^2 l^2 c_0^2} \\
0 &= 1 + z c_0 \sum_i \frac{|v_{ni}|^2(-\omega_I\lambda_i + \omega_I(\omega_R^2 - \omega_I^2) l c_0 - 2\omega_R^2\omega_I l c_0)}{(\lambda_i - (\omega_R^2 - \omega_I^2) l c_0)^2 + 4\omega_R^2\omega_I^2 l^2 c_0^2} \\
0 &= 1 + z c_0 \sum_i \frac{|v_{ni}|^2(-\omega_I\lambda_i - \omega_I^3 l c_0 - \omega_R^2\omega_I l c_0)}{(\lambda_i - (\omega_R^2 - \omega_I^2) l c_0)^2 + 4\omega_R^2\omega_I^2 l^2 c_0^2} \\
0 &= 1 + \omega_I z c_0 \sum_i \frac{|v_{ni}|^2(-\lambda_i - (\omega_R^2 + \omega_I^2) l c_0)}{(\lambda_i - (\omega_R^2 - \omega_I^2) l c_0)^2 + 4 l^2 c_0^2 \omega_R^2\omega_I^2} \qquad (3.7)
\end{aligned}
$$

From equation(3.7), $z\omega_I > 0$ (because each term inside the summation is negative). Thus

- If $z < 0$, poles are in the lower half plane
- If $z > 0$, poles are in the upper half plane

Thus, for $L = lI$, and $z < 0$, poles are trapped in the lower half plane. The previous theorem guarantees non-real poles if z is present. Now, if we vary L continuously, the poles have to cross the real line to move to the upper half plane. And since real poles are not allowed, the poles for the network are all trapped in the lower half plane. □

3.2.2 Sensitivity of $Y_1(\omega)$ with respect to k'th inductor L_k

Rewriting the expression for $Y_1(\omega)$, we have

$$Y_1(\omega) = j\omega c_0 \frac{\det(T - \omega^2 L\widehat{c_0 + j\omega z c_0 e_n e_n^T})}{\det(T - \omega^2 L c_0 + j\omega z c_0 e_n e_n^T)},$$

which can be simplified and written using continued fractions:

$$Y_1(\omega) = \cfrac{j\omega c_0}{1 - \omega^2 c_0 L_1 - \cfrac{1}{2 - \omega^2 c_0 L_2 - \cfrac{1}{\ddots_{2 - \omega^2 c_0 L_k - \cfrac{1}{\ddots_{- \cfrac{1}{1 - \omega^2 c_0 L_n + j\omega c_0 z}}}}}}}$$

$$\begin{aligned}
Y_1(\omega) &= \frac{j\omega c_0}{D_1} \\
\text{where } D_1 &= 1 - \omega^2 c_0 L_1 - \frac{1}{D_2} \\
\text{where } D_2 &= 2 - \omega^2 c_0 L_2 - \frac{1}{D_3} \\
&\vdots \\
\text{where } D_k &= 2 - \omega^2 c_0 L_k - \frac{1}{D_{k+1}}
\end{aligned}$$

Now if we denote derivative w.r.t L_k using prime, then $\frac{\partial Y}{\partial L_k}$ is given as

$$\begin{aligned}
Y' &= -j\omega c_0 \frac{D_1'}{D_1^2} \\
D_1' &= \frac{D_2'}{D_2^2} \\
D_2' &= \frac{D_3'}{D_3^2} \\
&\vdots \\
D_{k-1}' &= \frac{D_k'}{D_k^2} \\
D_k' &= -\omega^2 c_0 \\
\therefore D_{k-1}' &= \frac{-\omega^2 c_0}{D_k^2} \\
\therefore D_{k-2}' &= \frac{-\omega^2 c_0}{D_k^2 D_{k-1}^2} \\
&\vdots \\
\frac{\partial Y}{\partial L_k} &= \frac{\omega^3 c_0^2}{\prod_{m=1}^{k} D_m^2} \qquad (3.8)
\end{aligned}$$

where $\prod_{m=1}^{k} D_m^2$ is $O(\omega^{2k})$

Result (3.8) can be interpreted as

- If $L_k = l$ for all k's and if one of the l is changed, then the change can be "observed" in the low frequency region of the admittance.

Alternately for sensititvity we can ask the following question: Given that I am solving $Ax = \alpha e_1$, and now I modify the (k,k) entry of the coefficient matrix by δ i.e. solve $(A + \delta e_k e_k^T)y = \alpha e_1$. How different is y_1 from x_1? Here $A =$

$(T - \omega^2 l c_0 I + j\omega z c_0 e_n e_n^T)$, x is the current vector, $\alpha = j\omega c_0 V(\omega)$, and $\delta = \omega^2 \hat{l} c_0$.

$$\begin{aligned}
(A + \delta e_k e_k^T)y &= \alpha e_1 \\
\Rightarrow (I + \delta A^{-1} e_k e_k^T)y &= x \\
\Rightarrow y + (\delta y_k)(A^{-1})_{*k} &= x \\
\Rightarrow y_1 + (\delta y_k)(A^{-1})_{1k} &= x_1 \qquad (3.9) \\
\text{and } y_k + (\delta y_k)(A^{-1})_{kk} &= x_k \\
\Rightarrow y_k &= \frac{x_k}{1 + \delta(A^{-1})_{kk}}
\end{aligned}$$

Substituting the above equation in (3.9)

$$\begin{aligned}
\Rightarrow y_1 + \frac{\delta x_k}{1 + \delta(A^{-1})_{kk}}(A^{-1})_{1k} &= x_1 \\
\Rightarrow x_1 - y_1 &= \frac{\delta x_k (A^{-1})_{1k}}{1 + \delta(A^{-1})_{kk}} \qquad (3.10)
\end{aligned}$$

Substituting the value of δ in equation (3.10), we have

$$x_1 - y_1 = \frac{\omega^2 \hat{l} c_0 x_k (A^{-1})_{1k}}{1 + \omega^2 \hat{l} c_0 (A^{-1})_{kk}} \qquad (3.11)$$

Equation (3.11) suggests that slight change in one of the inductance, will cause the current to change, implying that the new value of the inductor can be recovered from the observed data. Figure(3.2) shows the $\Re(I_1(\omega))$ as a function of frequency. All inductors took the value one. Now L_5 was changed to 2 and the current plotted in figure (3.3). Note the change in the values of the two currents.

3.3 Explicit expression for current

Rewriting equation (3.4) we have

$$(\underbrace{T - \omega^2 c_0 L}_{A} + j\underbrace{\omega c_0 z e_n e_n^T}_{B})I(\omega) = j\underbrace{\omega c_0 V(\omega) e_1}_{b} \qquad (3.12)$$

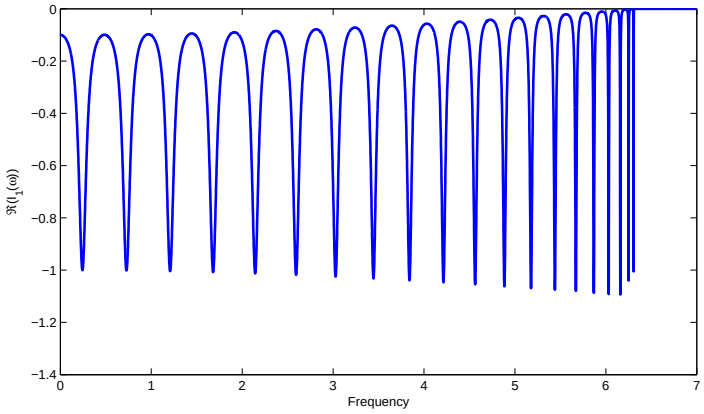

Figure 3.2. $\Re(I_1(\omega))$ vs frequency: N = 21, $L_k = 1, \forall k$.

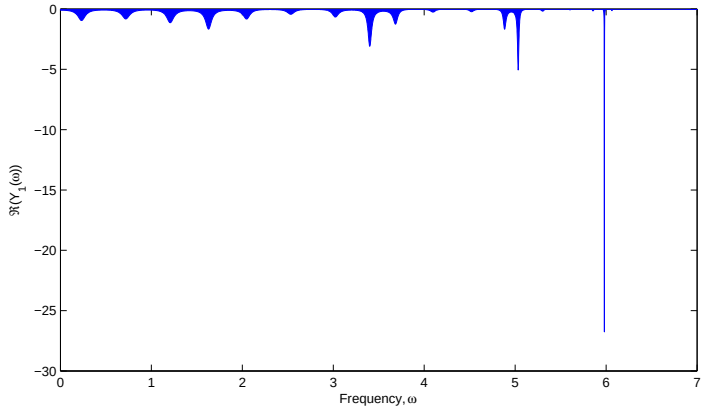

Figure 3.3. $\Re(I_1(\omega))$ vs frequency: N = 21, $L_k = 1, \forall k \neq 5$, $L_5 = 2$

Let the complex current be given as $I(\omega) = x + jy$. Then the current can be obtained by solving

$$\begin{pmatrix} A & -B \\ B & A \end{pmatrix} \begin{pmatrix} x \\ y \end{pmatrix} = \begin{pmatrix} 0 \\ b \end{pmatrix}$$

The first block equation gives

$$Ax = By = \omega c_0 z y_n e_n$$

Assuming A^{-1} exist, we have

$$x = (\omega c_0 z) y_n (A^{-1})_{*n}$$

The second block equation gives

$$\begin{aligned}
Bx + Ay &= b \\
\Rightarrow Ay &= (\omega c_0) e_1 - (\omega c_0 z)^2 y_n (A^{-1})_{nn} e_n \\
\Rightarrow y &= (\omega c_0)(A^{-1})_{*1} - (\omega c_0 z)^2 y_n (A^{-1})_{nn} (A^{-1})_{*n} \\
\Rightarrow y_n &= (\omega c_0)(A^{-1})_{n1} - (\omega c_0 z)^2 y_n (A^{-1})_{nn}^2 \\
\Rightarrow y_n &= \frac{(\omega c_0)(A^{-1})_{n1}}{1 + (\omega c_0 z)^2 (A^{-1})_{nn}^2} \\
\Rightarrow y_1 &= \omega c_0 (A^{-1})_{nn} - \frac{(\omega c_0 z)^2 \omega c_0 (A^{-1})_{n1} (A^{-1})_{1n} (A^{-1})_{nn}}{1 + (\omega c_0 z)^2 (A^{-1})_{nn}^2}
\end{aligned}$$

and

$$x_1 = \frac{(\omega c_0 z) \omega c_0 (A^{-1})_{n1} (A^{-1})_{1n}}{1 + (\omega c_0 z)^2 (A^{-1})_{nn}^2} \tag{3.13}$$

Some observations:

- The real part of current, x_1 (if A^{-1} exist) cannot have real poles, since the denominator is always greater than 1. Also, $(A^{-1})_{n1}$ $(= (A^{-1})_{1n})$ have the

asymptotics of $O(\omega^{-2N})$. Thus the real part of the current, which is used to recover L_1, decays rapidly.

- Figure (3.4) shows the real part of the current in the first loop. The pole like behavior that we observe is due to "large" values of $(A^{-1})_{n1}$ e.g. in one particular class of L (continuous and slowly varying), $(A^{-1})_{n1} \approx 40$ while $(A^{-1})_{nn} < 1$ and making the real part of current in the vicinity of 1000.

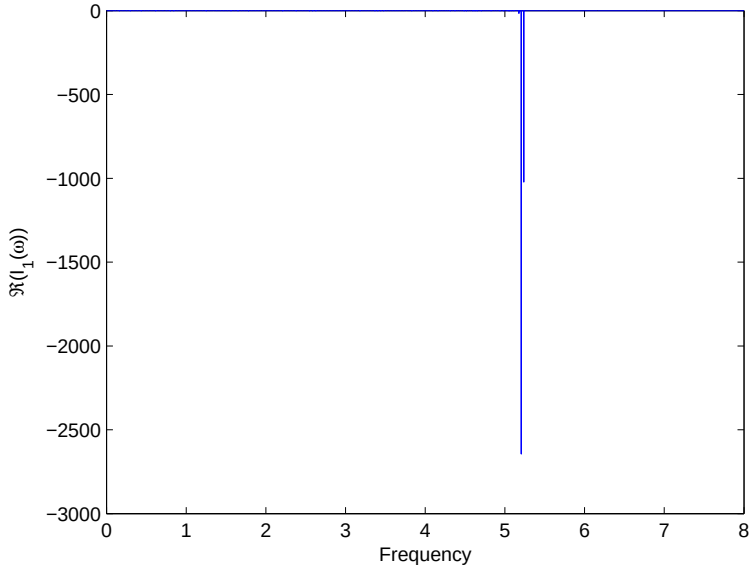

Figure 3.4. $\Re(I_1(\omega))$ vs frequency.

- It seems that making z large in magnitude might mitigate the effect of small $(A^{-1})_{nn}$, but what it does is suppress the pole location by some amount, but increases the magnitude of current at other frequency locations.

- Looking at the complete expression, we have that the imaginary part of the current has the asymptotics of $O(\omega^{-1})$, which is used to recover L.

- For the case when A^{-1} doesn't exist, we don't have an explicit expression for the current. But the asymptotics still hold true.

3.4 Discrete algorithm

The inverse algorithm consists of the following steps:

1. Measure data $Y_1(\omega)$ and obtain the inductor in the first loop, L_1, figure (3.5).

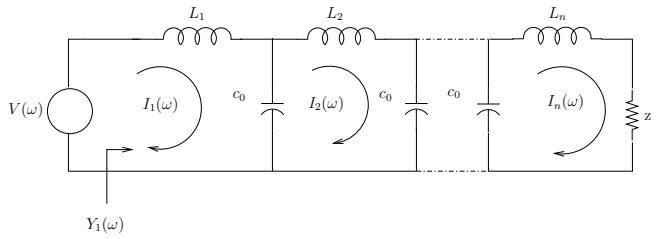

Figure 3.5. Obtain scattered data, $Y_1(\omega)$

2. Using L_1 and $Y_1(\omega)$, "peel" the network, i.e. obtain $Y_2(\omega)$ for the circuit consisting of n-1 inductors L_2 to L_n.

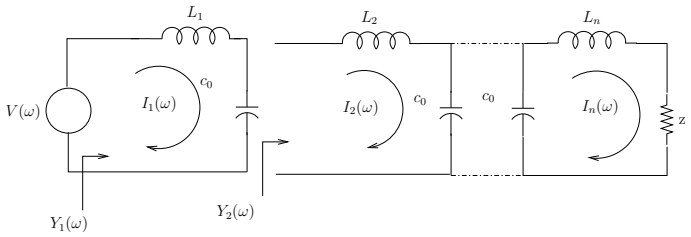

Figure 3.6. Peel the network to obtain $Y_2(\omega)$

3. Repeat step 1 with the new admittance $Y_2(\omega)$.

3.4.1 Obtain L_1 from $Y_1(\omega)$

Rewriting the admittance,

$$Y_1(\omega) = \cfrac{j\omega c_0}{2 - \omega^2 c_0 L_1 - \cfrac{1}{2-\omega^2 c_0 L_2 - \cfrac{1}{\ddots_{2-\omega^2 c_0 L_k - \cfrac{1}{\ddots_{-\cfrac{1}{1-\omega^2 c_0 L_n + j\omega c_0 z}}}}}}} \tag{3.14}$$

Next we find A_i's such that

$$Y_1(\omega) = A_0 + \frac{A_1}{j\omega} + O(\omega^{-2})$$

where A_0 and A_1 are the unknowns independent of ω and are to be determined from equation (3.14). The A_i's are found using high frequency approximation:

$$\begin{aligned} A_0 &= \lim_{\omega\to\infty} Y_1(\omega) = 0 \\ A_1 &= \lim_{\omega\to\infty} j\omega Y_1(\omega) = \frac{1}{L_1} \end{aligned}$$

$$Y_1(\omega) = \frac{1}{j\omega L_1} + O(\omega^{-2}) \tag{3.15}$$

Since there are no poles on the upper half plane, integration of $Y_1(\omega)$ along a closed contour indicated in the figure (3.7) yields 0.

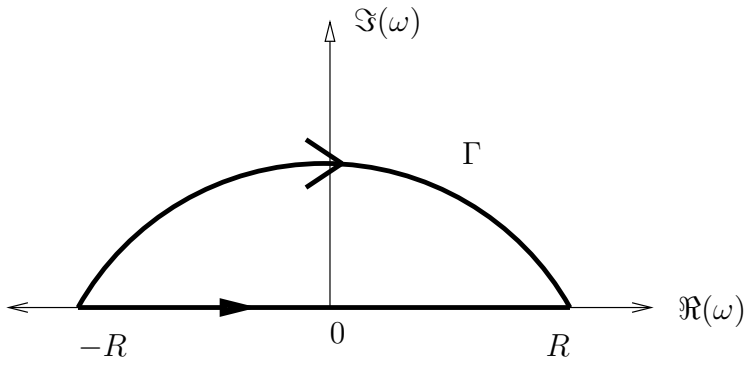

Figure 3.7. contour integration

$$\oint Y_1(\omega)d\omega = 0$$

Let Γ denote the curve (with clockwise orientation) in the upper half plane. Then the contour integral yields

$$\int_{-R}^{R} Y_1(\omega)d\omega = \int_{\Gamma} Y_1(\omega)d\omega \tag{3.16}$$

Integrating equation(3.15) along the curve

$$\begin{aligned}
\int_{\Gamma} Y_1(\omega)d\omega &= \int_{\Gamma} \frac{1}{j\omega L_1}d\omega \\
\text{Let } Re^{j\theta} &= \omega \\
\Rightarrow jRe^{j\theta}d\theta &= d\omega \\
\Rightarrow j\omega d\theta &= d\omega \\
\Rightarrow d\theta &= \frac{d\omega}{j\omega} \\
\omega = -R &\Rightarrow \theta = \pi \\
\omega = R &\Rightarrow \theta = 0 \\
\therefore \int_{\Gamma} Y_1(\omega)d\omega &= \int_{\pi}^{0} \frac{1}{L_1}d\theta \\
&= \frac{-\pi}{L_1}
\end{aligned} \tag{3.17}$$

Hence using equations (3.16) and (3.17) we have

$$L_1 = \frac{-\pi}{\int_{-R}^{R} Y_1(\omega)d\omega} \tag{3.18}$$

3.4.2 Layer Peeling

There are different ways to "peel" the layer i.e. given I_1, L_1, and V_s, we need to find, I_2 and V_2 which shall be used to find L_2 and so on.

1. Peel for I's and V's separately and then form admittance.

2. Peel directly for admittance Y.

Peeling using I's and V's

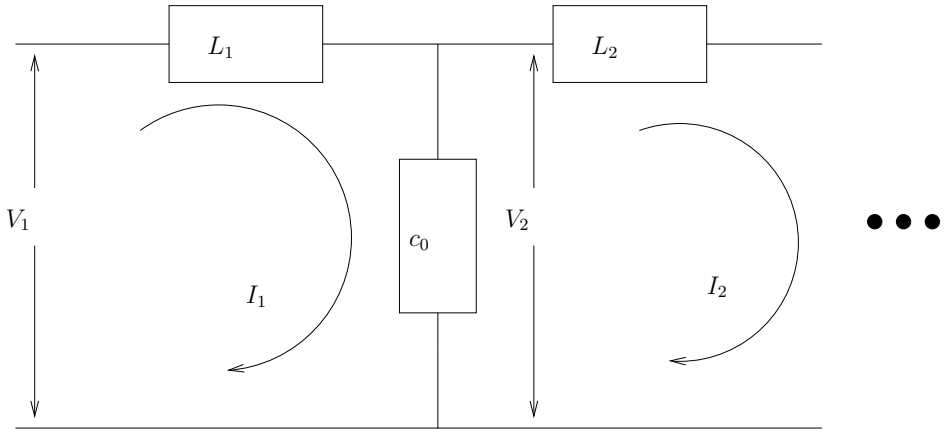

Figure 3.8. Layer Peeling using I's and V's

The figure (3.8) shows two immediate layers. V_1 is the supplied voltage (hence known), I_1 is the measured current, and L_1 is recovered from (3.18). As a next step, I_2 and V_2 need to be determined, so that the procedure can be repeated. Using KVL

$$V_2 = V_1 - j\omega L_1 I_1, \tag{3.19}$$

and since the right hand side is completely known, V_2 is now known. To get I_2, we rewrite V_2 as the voltage accross the capacitor.

$$\begin{aligned} V_2 &= (I_2 - I_1)\frac{1}{j\omega c_0} \\ \Rightarrow I_2 &= I_1 + j\omega C_0 V_2. \end{aligned} \tag{3.20}$$

Equations (3.18), (3.19), and (3.20) with $Y_2(\omega) = \frac{I_2(\omega)}{V_2(\omega)}$ constitute a recursive procedure to determine the L's. Note that V_2 can now be treated as the new known source voltage, I_2 as the new measured current and the new network is now the old network with the first section removed. Hence the proof for poles carry on for the new system.

Layer peeling using Y

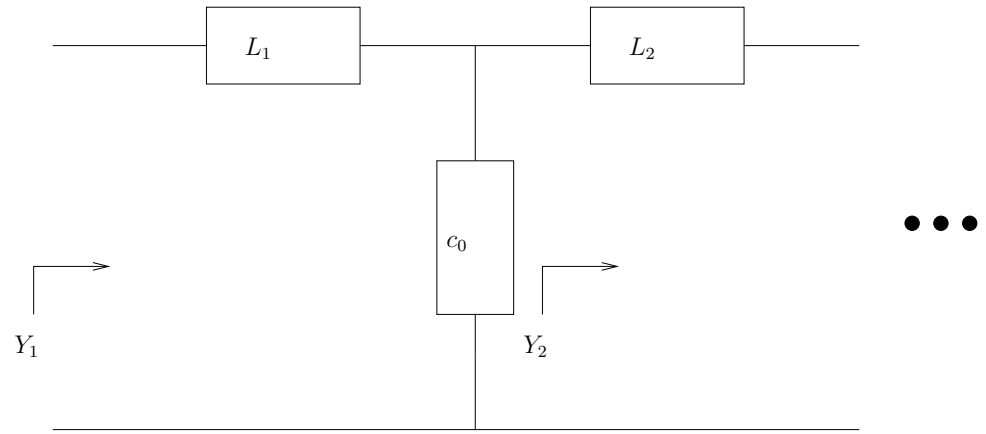

Figure 3.9. Layer Peeling using Y

Suppose instead of measuring the current separately, we measure the admittance of the network Y_1 (old admittance of the network shown in figure (3.9)). Again L_1 can be calculated using equation (3.18). Using standard circuit theory concepts, the old admittance can be written as

$$\begin{aligned}
Y_1 &= \frac{1}{j\omega L_1} || (Y_2 + j\omega c_0) \\
&\quad \text{where } || \text{ means a parallel combination} \\
Y_1 &= \frac{Y_2 + j\omega c_0}{j\omega L_1} \frac{1}{\frac{1}{j\omega L_1} + (Y_2 + j\omega c_0)} \\
&= \frac{Y_2 + j\omega c_0}{1 - \omega^2 L_1 c_0 + j\omega L_1 Y_2} \\
\Rightarrow Y_2 + j\omega c_0 &= Y_1(1 - \omega^2 L_1 c_0) + j\omega L_1 Y_1 Y_2 \\
\Rightarrow Y_2(j\omega L_1 Y_1 - 1) &= j\omega c_0 + Y_1(\omega^2 L_1 c_0 - 1) \\
\Rightarrow Y_2 &= \frac{j\omega c_0 + Y_1(\omega^2 L_1 c_0 - 1)}{j\omega L_1 Y_1 - 1} \qquad (3.21)
\end{aligned}$$

The right hand side of equation (3.21) is known and hence the admittance of the new network is now known. Equation (3.21) coupled with equation (3.18) constitute the inverse algorithm.

3.4.3 Stability of the Algorithm

Here it is shown how errors in measurement of current, and errors in reconstruction, are amplified and propagated due to layer peeling. This is also provides a range of frequency for which the data is usable.

Stability and experimental errors

Instead of measuring the true current $I_1(\omega)$, we measure $\hat{I}_1(\omega) = I_1(\omega) + \delta_I^e$.

$$\begin{aligned}
\therefore \hat{V}_2(\omega) &= V_1 - j\omega L_1 \hat{I}_1(\omega) \\
&= V_1 - j\omega L_1 (I_1(\omega) + \delta_I^e) \\
&= V_1 - j\omega L_1 I_1(\omega) - j\omega L_1 \delta_I^e \\
&= V_2 - \underbrace{j\omega L_1 \delta_I^e}_{\delta_V} \qquad (3.22)
\end{aligned}$$

Similarly

$$\begin{aligned}
\hat{I}_2 &= \hat{I}_1 - j\omega c_0 \hat{V}_2 \\
&= I_1 + \delta_I^e - j\omega c_0 \hat{V}_2 - \omega^2 L_1 c_0 \delta_I^e \\
&= I_2 + \underbrace{(1 - \omega^2 L_1 c_0)\delta_I^e}_{\delta_{I2}} \qquad (3.23)
\end{aligned}$$

Equations (3.22) and (3.23) suggest that the errors blow up as $O(\omega^2)$ for high frequencies and data for those frequencies are unusable.

Stability and reconstruction error

An error δ_L is made in reconstructing the inductor value so that $\hat{L_1} = L_1 + \delta_L$.

$$\begin{aligned} \therefore \hat{V_2} &= V_1 - j\omega\hat{L_1}I_1 \\ &= V_1 - j\omega(L_1 + \delta_L)I_1 \\ &= V_2 - \underbrace{j\omega\delta_L I_1}_{\delta_V^r} \end{aligned} \tag{3.24}$$

Similarly

$$\begin{aligned} \hat{I_2} &= I_1 - j\omega c_0 \hat{V_2} \\ &= I_1 - j\omega c_0 V_2 - \omega^2 c_0 \delta_L I_1 \\ &= I_2 - \underbrace{\omega^2 c_0 \delta_L I_1}_{\delta_{I2}^r}. \end{aligned} \tag{3.25}$$

Since $I_1(\omega)$ is of $O(\omega^{-1})$, the error in the voltage grows as $O(1)$ (equation(3.24)), whereas the error in the current blows up as $O(\omega)$ (equation(3.25)).

Stability and reconstruction error with $Y_1(\omega)$

Rewriting equation (3.21)

$$\hat{Y_2} = \frac{j\omega c_0 + Y_1(\omega^2 \hat{L}_1 c_0 - 1)}{j\omega \hat{L}_1 Y_1 - 1}$$

where $\hat{L}_1 = L_1 + \Delta L_1$ reprents error in reconstructing L_1.

$$\begin{aligned} \therefore \hat{Y_2} &= \frac{j\omega c_0 + Y_1(\omega^2 L_1 c_0 + \omega^2 \Delta L_1 c_0 - 1)}{j\omega L_1 Y_1 - 1 + j\omega \Delta L_1 Y_1} \\ &= \frac{j\omega c_0 + Y_1(\omega^2 L_1 c_0 - 1) + Y_1 \omega^2 \Delta L_1 c_0}{(j\omega L_1 Y_1 - 1) + j\omega \Delta L_1 Y_1} \\ &= \frac{j\omega c_0 + Y_1(\omega^2 L_1 c_0 - 1)}{(j\omega L_1 Y_1 - 1) + j\omega \Delta L_1 Y_1} + \frac{Y_1 \omega^2 \Delta L_1 c_0}{(j\omega L_1 Y_1 - 1) + j\omega \Delta L_1 Y_1} \end{aligned}$$

Substituting the expression for Y_1 from equation (3.14) we have

$$\begin{aligned}
\hat{Y}_2 &= \frac{j\omega c_0 + \left(\frac{j\omega c_0}{1-\omega^2 L_1 c_0 - D_2^{-1}}\right)(\omega^2(L_1+\Delta L_1)c_0 - 1)}{j\omega(L_1+\Delta L_1)\left(\frac{j\omega c_0}{1-\omega^2 L_1 c_0 - D_2^{-1}}\right) - 1} \\
&= \frac{j\omega c_0(1-\omega^2 L_1 c_0) - j\omega c_0 D_2^{-1} + j\omega c_0(\omega^2(L_1+\Delta L_1)c_0 - 1)}{-\omega^2(L_1+\Delta L_1)c_0 - (1-\omega^2 L_1 c_0 - D_2^{-1})} \\
&= \frac{-j\omega c_0 D_2^{-1} + j\omega c_0(\omega^2(\Delta L_1)c_0)}{-\omega^2(\Delta L_1)c_0 - 1 + D_2^{-1}} \\
&= \underbrace{\frac{-j\omega c_0 D_2^{-1}}{-\omega^2(\Delta L_1)c_0 - 1 + D_2^{-1}}}_{A} + \underbrace{\frac{j\omega c_0(\omega^2(\Delta L_1)c_0)}{-\omega^2(\Delta L_1)c_0 - 1 + D_2^{-1}}}_{B}
\end{aligned}$$

where $D_2 = 2 - \omega^2 L_2 c_0 - \frac{1}{D_3}$.

$$\begin{aligned}
A &= \frac{-j\omega c_0 D_2^{-1}}{-\omega^2(\Delta L_1)c_0 - 1 + D_2^{-1}} \\
&= \frac{j\omega c_0}{(2-\omega^2 L_2 c_0 - D_3^{-1}) + \omega^2 \Delta L_1 c_0 D_2 - 1} \\
&= \frac{j\omega c_0}{(1-\omega^2 L_2 c_0 - D_3^{-1})(1 + \frac{\omega^2 \Delta L_1 c_0 D_2}{(1-\omega^2 L_2 c_0 - D_3^{-1})})} \\
&= \frac{Y_2}{1 + \frac{\omega^2 \Delta L_1 c_0 D_2}{(1-\omega^2 L_2 c_0 - D_3^{-1})}} \\
&= \frac{Y_2}{1 - \Delta L_1 j\omega c_0 D_2 Y_2}
\end{aligned}$$

Hence for small ω, A becomes

$$A \approx Y_2\,(1 + j\omega \Delta L_1 Y_2 D_2)$$

For large ω

$$A \approx \frac{-1}{j\omega D_2 \Delta L_1}$$

Similarly B is given by

$$B = \frac{j\omega c_0(\omega^2 \Delta L_1 c_0)}{-\omega^2(\Delta L_1)c_0 - 1 + D_2^{-1}}$$

Hence for large ω, we have

$$\begin{aligned}
B &\approx \frac{-j\omega c_0(\omega^2 \Delta L_1 c_0)}{1 + \omega^2(\Delta L_1)c_0} \\
&\approx -j\omega c_0
\end{aligned}$$

While for small ω, we have

$$\begin{aligned} B &= \frac{-j\omega c_0(\omega^2 \Delta L_1 c_0 D_2)}{\omega^2(\Delta L_1)c_0 D_2 + D_2 - 1} \\ &= \frac{-j\omega c_0(\omega^2 \Delta L_1 c_0 D_2)}{1 - \omega^2 L_2 c_0 - D_3^{-1} + \omega^2(\Delta L_1)c_0 D_2} \\ &= \frac{-j\omega c_0(\omega^2 \Delta L_1 c_0 D_2)}{(1 - \omega^2 L_2 c_0 - D_3^{-1})\left(1 + \frac{\omega^2(\Delta L_1)c_0 D_2}{(1-\omega^2 L_2 c_0 - D_3^{-1})}\right)} \\ &= \frac{-\omega^2 c_0 D_2 Y_2 \Delta L_1}{1 - j\omega Y_2 D_2 \Delta L_1} \\ &\approx -\omega^2 \Delta L_1 c_0 D_2 Y_2 \end{aligned}$$

for large ω

$$\therefore \hat{Y}_2 = \frac{-1}{j\omega D_2 \Delta L_1} - j\omega c_0 \tag{3.26}$$

for small ω

$$\hat{Y}_2 = Y_2 + j\omega \Delta L_1 Y_2^2 D_2 - \omega^2 c_0 D_2 Y_2 \Delta L_1 \tag{3.27}$$

This seems to suggest that the error in imaginary part of Y grows like $O(\omega)$.

3.5 Signal to Noise Ratio

To model noise, a resistor is connected in series with the inductor. Here we define some notion of Signal to Noise ratio (SNR) as a function of resistor value. In the case of one section, we define the admittance without resistance as

$$Y(\omega) = \frac{1}{j\omega L + \frac{1}{j\omega c_0}},$$

and that with resistance as

$$\begin{aligned}
\hat{Y}(\omega) &= \frac{1}{j\omega L + R + \frac{1}{j\omega c_0}} \\
&= \frac{1}{\left(j\omega L + \frac{1}{j\omega c_0}\right)\left(1 + R\frac{1}{\left(j\omega L + \frac{1}{j\omega c_0}\right)}\right)} \\
&= \frac{Y}{1+RY} \\
&= Y(1 - RY + R^2Y^2 - \cdots) \\
&= Y - RY^2 + R^2Y^3 - \cdots \\
&= Y + \underbrace{N}_{noise} \\
N &= -RY^2 + R^2Y^3 - \cdots \\
&= -RY^2(1 - RY + R^2Y^2 - \cdots) \\
N(\omega) &= \frac{-RY^2}{1+RY}
\end{aligned} \tag{3.28}$$

Hence the SNR can be defined as

$$\begin{aligned}
SNR &= \frac{Y(\omega)}{N(\omega)} \\
&= -\frac{1+RY}{RY} \\
SNR &= -\left(1 + \frac{1}{RY}\right)
\end{aligned} \tag{3.29}$$

Thus with no noise, $R \to 0$ and hence the $SNR \to \infty$, while with large noise i.e. $R \to \infty$, $SNR \to 1$, meaning the signal cannot be distinguished from noise.

Similarly we define the SNR for the case when there is a ladder network with

more than one inductor.

$$
\begin{aligned}
(T - \omega^2 c_0 L + j\omega z c_0 e_n e_n^T + j\omega c_0 R)\hat{I}(\omega) &= V(\omega)e_1 \\
(I + (T - \omega^2 c_0 L + j\omega z c_0 e_n e_n^T)^{-1} j\omega c_0 R)\hat{I}(\omega) &= I(\omega) \\
\Rightarrow (I + (T - \omega^2 c_0 L + j\omega z c_0 e_n e_n^T)^{-1} j\omega c_0 R)^{-1} I(\omega) &= \hat{I}(\omega) \\
\Rightarrow (I - (T - \omega^2 c_0 L + j\omega z c_0 e_n e_n^T)^{-1} j\omega c_0 R) I(\omega) &\approx \hat{I}(\omega) \\
\Rightarrow I(\omega) - \underbrace{(T - \omega^2 c_0 L + j\omega z c_0 e_n e_n^T)^{-1} j\omega c_0 R I(\omega)}_{noise} &= \hat{I}(\omega)
\end{aligned}
$$

$$
\therefore N(\omega) = (T - \omega^2 c_0 L + j\omega z c_0 e_n e_n^T)^{-1} j\omega c_0 R I(\omega) \tag{3.30}
$$

Note that all the currents come into play

$$
\begin{aligned}
\therefore ||N(\omega)|| &= ||(T - \omega^2 c_0 L + j\omega z c_0 e_n e_n^T)^{-1} j\omega c_0 R I(\omega)|| \\
&\leq ||(T - \omega^2 c_0 L + j\omega z c_0 e_n e_n^T)^{-1} j\omega c_0 R|| ||I(\omega)|| \\
\Rightarrow \frac{||N(\omega)||}{||I(\omega)||} &\leq |\omega c_0| ||(T - \omega^2 c_0 L + j\omega z c_0 e_n e_n^T)^{-1} R|| \\
&\leq |\omega c_0| ||(T - \omega^2 c_0 L + j\omega z c_0 e_n e_n^T)^{-1}|| ||R|| \\
\Rightarrow \frac{||I(\omega)||}{||N(\omega)||} &\geq \frac{1}{|\omega c_0| ||(T - \omega^2 c_0 L + j\omega z c_0 e_n e_n^T)^{-1}|| R_{max}} \\
&= \frac{\sigma_{min}}{|\omega c_0| R_{max}}
\end{aligned}
$$

where $\sigma_{min} = \min \sigma(T - \omega^2 c_0 L + j\omega z c_0 e_n e_n^T)$

The above equation gives a feel for the SNR, whenever there are resistance present in the circuit.

3.6 Implementation Details

All the simulations are carried out in MATLAB [21]. The whole process can be broken down into two parts:

1. *Forward problem:* Given the parameters inductance vector, L, capacitance, c_0, negative impedance, z, we solve the linear system of equations (3.4), to obtain the admittance $Y_1(\omega)$, for different frequencies, ω_k.

2. *Inverse problem:* The inverse problem can be divided into two parts:

   - Numerical integration to evaluate L_1 (equation (3.18)).
   - Evaluate $Y_2(\omega)$ using the layer peeling equation (3.21).

   The layer peeling equation is straight forward to implement. For the numerical integration, we use an adaptive quadrature rule. Say we wish to integrate from $[a, b]$.

   - First we evaluate the integral, Q, using $N_{\max}$ points in the interval $[a, b]$.
   - Next we evaluate the integral Q_l in the region $[a, c]$, and Q_r in the region $[c, b]$, where c is the midpoint of $[a, b]$. $N_{\max}$ points are used in each of the intervals.
   - If $|Q - (Q_l + Q_r)|$ is less than some prescribed tolerance, we stop, else we go back to the first step with two intervals now, i.e. we repeat the procedure for $[a, c]$ and $[c, b]$.

   The integral for each region is evaluated using trapezoidal rule. A thing to note is that due to the nature of the admittacne function, MATLAB's adaptive Gauss-Lobatto quadrature rule [24] didn't converge to the right answer.

3.7 Results

In this section the performance of the inverse algorithm is demonstrated for different profiles for L. The scattered data, $Y_1(\omega)$ is shown for each different profile. The admittance shows N peaks, where N is the number of inductors. And as pointed in equation (3.13), the current tends to become rough, as a result the quadrature rules for the integration don't perform well. This is one of the reasons for the poor performance of the algorithm.

3.7.1 Quantized L's

Here we consider the profile such that

$$L_k = \begin{cases} 5 & \forall k \neq N_0 \\ 6 & \text{for some } k = N_0 \end{cases}$$

The admittance is shown in figure (3.10). In this case, after each integration, a hard decoding decision is made. If the value of the integral suggest L_k less than 5.5, then L_k is set to 5, else it is set to 6. All the values of L were recovered successfully.

Now instead of only one inductor of different value, a bunch of inductors take the value 6. The inductor profile is shown in figure(3.11), and the corresponding admittance profile is shown in figure(3.12). Again, all the L's were recovered successfully

Next we take a continuous function and quantize it to two levels. The inductor profile is shown in figure (3.13). Except for the last inductor, all the inductors were recovered correctly. For this case, adaptive quadrature rule was used.

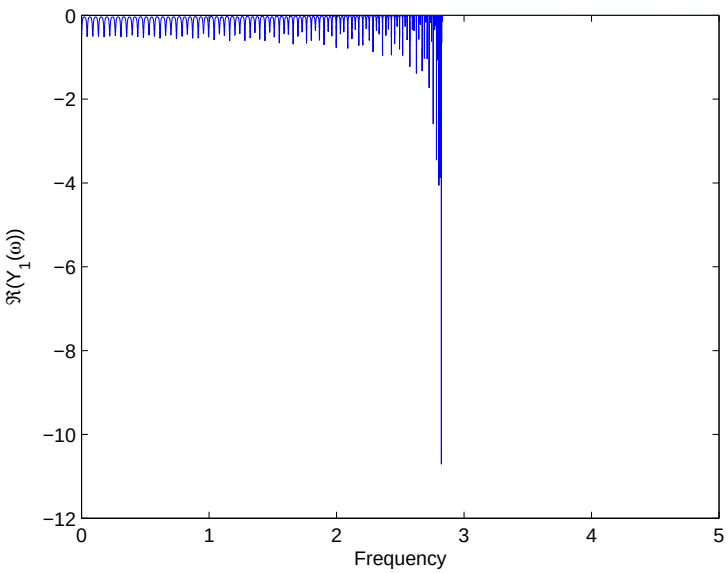

Figure 3.10. $\Re(Y_1(\omega))$ vs frequency: N = 100, $L_k = 5, \forall k \neq 70, L_{70} = 6$

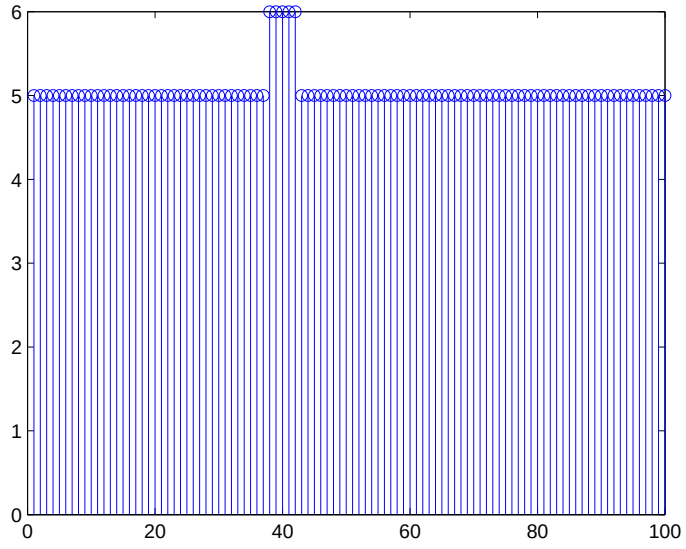

Figure 3.11. Inductor profile

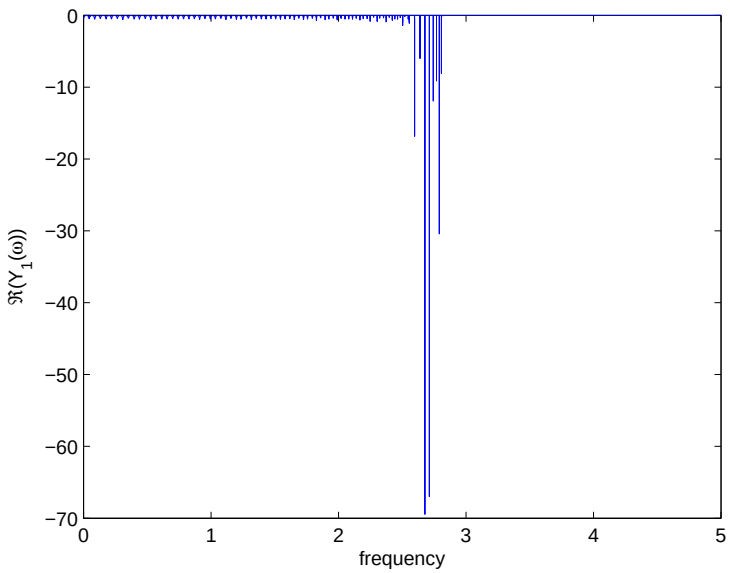

Figure 3.12. $\Re(Y_1(\omega))$ vs frequency for inductor profile shown in figure(3.11)

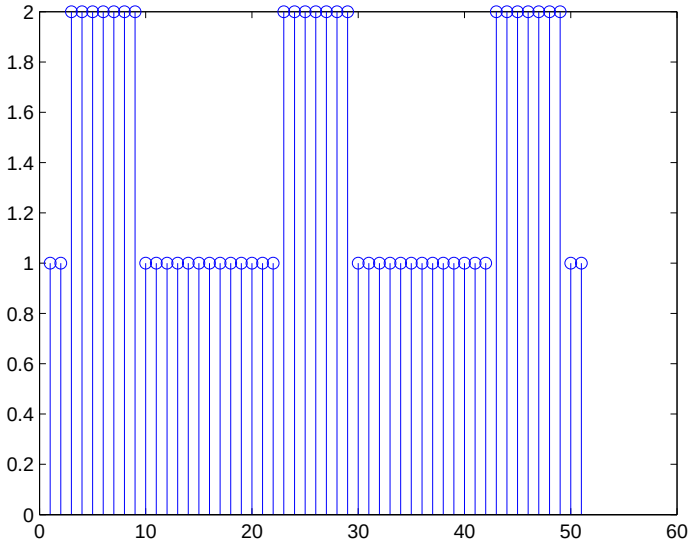

Figure 3.13. Inductor profile

3.7.2 Continuous L

Here we sample a continuous function to obtain the values of L.

$$\begin{aligned} L_k &= 1 + q(x_k) \\ \text{where } q(x_k) &= .01 \sin^3(\pi x_k) \\ & \quad \text{and } x_k \text{ are equidistant samples in } [0, 1] \end{aligned}$$

The admittance profile is shown in figure (3.14). The recovered profile is shown

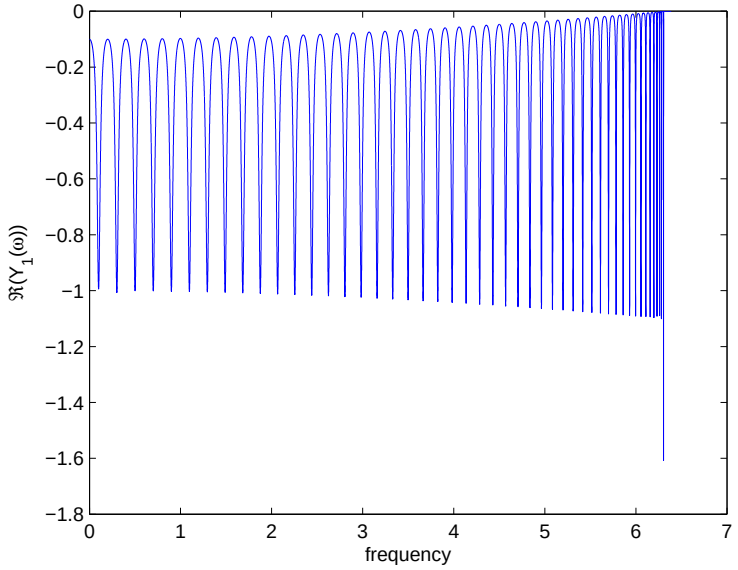

Figure 3.14. $\Re(Y_1(\omega))$ vs frequency: $N = 100$,$L_k = .01 \sin^3(\pi x_k)$

in figure (3.15). Although the errors towards the later part are huge, there is no exponential blow-up as in the existing algorithms in the literature [8]. The zoomed version of the recovered profile is shown in figure (3.16).

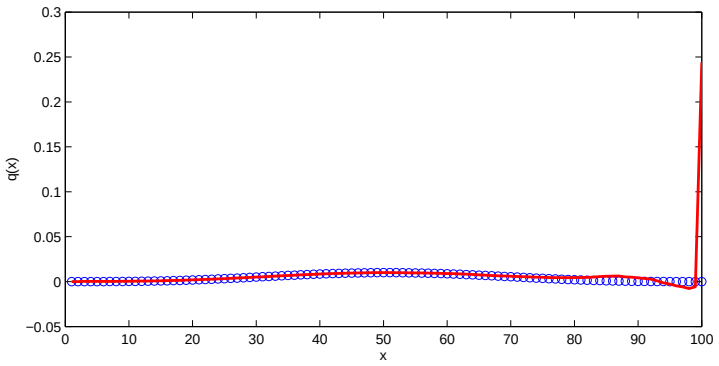

Figure 3.15. Recovered $q(x)$ (in red): $||q - \hat{q}||_2 = .2448, ||q - \hat{q}||_\infty = .2440$

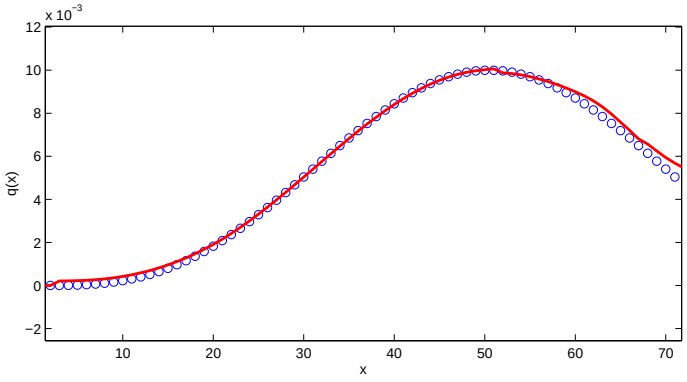

Figure 3.16. Recovered $q(x)$ (in red) is zoomed for the first 50 sensors:$||q - \hat{q}||_2 = 8.7225e - 004$, $||q - \hat{q}||_\infty = 2.9103e - 004$

3.7.3 Error in Recovering the last inductor, L_n

In most of the experiments, the last inductor L_n, is never recovered faithfully. This happens because the admittance for just one loop does not decay as fast as it does for the other admittances. Figure (3.17) shows the circuit when the last loop has been reached.

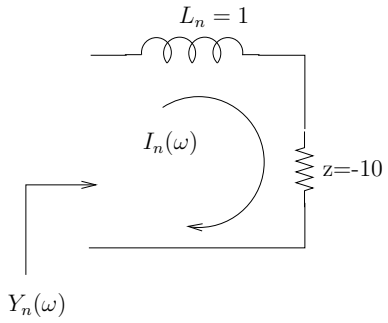

Figure 3.17. Circuit corresponding to the last loop.

Figure (3.18) shows the actual admittance profile, $Y(\omega)$, for the circuit shown in figure (3.17). Note that even for the bandwidth as high as 50, the admittance

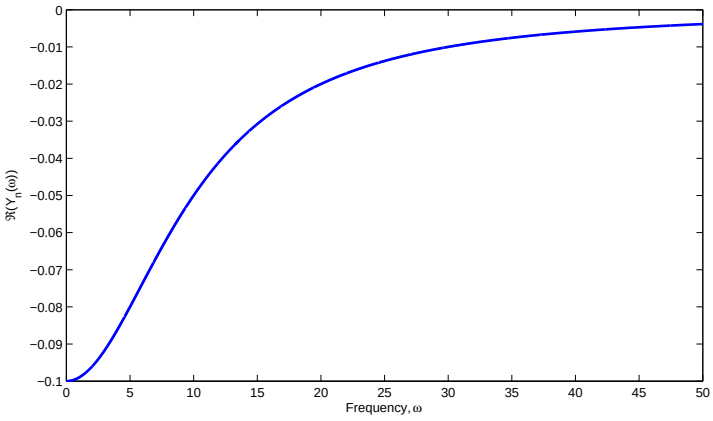

Figure 3.18. Admittance $Y(\omega)$ for the last loop.

has not decayed completely, resulting in a finite error in computing the integral. There are a couple of ways to remedy the situation:

1. Since L_n corresponds to the boundary inductor at the other end, we can assume it is known as a part of the boundary condition.

2. We can conduct a similar set of experiments from the other side, and recover L_n faithfully.

3.7.4 Three section analysis

In this section we analyze the LC ladder circuit with three sections. The inductance vector is given as

$$L = [1, 0.9990, 1]$$

- Let Y_1 represent the admittance function of the three section network.
- Let Y_2 represent the admittance function of the two section network, with $L = [0.9990, 1]$.
- A rational function expression for Y_2 is evaluated, and poles found using MATLAB's root function. The poles are

$$\begin{aligned} p_1 &= 0.0000 - 9.0121i \\ p_2 &= 3.2959 - 0.4939i \\ p_3 &= -3.2959 - 0.4939i \end{aligned}$$

- Let $\hat{Y}_2$ represent the admittance function for two section LC ladder networks, obtained after peeling Y_1 using inexact values L_1. Here the erroneous L_1 is given by $\hat{L}_1 = L_1 + \delta$, where $\delta = 10^{-7}$. A rational function for

$\hat{Y}_2$ is found and the poles calculated.

$$\begin{aligned} p_1 &= -3.6380e-012-1.0000e+004i \\ p_2 &= -3.2401e-012+1.0000e+004i \\ p_3 &= 0.0000-9.0121i \\ p_4 &= 3.2960-0.4939i \\ p_5 &= -3.2960-0.4939i \end{aligned}$$

A pole, p_2 thus moves to the upper half plane, which makes the integration formula erroneous. The recovered L's are

$$\hat{L} = [1.0000, 0.9992, 1.6560]$$

Figures (3.19), and (3.20) represents the errors (due to peeling formula) in real and imaginary part of $Y2$, respectively. This is the case when peeling is done using exact values of L's.

Figures (3.21), and (3.22) represents the errors (due to peeling formula) in real and imaginary part of $Y2$, respectively. This is the case when peeling is done using inexact values of L's.

Thus the sources of errors are:

1. The movement of poles in the upper half plane.

2. The $O(\omega)$ error in the imaginary part, for each stage of layer peeling (equation 3.27). To begin with, the real part of $Y(\omega)$ is of $O(\omega^{-(4n-2)})$, but as the peeling progresses, it gets multiplied by the error in the imaginary part. This seems to affect the recovery formula around the half way mark. The error in peeling around the half way mark is apparent for the ten section network.

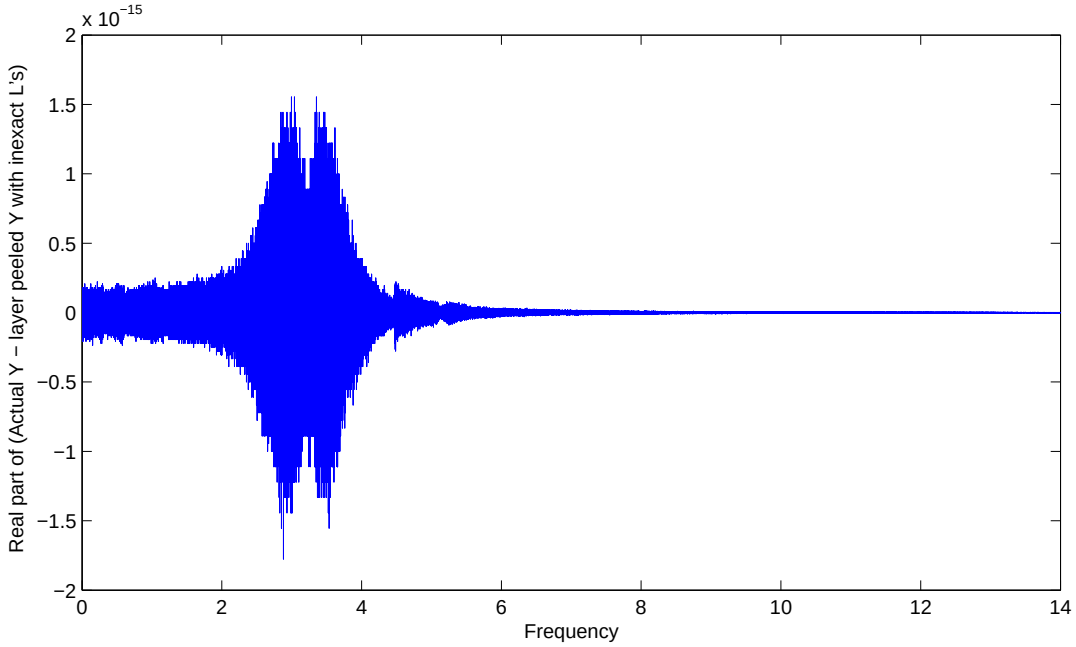

Figure 3.19. Error in $\Re(Y(\omega))$, when exact peeling formula is used. This error is calculated for Y_2, i.e. when we have peeled the first section.

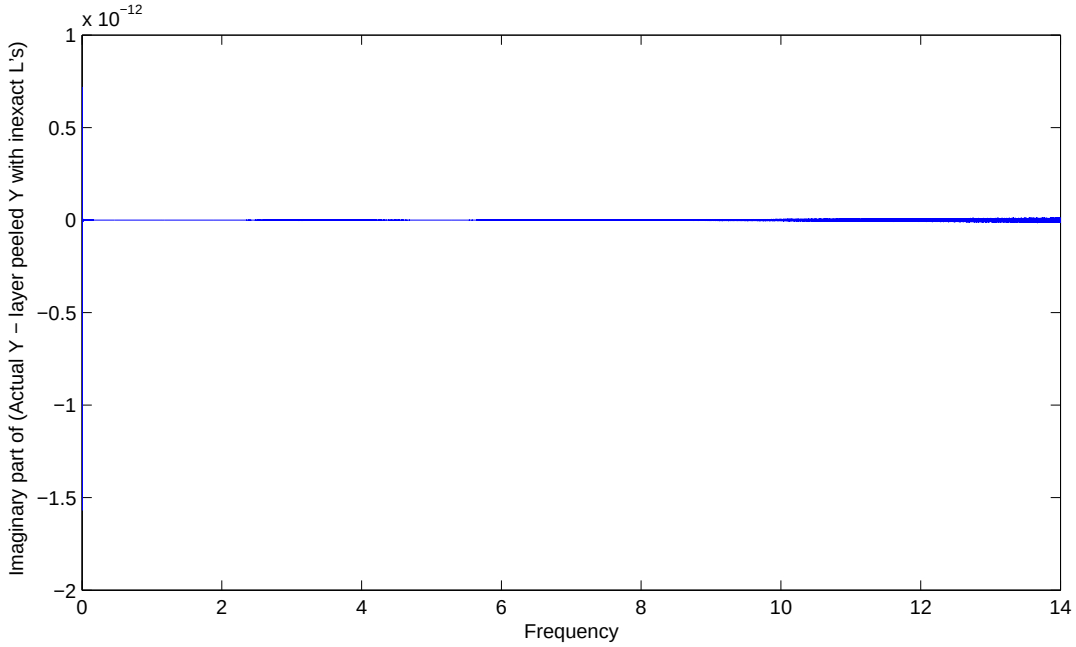

Figure 3.20. Error in $\Im(Y(\omega))$, when exact peeling formula is used. This error is calculated for Y_2, i.e. when we have peeled the first section.

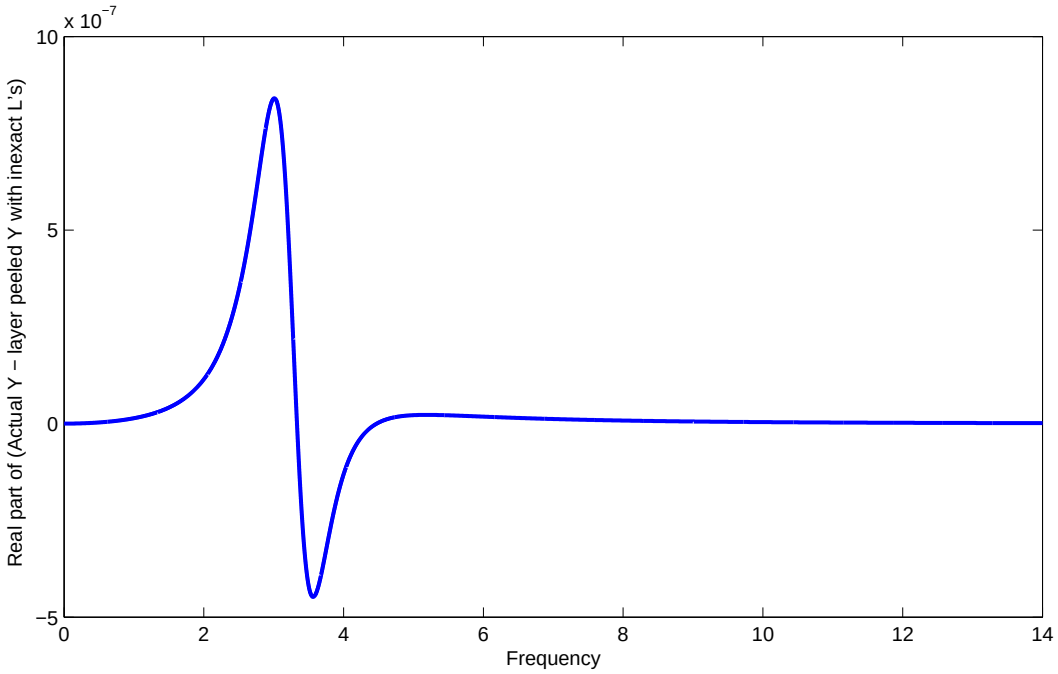

Figure 3.21. Error in $\Re(Y(\omega))$, when inexact peeling formula is used. This error is calculated for Y_2, i.e. when we have peeled the first section.

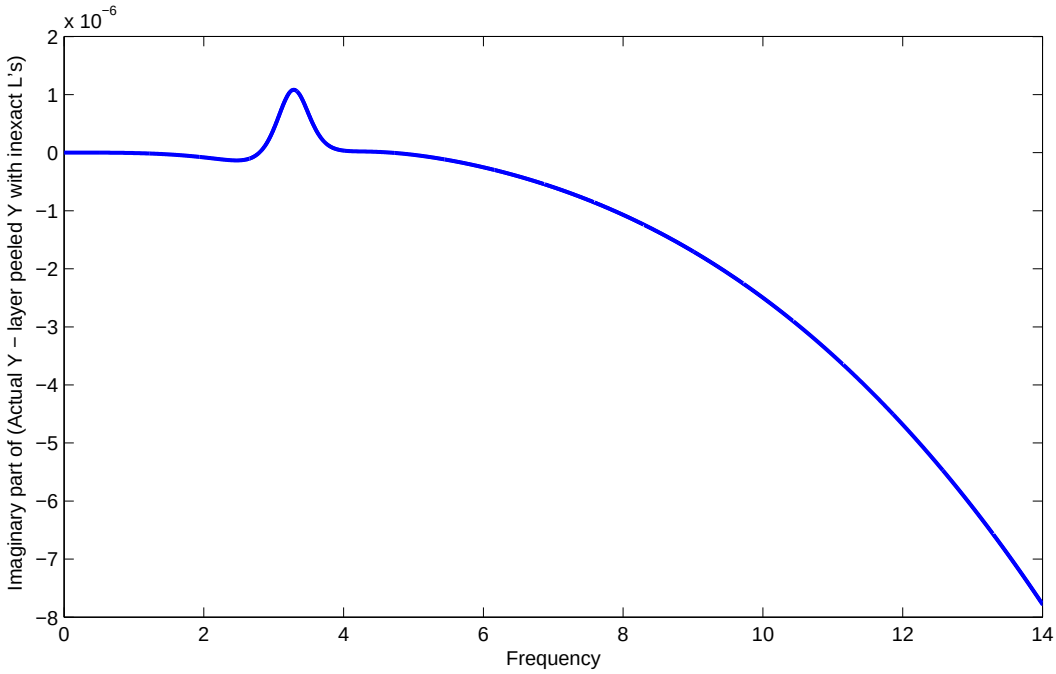

Figure 3.22. Error in $\Im(Y(\omega))$, when inexact peeling formula is used. This error is calculated for Y_2, i.e. when we have peeled the first section.

3.7.5 Ten section results

In this section, results for an LC ladder network with 10 L's is shown. The L's are chosen using a random walk, with step size of .001, i.e.

$$\begin{aligned} L_k &= L_{k-1} \pm .001 \\ L_1 &= 1 \end{aligned}$$

The inverse algorithm does not know about the specific nature of L's. Figure (3.23) shows a plot of the logarithm of the error. The error is calculated by first calculating vector q as

$$q_k = L_k - L_{k-1}, \text{ and } q_0 = 0$$

and similarly $\hat{q}$ is calculated using recovered values of L.

$$\hat{q}_k = \hat{L}_k - \hat{L}_{k-1}, \text{ and } q_0 = \hat{L}_0$$

and the error is

$$e = log_{10}|q - \hat{q}|$$

Figures (3.24), and (3.25) represents the errors (due to peeling formula) in real and imaginary part of $Y4$, respectively. This is the case when peeling is done using exact values of L's.

Figures (3.26), and (3.27) represents the errors (due to peeling formula) in real and imaginary part of $Y4$, respectively. This is the case when peeling is done using inexact values of L's.

Figures (3.28), and (3.29) represents the errors (due to peeling formula) in real and imaginary part of $Y5$, respectively. This is the case when peeling is done using exact values of L's.

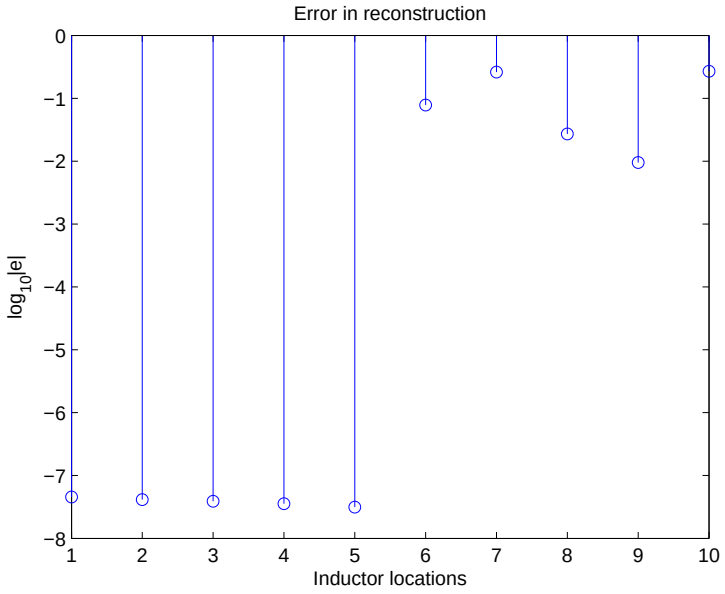

Figure 3.23. $log_{10}|q - \hat{q}|$ vs k: $N = 10$, and L's are given by random walk

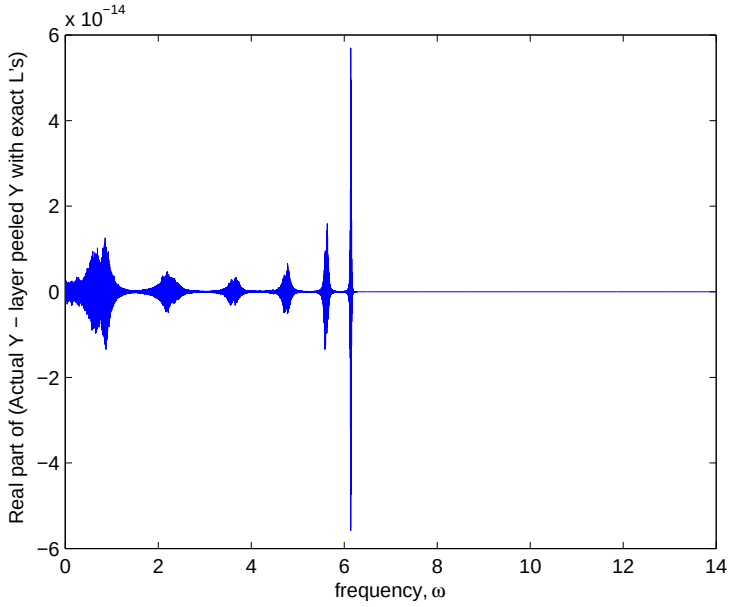

Figure 3.24. Error in $\Re(Y(\omega))$, when exact peeling formula is used. This error is calculated for Y_4, i.e. when we have peeled three sections off.

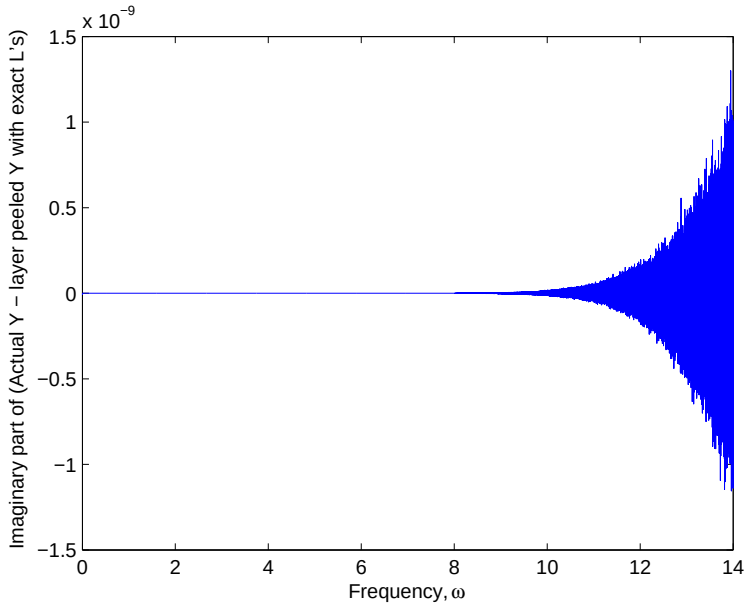

Figure 3.25. Error in $\Im(Y(\omega))$, when exact peeling formula is used. This error is calculated for Y_4, i.e. when we have peeled three sections off.

Figures (3.30), and (3.31) represents the errors (due to peeling formula) in real and imaginary part of $Y5$, respectively. This is the case when peeling is done using inexact values of L's.

Figures (3.32), and (3.33) represents the errors (due to peeling formula) in real and imaginary part of $Y6$, respectively. This is the case when peeling is done using exact values of L's.

Figures (3.34), and (3.35) represents the errors (due to peeling formula) in real and imaginary part of $Y6$, respectively. This is the case when peeling is done using inexact values of L's.

We can see from the above plots that the error at the half way mark is a result of the peeling formula.

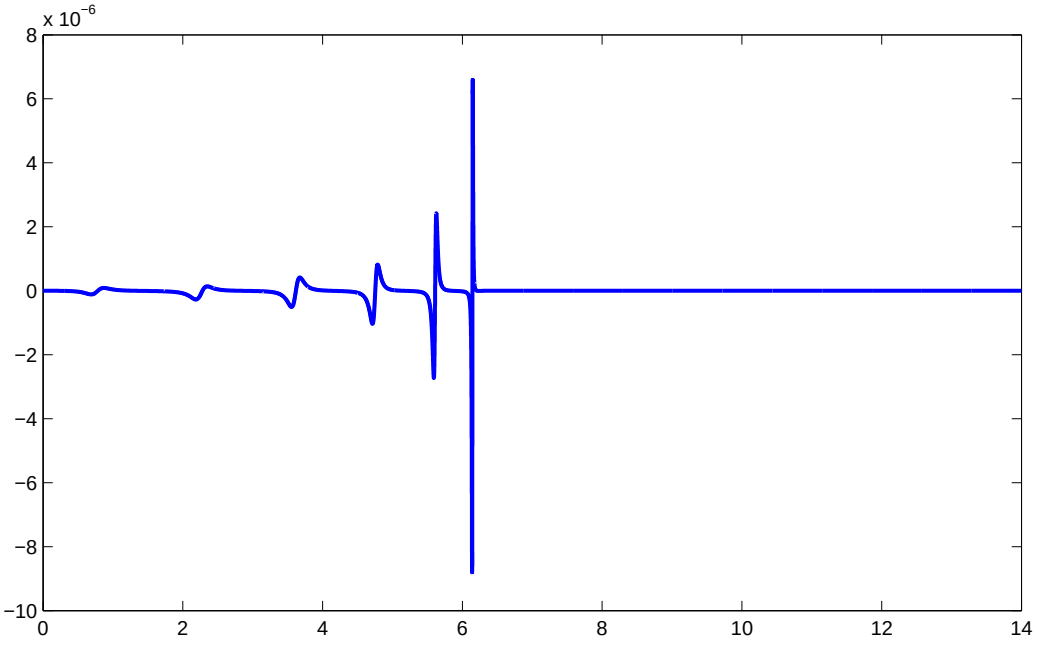

Figure 3.26. Error in $\Re(Y(\omega))$, when inexact peeling formula is used. This error is calculated for Y_4, i.e. when we have peeled three sections off.

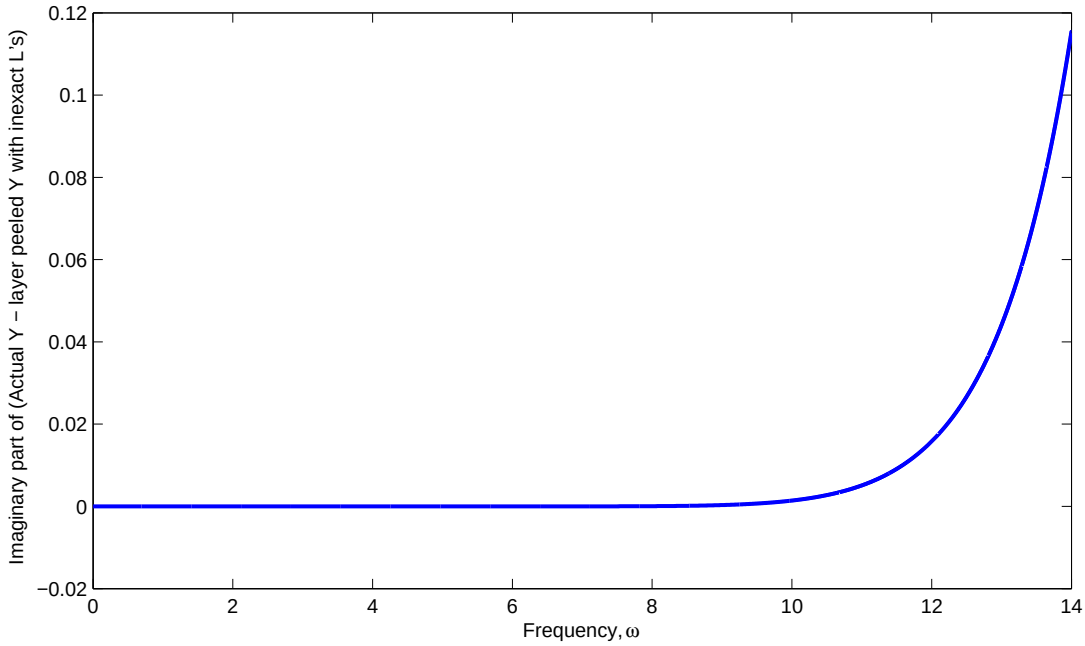

Figure 3.27. Error in $\Im(Y(\omega))$, when inexact peeling formula is used. This error is calculated for Y_4, i.e. when we have peeled three sections off.

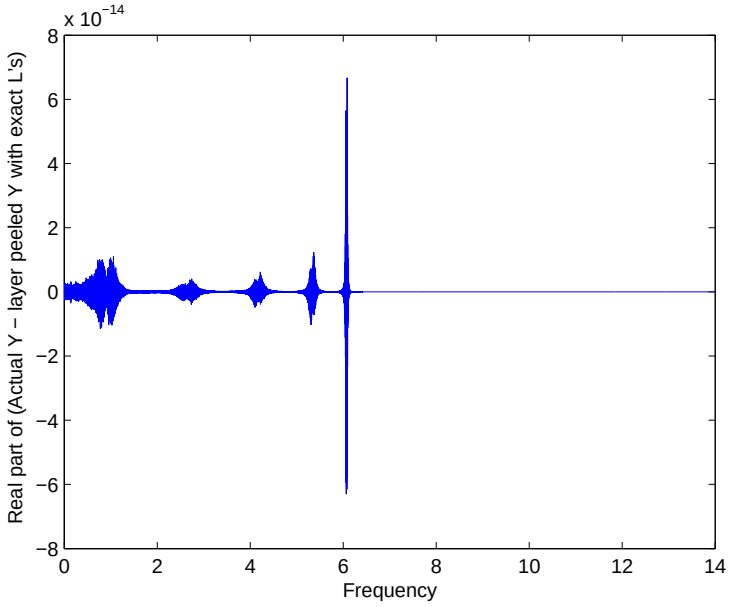

Figure 3.28. Error in $\Re(Y(\omega))$, when exact peeling formula is used. This error is calculated for Y_5, i.e. when we have peeled four sections off.

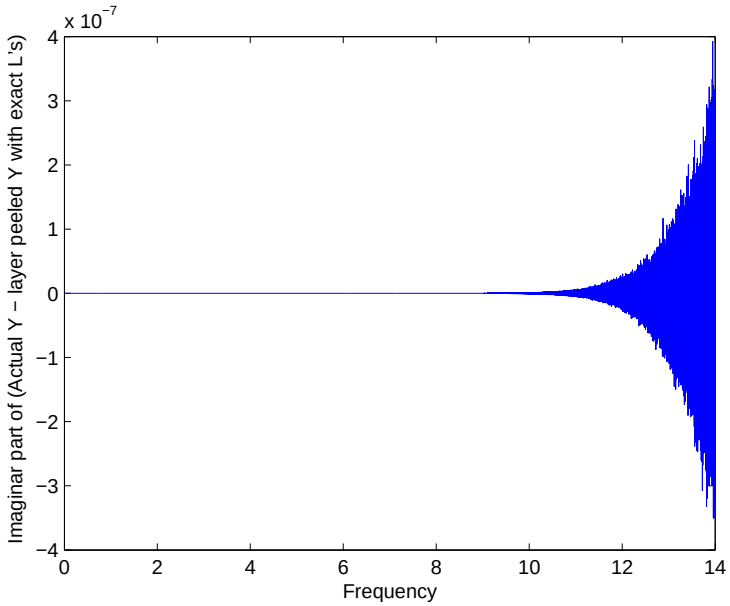

Figure 3.29. Error in $\Im(Y(\omega))$, when exact peeling formula is used. This error is calculated for Y_5, i.e. when we have peeled four sections off.

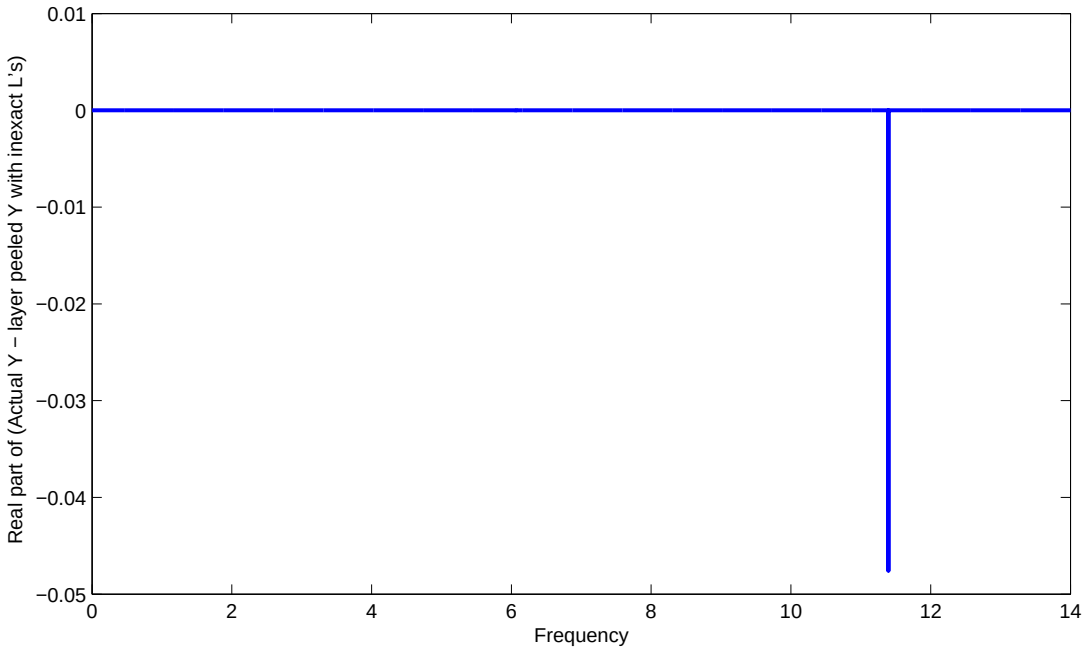

Figure 3.30. Error in $\Re(Y(\omega))$, when inexact peeling formula is used. This error is calculated for Y_5, i.e. when we have peeled four sections off.

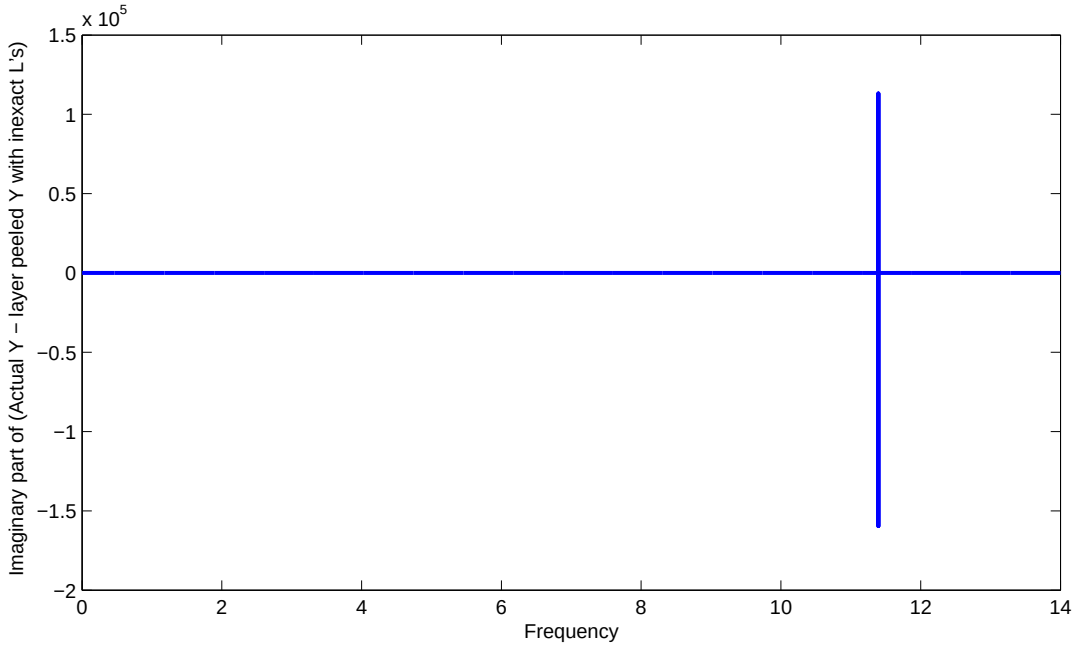

Figure 3.31. Error in $\Im(Y(\omega))$, when inexact peeling formula is used. This error is calculated for Y_5, i.e. when we have peeled four sections off.

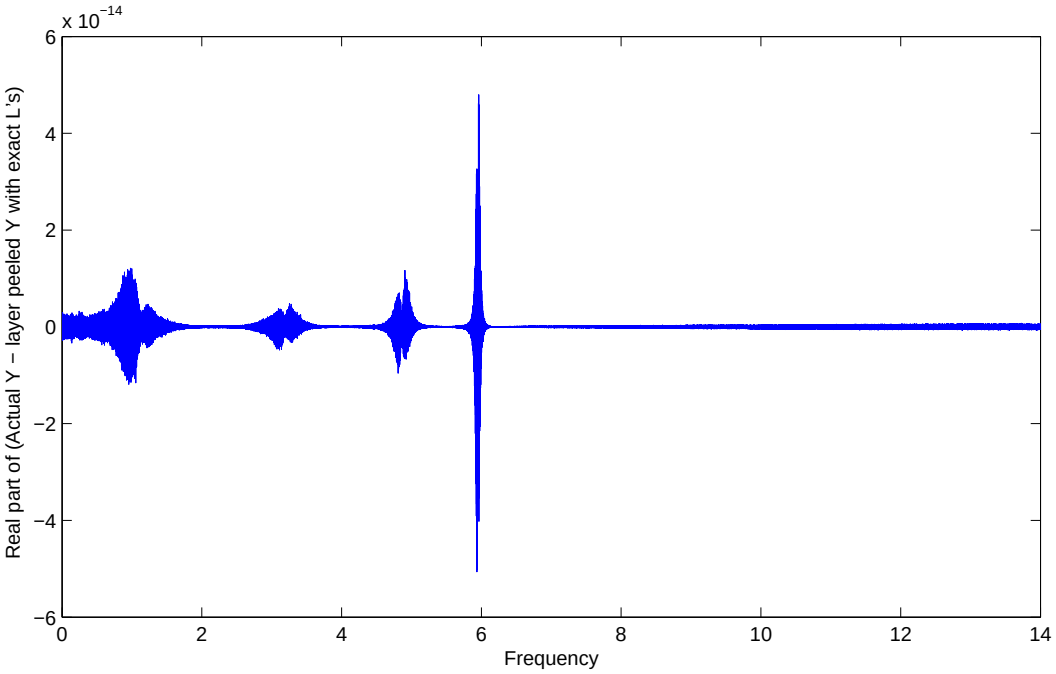

Figure 3.32. Error in $\Re(Y(\omega))$, when exact peeling formula is used. This error is calculated for Y_6, i.e. when we have peeled five sections off.

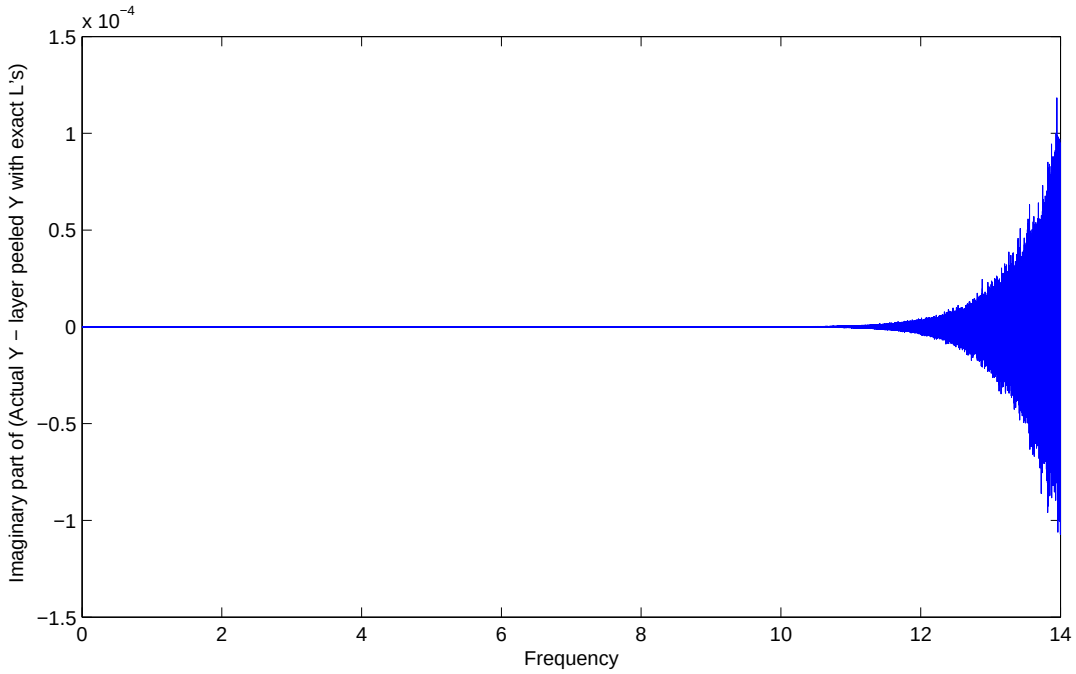

Figure 3.33. Error in $\Im(Y(\omega))$, when exact peeling formula is used. This error is calculated for Y_6, i.e. when we have peeled five sections off.

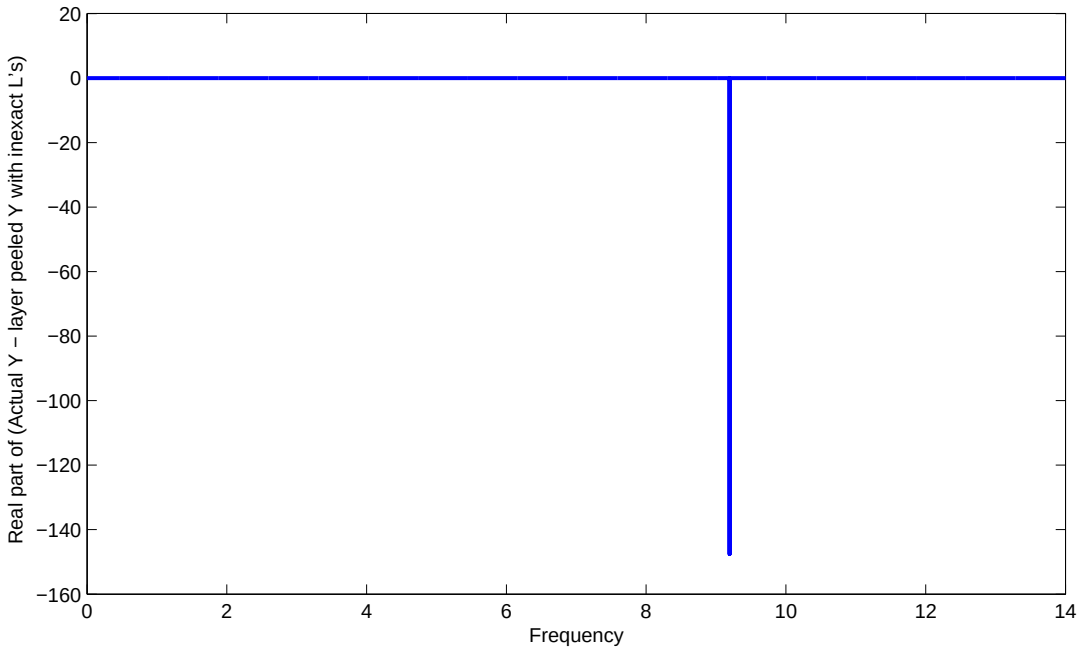

Figure 3.34. Error in $\Re(Y(\omega))$, when inexact peeling formula is used. This error is calculated for Y_6, i.e. when we have peeled five sections off.

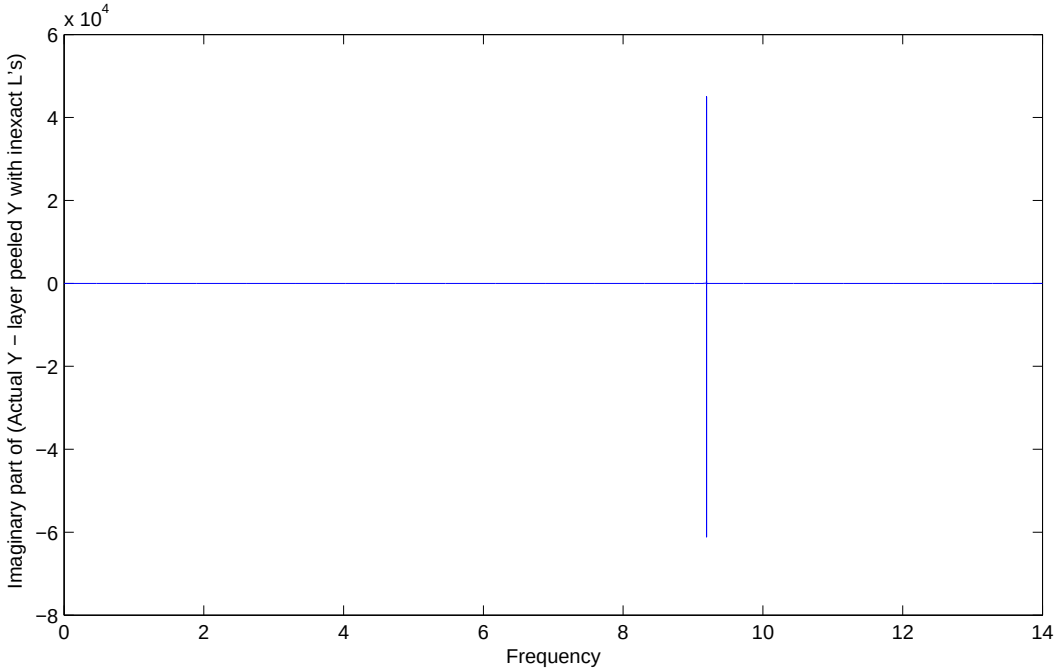

Figure 3.35. Error in $\Im(Y(\omega))$, when inexact peeling formula is used. This error is calculated for Y_6, i.e. when we have peeled five sections off.

3.8 Comments

- An extension of Chen-Rokhlin algorithm in the discrete domain is provided. This analysis helps in actual implementation of the stable inverse scattering algorithm.

- Of all the results, the one with quantized values of L seem to work the best. In part this is because we use the extra information while decoding. This suggests a need for an extra piece of information to control the error.

- Recovery after the half way mark is always in error. One way to remedy the situation would be to conduct experiments from the other end, and peel the network from the right.

- Although, the poles are proven to be non-real, the impedance profile is rough for non-constant L's. This causes problems with the integration using quadrature formula. Also, errors in reconstruction, causes the poles to move in the upper half plane.

Chapter 4

Other Approaches

In this chapter, we consider two different approaches:

- It is shown that the LC ladder network synthesis using admittance function, is equivalent to generating a symmetric tridiagonal matrix with non-zero upper diagonal, from its eigenvalues and the eigenvalues of the matrix with first row and column removed.

- Inverse Scattering algorithm developed by Sylvester *et. al.*. The problem setup is different from the Chen-Rokhlin (CR) algorithm. The problem is defined on a semi infinite line, i.e. unlike CR algorithm, they don't need infinite sections at both ends. Also, the authors have a single nonlinear differential equation, which they use to both recover the unknown, and "peel" the network.

4.1 LC ladder network and inverse spectral problem

We redefine the circuit synthesis problem. Figure 4.1 shows an LC ladder network. Here L's are the unknown inductance value to be determined. c_0 is the known capacitance, $V(\omega)$ is a known source voltage, $I_k(\omega)$ is the current in the k-th loop, and $Y_1(\omega)$ is the input admittance. Once again the problem is to

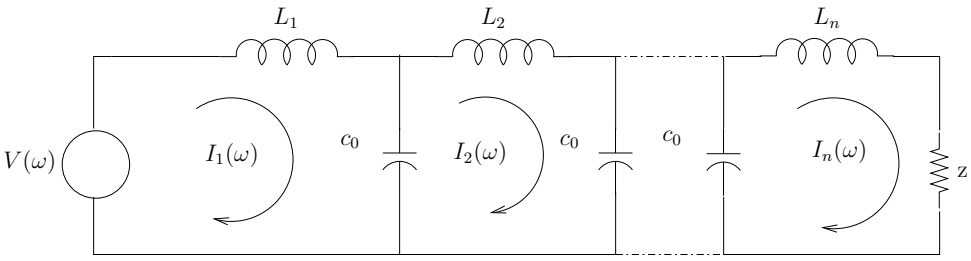

Figure 4.1. LC Ladder Network

observe $Y_1(\omega)$ at different frequencies ω and determine the unknown L's. The only difference between this problem and the circuit synthesis problem considered in the previous chapter, is the absence of the negative impedance, z. Writing the Kirchhoff's voltage equation for each loop (as done in chapter 3), we get the matrix vector equation:

$$(T - \omega^2 L c_0) I(\omega) = j\omega c_0 \hat{V}(\omega) e_1 \tag{4.1}$$

where T is the known symmetric tridiagonal matrix, $I(\omega)$ is the loop current vector, V is the source voltage, c_0 is the known capacitance and L is the diagonal matrix with the unknown inductance values (Refer chapter 3 for the exact structure of the matrix). The goal of this section is to covert the above problem to a spectral problem:

$$(A - sI)x(s) = y(s)e_1 \tag{4.2}$$

where A is the symmetric tridiagonal matrix with unknown entries. Given the equation for currents in loops,

$$\begin{aligned}(T-\omega^2 Lc_0)\hat{I}(\omega) &= j\omega c_0 \hat{V}(\omega)e_1 \\ (\frac{1}{c_0}L^{\frac{1}{2}}TL^{\frac{1}{2}}-\omega^2 I)(L^{\frac{1}{2}}\hat{I}(\omega)) &= j\omega c_0 \hat{V}(\omega)L^{\frac{1}{2}}e_1 \\ (A-\omega^2 I)x &= ye_1\end{aligned}$$

The matrix A containing the unknowns is given by

$$A = \begin{pmatrix} L_1 & -\sqrt{L_1L_2} & & & & \\ -\sqrt{L_1L_2} & 2L_2 & -\sqrt{L_2L_3} & & & \\ & \ddots & \ddots & \ddots & & \\ & & & & -\sqrt{L_{N-1}L_N} & \\ & & & -\sqrt{L_{N-1}L_N} & L_N & \end{pmatrix} \tag{4.3}$$

And the admittance function is given by

$$\begin{aligned}(A-\omega^2 I)^{-1}_{11} = \frac{x_1}{y} &= \frac{L_1^{\frac{1}{2}}\hat{I}_1(\omega)}{j\omega c_0 \hat{V}(\omega)L_1^{\frac{1}{2}}} \\ \therefore \frac{\hat{I}_1(\omega)}{\hat{V}(\omega)} &= j\omega c_0 (A-\omega^2 I)^{-1}_{11} \\ \Rightarrow \frac{\hat{I}_1(\omega)}{\hat{V}(\omega)} &= j\omega c_0 \frac{\det(\widehat{A-\omega^2 I})}{\det(A-\omega^2 I)}\end{aligned}$$

where $(\widehat{A-\omega^2 I})$ is the matrix $(A-\omega^2 I)$ with first row and column removed. The poles and zeros of the admittance function are basically the eigenvalues of A and $\hat{A}$ respectively. Hence, the inverse spectral problem can be stated as:

> ***Inverse Spectral Problem:*** *Observe the poles and zeros of the admittance profile, and obtain the values of L_k's from these observations.*

4.1.1 Existence of unique poles and zeros of the admittance function

If a pole or zero is repeated, one cannot recover that information by simply measuring them, and hence cannot generate the matrix. In this section we prove that poles and zeros of the admittance function arising due to matrix A in (4.3), are indeed unique [9].

Since eigenvalues of A correspond to the poles of the admittance function, we show that the matrix A has unique eigenvalues. Symmetric tridiagonal matrix with non-zero sub diagonals is also known as Jacobi matrix. Given A

$$A = \begin{pmatrix} a_1 & b_1 & & & \\ b_1 & a_2 & b_2 & & \\ & \ddots & \ddots & \ddots & \\ & & b_{n-2} & a_{n-1} & b_{n-1} \\ & & & b_{n-1} & a_n \end{pmatrix},$$

we can find a sequence of polynomials $\{\phi_i(\lambda)\}_{i=1}^{n}$ such that

$$\begin{pmatrix} a_1-\lambda & b_1 & & & \\ b_1 & a_2-\lambda & b_2 & & \\ & \ddots & \ddots & \ddots & \\ & & b_{n-2} & a_{n-1}-\lambda & b_{n-1} \\ & & & b_{n-1} & a_n-\lambda \end{pmatrix} \begin{pmatrix} \phi_1(\lambda) \\ \phi_2(\lambda) \\ \vdots \\ \phi_{n-1}(\lambda) \\ \phi_n(\lambda) \end{pmatrix} = \begin{pmatrix} 0 \\ 0 \\ \vdots \\ 0 \\ p(\lambda) \end{pmatrix}$$

such that $\phi(\lambda) = 1$. The $\phi_i(\lambda)$'s satisfy a recurrence relation

$$\begin{aligned} b_{j-1}\phi_{j-1}(\lambda) + (a_j - \lambda)\phi_j(\lambda) + b_j\phi_j(\lambda) \quad &= \quad 0 \text{ for } j = 2, \ldots, n-1 \\ \phi_0(\lambda) = 0 \quad \text{and} \quad \phi_1(\lambda) &= 1 \end{aligned}$$

The characteristic polynomial $p(\lambda)$ is then given by

$$b_{n-1}\phi_{n-1}(\lambda) + (a_n - \lambda)\phi_n(\lambda) = p(\lambda) \tag{4.4}$$

and the roots of $p(\lambda) = 0$ form the eigenvalues of the matrix A. Now if A has a repeated eigenvalue λ, then $A - \lambda I$ has rank deficiency of more than one. This implies that all $(n-1)$ principal minors of the matrix are zeros making $\phi_n(\lambda) = 0$. From equation (4.4), $\phi_{n-1}(\lambda) = 0$ and from the recurrence relation each $phi_j(\lambda) = 0$, leading to a contradiction. Hence, A cannot have a repeated eigenvalue which means the network has unique poles and zeros.

4.1.2 Circuit Synthesis from poles and zeros of the admittance

In this section, we show a way to generate the matrix A from its eigenvalues (poles of admittance), and the eigenvalues of A, with first row and column removed (zeros of admittance). Although the method described here is unstable, there are stable algorithms for such synthesis [25], [9].

Let A_n be the Jacobi matrix of order n, and A_i be the left principal sub matrix of order i, that is a sub matrix obtained by removing first $n-i$ rows and columns from A_n. Let

$$p_i(t) = \det(t - A_i) \text{ for } i = 1, \ldots, n$$

then $p_i(t)$ is a monic polynomial of degree i. Writing the recurrence relation for the determinants

$$\begin{aligned} p_i(t) &= (t - a_i)p_{i-1}(t) - b_{i-1}^2 p_{i-2}(t) \text{ for } i = 1, \ldots n \\ p_1(t) = 0 \qquad & p_0(t) = 1 \end{aligned}$$

Given $\{\lambda_i\}_{i=1}^n$ and $\{\mu_i\}_{i=1}^n$, such that $\lambda_i < \mu_i < \lambda_{i+1}$ for all i, we wish to construct A_n such that the recurrence relation holds, and λ_i and μ_i correspond to the poles and zeros of the admittance function, i.e.

$$\det(t - A_n) = p_n = \prod_{j=1}^{n}(t - \lambda_j) \tag{4.5}$$

$$\det(t - A_{n-1}) = p_{n-1} = \prod_{j=1}^{n-1}(t - \mu_j) \tag{4.6}$$

1. Given p_i and p_{i-1}, find a_i so that

   $$q(t) = p_i(t) - (t - a_i)p_{i-1}(t)$$

   is a polynomial of degree $(i - 2)$.

2. coefficient of t^{i-2} is $-b_{i-2}^2$.

3. $\frac{q(t)}{-b_{i-2}^2} = p_{i-2}$

4. Take p_{i-1} and p_{i-2} and go to step 1.

Although the algorithm of generating the matrix from the poles and zeros of the admittance function, is stable, the method of obtaining poles and zeros is highly unstable [23]. Hence we tried a method of generating the matrix without measuring the poles or zeros. The method is described next.

4.2 Matrix synthesis using scattered data

One of the methods we tried was to sample the admittance function at different frequencies (need not be the pole frequencies) and then reconstruct the admittance function through rational function interpolation. The instabilities

are inherent in the rational function interpolation algorithm and the "peeling" formula. To obtain the algorithm, we start with equation (4.2)

$$(A_n + sI)x(s) = y(s) \tag{4.7}$$

where, $A_n = \begin{pmatrix} a_n & b_n & & & \\ b_n & a_{n-1} & b_{n-1} & & \\ & \ddots & \ddots & \ddots & \\ & & b_3 & a_2 & b_2 \\ & & & b_2 & a_1 \end{pmatrix}, x(s) = \begin{pmatrix} X_n(s) \\ X_{n-1}(s) \\ \vdots \\ X_1(s) \end{pmatrix},$

$y(s) = \begin{pmatrix} Y_n(s) \\ 0 \\ \vdots \\ 0 \end{pmatrix}$

$$f(s) = \frac{Y_n(s)}{X_n(s)} = \frac{1}{(A^{-1})_{11}} = \frac{\det(A_n)}{\det(A_{n-1})} \tag{4.8}$$

Objective: Given samples of $f(s)$ at different frequencies, determine the matrix A.

Rewriting the recursive expression for $\det(A_n)$, we have,

$$\det(A_n) = (s + a_n)\det(A_{n-1}) - (b_n)^2 \det(A_{n-2}) \tag{4.9}$$

where A_{n-1} is the matrix obtained after deleting first row and column of A_n. Also, $\det(A_0) = 1$ and $\det(A_{-1}) = 0$.

Theorem 3. *The determinant of A_n is given by the following polynomial expression*

$$\det(A_n) = s^n + (\sum_{i=1}^{n} a_i)s^{n-1} + (\sum_{i=2}^{n} a_i \sum_{j=1}^{i-1} a_j - \sum_{i=2}^{n} b_i^2)s^{n-2} + \cdots \tag{4.10}$$

Proof. We prove the theorem using mathematical induction. For $n = 1$,

$$\begin{aligned} A_1 &= (s + a_1) \\ \det(A_1) &= s + a_1 \end{aligned}$$

$\therefore$ equation 4.10 is true for $n = 1$. For $n = 2$,

$$\begin{aligned} A_2 &= \begin{pmatrix} s + a_2 & b_2 \\ b_2 & s + a_1 \end{pmatrix} \\ \det(A_2) &= (s + a_2)(s + a_1) - b_2^2 \\ &= s^2 + (a_1 + a_2)s + a_2 a_1 - b_2^2 \end{aligned}$$

$\therefore$ equation (4.10) is true for n = 2.

Now suppose that the expression is true for $n = k$ and $n = k - 1$ i.e.

$$\det(A_k) = s^k + (\sum_{i=1}^{k} a_i)s^{k-1} + (\sum_{i=2}^{k} a_i \sum_{j=1}^{i-1} a_j - \sum_{i=2}^{k} b_i^2)s^{k-2} + \cdots$$

and

$$\det(A_{k-1}) = s^{k-1} + (\sum_{i=1}^{k-1} a_i)s^{k-2} + (\sum_{i=2}^{k-1} a_i \sum_{j=1}^{i-1} a_j - \sum_{i=2}^{k-1} b_i^2)s^{n-3} + \cdots$$

using equation (4.9) we have

$$\begin{aligned}
\det(A_{k+1}) &= (s+a_{k+1})\left(s^k+(\sum_{i=1}^{k}a_i)s^{k-1}+(\sum_{i=2}^{k}a_i\sum_{j=1}^{i-1}a_j-\sum_{i=2}^{k}b_i^2)s^{k-2}+\cdots\right)- \\
&\quad b_{k+1}^2\left(s^{k-1}+(\sum_{i=1}^{k-1}a_i)s^{k-2}+(\sum_{i=2}^{k-1}a_i\sum_{j=1}^{i-1}a_j-\sum_{i=2}^{k-1}b_i^2)s^{n-3}+\cdots\right) \\
&= s^{k+1}+\overbrace{\left(\sum_{i=1}^{k}a_i\right)s^k}^{1}+\left(\overbrace{\sum_{i=2}^{k}a_i\sum_{j=1}^{i-1}a_j}^{2}-\overbrace{\sum_{i=2}^{k}b_i^2}^{3}\right)s^{k-1}+\cdots+ \\
&\quad \overbrace{a_{k+1}s^k}^{1}+\overbrace{a_{k+1}\left(\sum_{i=1}^{k}a_i\right)s^{k-1}}^{2}+\cdots-\overbrace{b_{k+1}^2}^{3}s^{k-1}-\cdots
\end{aligned}$$

combining the coefficients of s^k in the above equation, we get

$$\det(A_{k+1}) = s^{k+1}+(\sum_{i=1}^{k+1}a_i)s^k+(\sum_{i=2}^{k+1}a_i\sum_{j=1}^{i-1}a_j-\sum_{i=2}^{k+1}b_i^2)s^{k-1}+\cdots$$

□

So the algorithm can be described as:

1. Given the sampled function $f(s_k)$ for different values of k, use rational function interpolation technique, to generate a rational function such that

$$f(s_k)=\frac{p(s_k)}{q(s_k)}=\frac{p_0+p_1s_k+p_2s_k^2+\cdots+p_ns_k^n}{q_0+q_1s_k+q_2s_k^2+\cdots+q_{n-1}s_k^{n-1}}=\frac{\det(A_n)}{\det(A_{n-1})} \quad (4.11)$$

2. From equations 4.10, and 4.11 we can see that

$$p_{n-1}-q_{n-2}=\sum_{i=1}^{n}a_i-\sum_{i=1}^{n-1}a_i=a_n \quad (4.12)$$

and

$$a_nq_{n-2}+q_{n-3}-p_{n-3}=b_n^2 \quad (4.13)$$

3. Once a_n and b_n are determined we need to update the data $f(s_k)$ to remove their influence and then calculate the other terms. The update formula can be determined in the following way: Divide equation (4.10) by $\det(A_{n-1})$ to obtain

$$\frac{\det(A_n)}{\det(A_{n-1})} = (s + a_n) - b_n^2 \frac{\det(A_{n-2})}{\det(A_{n-1})}$$

$$f(s) = (s + a_n) - b_n^2 \frac{1}{\hat{f(s)}} \tag{4.14}$$

where $\hat{f(s)}$ is the updated function that needs to be determined

From (4.14),

$$\hat{f(s)} = \frac{b_n^2}{s + a_n - f(s)} \tag{4.15}$$

4. Go back to step 1, with $f(s) = \hat{f}(s)$.

It turns out that even this method is highly unstable, and only first two entries were recovered, after which the error exponentially blows up.

Next, we describe an alternative approach to one dimensional inverse scattering problem. Sylvester *et. al.* proposed this algorithm [11] in 1996, and their problem setup is different from that considered by Chen-Rokhlin.

4.3 Layer stripping by Sylvester, Winebrenner, and Gylys-Colwell

Consider the Helmholtz equation on the half line $L^2(-\infty, 0)$

$$\frac{d^2v}{dy^2} + \omega^2 n^2(y) v = 0$$

with the boundary condition

$$v \sim e^{-i\omega \int_0^y n(s)ds} \text{ as } y \to -\infty$$

Here $n(y)$ is the unknown scatterer to be determined. The authors consider a class of $n(y)$, where $\frac{d}{dy}\frac{1}{\sqrt{n(y)}} \in L^2(-\infty, 0)$. Also, $n(y)$ is a constant in the region $y > 0$, i.e. $n(y) = n_0$ for $y \in (0, \infty)$. Therefore, for $y > 0$, $v(y)$ may be written as

$$v(y) = \frac{1}{T(\omega)}\left(e^{-\omega n_0 y} + R(\omega)e^{-\omega n_0 y}\right)$$

The above equation defines the reflection coefficient $R(\omega)$.

Since $\frac{1}{n(y)}$ has the units of velocity, perform a change of variables to obtain a PDE in terms of travel time coordinate

$$\begin{aligned}
x(y) &\triangleq \int_0^y n(s)ds \\
\Rightarrow \frac{dx}{dy} &= n(y) \\
u(x) &= v(y(x)) \\
\gamma(x) &= n(y(x)) \\
\alpha(x) &= (\gamma(x))^{-1}\frac{d\gamma}{dx} \\
&= (n)^{-1}\frac{dn}{dy}\frac{dy}{dx} = (n)^{-2}\frac{dn}{dy} \\
\text{Now } \frac{dv}{dy} &= \frac{du}{dx}\frac{dx}{dy} \\
&= u'n = u'\gamma
\end{aligned}$$

where prime is derivative w.r.t. x. The Helmholtz equation is now transformed to

$$\begin{aligned}
(\gamma u')'\gamma + \omega^2\gamma^2 u &= 0 \\
\Rightarrow \frac{1}{\gamma}(\gamma u')' + \omega^2 u &= 0 \\
\text{with } u &\sim e^{-i\omega x} \text{ as } x \to -\infty
\end{aligned}$$

Define a reflection coefficient $r(x,\omega)$ for any $x < 0$

$$r(x,\omega) \triangleq f\left(\frac{u'(x,\omega)}{-i\omega u(x,\omega)}\right), \tag{4.16}$$

where $f(z) = \frac{1-z}{1+z}$ is the bilinear transform. To obtain the differential equation, which describes the evolution of reflection data $r(x,\omega)$, with "depth" x, differentiate equation (4.16) with respect to x

$$\begin{aligned}
r' &= \frac{df}{dz}\frac{dz}{dx} \\
\frac{df}{dz} &= \frac{-2}{(1+z)^2} \\
\frac{dz}{dx} &= \frac{d}{dx}\left(\frac{u'}{-i\omega u}\right) \\
&= \frac{u(u'') - (u')^2}{-i\omega(u)^2} \\
&= \frac{u(-\alpha u' - \omega^2 u) - (u')^2}{-i\omega(u)^2} \\
&= \frac{-\alpha u'}{-i\omega u} - i\omega + \frac{(u')^2}{-i\omega(u)^2} \\
&= -\alpha z - i\omega + i\omega z^2 \\
&= i\omega(z-1)(z+1) - \alpha z \\
\therefore r' &= -2i\omega\frac{z-1}{z+1} + 2\alpha\frac{z}{(1+z)^2} \\
&= 2i\omega r + \frac{\alpha}{2}\frac{4z}{(1+z)^2} \\
&= 2i\omega r + \frac{\alpha}{2}\frac{(1+z)^2 - (1-z)^2}{(1+z)^2} \\
&= 2i\omega r + \frac{\alpha}{2}(1-r^2)
\end{aligned} \tag{4.17}$$

The boundary conditions, for $x \geq 0$ can be obtained as:

$$\begin{aligned} u(x,\omega) &= \frac{1}{T(\omega)}\left(e^{-i\omega x} + R(\omega)e^{i\omega x}\right) \\ u'(x,\omega) &= \frac{i\omega}{T(\omega)}\left(-e^{-i\omega x} + R(\omega)e^{i\omega x}\right) \\ \therefore \frac{u'(0,\omega)}{-i\omega u(0,\omega)} &= \frac{1-R(\omega)}{1+R(\omega)} \\ \therefore r(0,\omega) &= f(\frac{u'(0,\omega)}{-i\omega u(0,\omega)}) \\ &= R(\omega) \end{aligned}$$

For $x \to -\infty$

$$\begin{aligned} u(x,\omega) &\sim e^{-i\omega x} \\ u'(x,\omega) &\sim -i\omega e^{-i\omega x} \\ \Rightarrow \frac{u'(x,\omega)}{-i\omega u(x,\omega)} &= 1 \\ \Rightarrow r(-\infty,\omega) &= 0 \end{aligned}$$

The authors now have a non linear ODE which states

- For the inverse problem, observe the scattering data $r(0,\omega) = R(\omega)$
- Determine the unknown $\alpha(x)$ by running the ODE

$$r' = 2i\omega r + \frac{\alpha}{2}(1-r^2)$$

  backwards such that $r(-\infty,\omega) = 0$.

The difference between the Chen-Rokhlin algorithm and this approach is that the authors here use a single ODE (4.17) to both "peel" the network, and to recover the unknown.

4.3.1 SWG algorithm

Before describing the complete algorithm, the authors describe a simpler case when the unknown $\alpha(x)$ is almost close to zero. This corresponds to the case when the velocity profile is almost constant which in the LC ladder network would imply that the L's are almost the same. This is the so called Born approximation. Next I describe the approximate algorithm, with ample explanation and a circuit analogy wherever possible.

- Let S be the scattering transform, i.e. a non linear operator such that given $\alpha(x)$, the operator gives the reflection coefficient

$$R(\omega) = S(\alpha(x))$$

- Let B be the Born approximation operator such that instead of $\alpha(x)$ we have an almost zero unknown ϵa and the reflection coefficient $\rho_0(\omega)$

$$\rho_0(\omega) = B(a)$$

  where

$$\rho_0(\omega) \triangleq \frac{d}{d\epsilon} S(0 + \epsilon a) \mid_{\epsilon=0}$$

  This approximation gives an approximate linear version of the nonlinear

ODE (4.17)

$$\begin{aligned}
\rho(x,\omega) &\triangleq \frac{dr}{d\epsilon} \\
\Rightarrow \frac{d\rho(x,\omega)}{dx} &= \frac{d}{dx}\frac{dr}{d\epsilon} \\
&= \frac{d}{d\epsilon}\frac{dr}{dx} \\
&= \frac{d}{d\epsilon}\left(2i\omega r + \frac{\epsilon a}{2}(1-r^2)\right) \\
&= 2i\omega\rho + \frac{a}{2}(1-r^2) + \frac{\epsilon a}{2}(1-2r\rho) \\
\therefore \epsilon &= 0 \\
\Rightarrow \rho' &= 2i\omega\rho + \frac{a}{2}(1-r^2)
\end{aligned}$$

For the approximate case, the original nonlinear ODE (4.17) now becomes

$$\begin{aligned}
r'(x,\omega,\epsilon) &= 2i\omega r + \frac{\epsilon a}{2}(1-r^2) \\
\therefore \epsilon = 0 \Rightarrow r' &= 2i\omega r \\
\text{and the boundary condition } r(-\infty,\omega) &= 0 \\
\Rightarrow r(x,\omega,0) &= 0 \\
\text{which gives } \rho' &= 2i\omega\rho + \frac{a}{2}
\end{aligned}$$

- Thus the approximate system is

$$\rho' = 2i\omega\rho + \frac{a}{2} \tag{4.18}$$

$$\rho(-\infty,\omega) = 0 \tag{4.19}$$

$$\rho(0,\omega) = \rho_0(\omega) \tag{4.20}$$

and the inverse problem is: given the measurements (4.20), and the evolution equation (4.18), determine the unknown a. Note that under this approximation, the evolution equation (4.18) is a linear differential equation with a closed form solution.

- Solution to equation(4.18):

$$\begin{aligned}
\frac{d}{dx}\left(\rho(x,\omega)e^{-2i\omega x}\right) &= e^{-2i\omega x}\frac{a(x)}{2} \\
\Rightarrow \rho(x,\omega) &= \int_{-\infty}^{x} e^{2i\omega(x-y)}\frac{a(y)}{2}dy \qquad (4.21) \\
\Rightarrow \rho_0(\omega) &= \int_{-\infty}^{0} e^{-2i\omega y}\frac{a(y)}{2}dy \qquad (4.22) \\
&= \left(H_{y<0}\frac{a(y)}{2}\right)^{\wedge} \\
\text{where } H_{y<0} &\triangleq \begin{cases} 1 \text{ if } y<0 \\ 0 \text{ else} \end{cases} \text{ is the unit step function} \\
\text{and } (f(\omega))^{\wedge} &= \text{Fourier transform of } f(t) \\
&\triangleq \int_{-\infty}^{\infty} f(t)e^{-2i\omega t}dt
\end{aligned}$$

  Thus the inverse problem is equivalent to inverting the Fourier transform in equation (4.22).

- Using equation 4.18, the authors prove an identity called Plancherel equality, which says that the reflection data is of finite energy.

$$\int_{-\infty}^{+\infty} |\rho(x,\omega)|^2 d\omega = \frac{1}{4\pi}\int_{-\infty}^{x} a^2(y)dy \qquad (4.23)$$

- Mathematical Aside - Hardy Spaces: The integral (4.22) may not exist if $a(y) \notin L^1$. To address this situation we let ω be complex so that $\omega = \alpha + i\beta$. Now the integral (4.22) transforms to

$$\begin{aligned}
\rho_0(\alpha+i\beta) &= \int_{-\infty}^{0} e^{-2i(\alpha+i\beta)y}\frac{a(y)}{2}dy \\
&= \int_{-\infty}^{0} e^{2\beta y}e^{-2i\alpha y}\frac{a(y)}{2}dy \qquad (4.24)
\end{aligned}$$

  For $\beta > 0$ the integrand in equation (4.24) is an exponentially decaying and hence in L^2. Such functions, which are analytic in one of the half planes

with finite norm are called the Hardy functions. (For detailed discussion on Hardy functions refer [26].) Hardy space, $H^2(\mathbb{C}^+)$, is the space of analytic functions in the upper half plane with

$$||\rho||_{H^2} = \sup_{\beta>0} \left(\int |\rho(\alpha + i\beta)|^2 d\alpha \right)^{\frac{1}{2}} < \infty$$

Similarly defining $H^2(\mathbb{C}^-)$, we have

$$L^2(\mathbb{R}) = H^2(\mathbb{C}^+) \oplus H^2(\mathbb{C}^-)$$

Thus, finite energy functions on the real line can be obtained from the two Hardy spaces.

- Let P^+ and P^- denote orthogonal projection operators, which project a function onto $H^2(\mathbb{C}^+)$ and $H^2(\mathbb{C}^-)$, respectively. $P^+\rho^\wedge(x,\omega)$ is obtained by:

  1. Obtain the inverse transform of $\rho^\wedge(x,\omega)$, i.e. $\rho^\vee(x,y)$
  2. Make the signal $\rho^\vee(x,y)$ zero for $y > 0$, i.e. obtain $H_{(-\infty,0)}\rho^\vee(x,y)$.
  3. Finally, take the Fourier transform of the truncated signal, i.e.

$$P^+\rho^\wedge(x,\omega) = \left(H_{(-\infty,0)}\rho^\vee(x,y)\right)^\wedge$$

- Rewriting the solution to the differential equation (4.18)

$$\rho(x,\omega) = e^{2i\omega x}\rho_0(\omega) + \int_0^x e^{2i\omega(x-y)}\frac{a(y)}{2}dy$$

Since $y > x$, the integral in the above equation lies in $H^2(\mathbb{C}^-$, while $\rho(x,\omega)$ lies in $H^2(\mathbb{C}^+)$ (equation (4.24)). So applying the projection operators, we have

$$\begin{aligned} \rho(x,\omega) &= P^+\rho(x,\omega) \\ &= P^+\left(e^{2i\omega x}\rho_0(\omega) + \int_0^x e^{2i\omega(x-y)}\frac{a(y)}{2}dy\right) \\ &= P^+\left(e^{2i\omega x}\rho_0(\omega)\right) \end{aligned} \tag{4.25}$$

Equation (4.25) is equivalent to the layer peeling formula, i.e. given the data at the boundary, $\rho_0(\omega)$, one can obtain the data at a depth x, $\rho(x,\omega)$ by applying the projection operator to the boundary data.

Similarly applying P^-, we have

$$\begin{aligned} P^-\rho(x,\omega) &= 0 \\ \Rightarrow P^-\left(e^{2i\omega x}\rho_0(\omega)\right) &= -P^-\left(\int_0^x e^{2i\omega(x-y)}\frac{a(y)}{2}dy\right) \\ &= -\int_0^x e^{2i\omega(x-y)}\frac{a(y)}{2}dy \\ \Rightarrow P^-\left(e^{2i\omega x}\rho_0(\omega)\right) &= \left(H_{(x<y<0)}\frac{a(y+x)}{2}\right)^\wedge \end{aligned} \tag{4.26}$$

Equation (4.26), gives a way to recover the value of unknown $a(y)$ for small depths, i.e when $0 < y < x$, by projecting the data onto $H^2(\mathbb{C}^-)$.

Thus the equations (4.25) and (4.26) constitute the inverse scattering algorithm to recover the unknown $a(y)$.

- Similar ideas are applied to solve the nonlinear problem (4.17) [11].

4.3.2 SWG algorithm and LC ladder networks

Although we don't have discrete equivalent of equations (4.25) and (4.26), we know that for LC ladder networks, the reflection data $Y_1(\omega)$, lies in $H^2(\mathbb{C}^+)$. This is because all the poles of $Y_1(\omega)$ lie in the lower half plane. In the discrete algorithm we nowhere verify this condition. In chapter 3, it was shown that for three section LC ladder network , the layer peeling equations cause the poles to move in the upper half plane, which causes errors in the recovery. We tried using the projection operator to enforce this condition after each stage of peeling. But this did not help improve the accuracy of the recovered data.

Understanding of SWG approach with respect to LC ladder network is not complete, and forms a part of the future work.

In the next chapter we summarize the contributions of the dissertation along with a list of open problems.

Chapter 5

Conclusions and Future Work

We summarize the main contributions of the dissertation:

1. An LC ladder circuit, whose L's can be recovered using Chen-Rokhlin algorithm, is identified. This circuit realization reveals the presence of a negative impedance component, which is believed to be the reason behind the stability of the inverse scattering algorithm. Faithful reconstruction of L's from noisy data, using Chen-Rokhlin algorithm, is experimentally verified.

   The circuit realization is important for two reasons:

   - It provides a new way to set up the discrete inverse scattering problem.
   - It provides with a way to model a wired network of sensors.

2. Discrete model for the one dimensional inverse scattering problem is proposed, along with some simulation results, and associated theorems:

   - The presence of negative impedance guarantees non-real poles, all trapped in the lower half plane.

- A discrete extension of the Chen-Rokhlin algorithm, which recovers the L's faithfully, is provided.

3. Another stable, continuous inverse scattering algorithm by Sylvester *et. al.* is explored, discrete extension of which, might provide a different way to recover the values of L's.

The discrete problem setup and the associated algorithm leads to a host of open problems, which are listed below:

1. *Different Discrete Model:* The discrete model proposed in the dissertation, identifies the unknowns as point wise discontinuity in the region. Alternately one can set up a problem so that the unknowns are modeled as piecewise constant (figure (5.1)). The model will now be governed by dif-

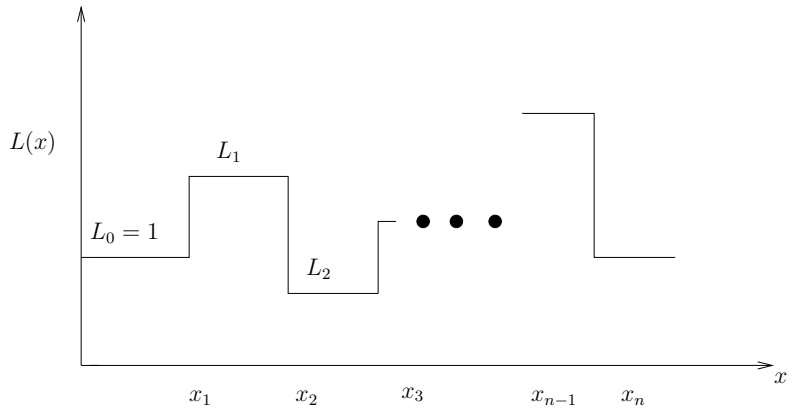

Figure 5.1. Discrete model with piecewise constant inductance

ferential equations [8], rather than algebraic equation. Also, the modeling of negative impedance in this setting needs to be figured out.

2. Identify the sources of instability and factors that mitigate it. A possible source of instability could be the layer peeling formula. One way to remedy the situation is to consider a different "trace" formula, i.e. instead of

using $Y(\omega)$ to recover L, one might want to try a function of $Y(\omega)$. This might lead to stable peeling formula. A couple of approaches that are not mentioned here were tried:

- $(A^{-1})_{n1}$ entry, which corresponds to the current in the last loop, was used as measured data, along with $Y(\omega)$. Asymptotically, this entry has the products of all L's into it.

3. Analyze the operation in time domain, specifically need to address the following two issues:

   - Come up with a stable operation of the LC ladder circuit.
   - Determine the settling time of the circuit, or in other words how long will it take to make the measurements.

4. *Setup a problem in higher dimensions:* Figure (5.2) shows a pictorial way to setup the problem in two dimensions. Here the bold circle in the center (blue) represents termination using negative impedance.

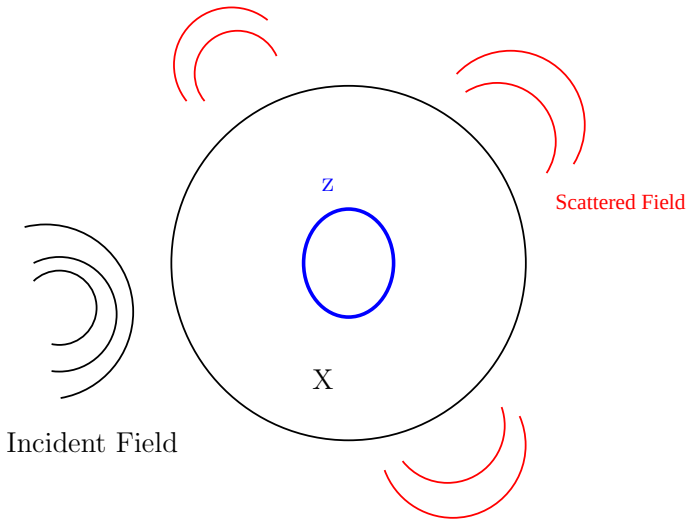

Figure 5.2. Inverse scattering model in two dimensional space

X is the unknown inhomogeneity, the field on the left represents the incident energy, and the one in right represents the scattered energy, which is measured along the entire periphery.

Bibliography

[1] Banff international research station. [Online]. Available: http://www.birs.ca/birspages.php?task=displayevent&event_id=06w5092

[2] K. Chadan and P. Sabatier, *Inverse Problems in Quantum Scattering Theory.* Springer-Verlag, 1989.

[3] M. Kaveh and M. Soumekh, *Image Recovery: Theory and Application.* Academic Press, 1987, ch. Computer assisted diffraction tomography, pp. 369–413.

[4] Center for remote imaging, sensing and processing. [Online]. Available: http://www.crisp.nus.edu.sg/~research/tutorial/mw.htm

[5] D. Colton, J. Coyle, and P. Monk, "Recent developments in inverse acoustic scattering theory," *SIAM Review*, vol. 42, no. 3, pp. 369–414, 2000.

[6] Non destructive testing figure. [Online]. Available: http://spie.org/Images/Graphics/Newsroom/Imported/0862/0862_fig1.jpg

[7] I. Gel'fand and B. Levitan, "On a determination of differential equation from its spectral function," *American Mathematical Society Translation, Series 2*, vol. 1, pp. 253–304, 1955.

[8] A. Bruckstein and T. Kailath, "Inverse scattering for discrete transmission-line models," *Siam Review*, vol. 29, no. 3, pp. 359–389, 1987.

[9] G. Gladwell, *Inverse problems in scattering: An introduction.* Kluwer Academic Publishers, 1993.

[10] Y. Chen and V. Rokhlin, "On the inverse scattering problem for the helmholtz equation in one dimension," *Inverse Problems*, vol. 8, no. 3, pp. 365–391, 1992.

[11] J. Sylvester, D. Winebrenner, and F. Gylys-Colwell, "Layer stripping for helmholtz equation," *SIAM Journal of Applied Mathematics*, vol. 56, no. 3, pp. 736–754, June 1996.

[12] J. Sylvester and D. Winebrenner, "Linear and nonlinear inverse scattering," *SIAM Journal of Applied Mathematics*, vol. 59, no. 2, pp. 669–699, 1998.

[13] J. Sylvester, "Layer stripping." [Online]. Available: http://www.math.washington.edu/~sylvest/

[14] Transmission line. [Online]. Available: http://en.wikipedia.org/wiki/Transmission_line

[15] M. R. Wohlers, *Lumped and distributed passive networks*. Academic Press, New York, 1969.

[16] B. Gopinath and M. Sondhi, "Inversion of the telegraph equation and synthesis of nonuniform lines," *Proceedings of the IEEE*, vol. 59, no. 3, pp. 383–392, 1971.

[17] M. Krein, "On a method for the effective solution of the inverse boundary value problem," *Doklady Akademiya Nauk SSSR*, vol. 94, pp. 987–990, 1954.

[18] Y. Chen and V. Rokhlin, "On the inverse scattering problem for the helmholtz equation in one dimension," *Research Report YALE/DCS/RR-838*, 1990.

[19] J. D. Ryder, *Networks, Lines and Fields*. Prentice Hall of India Pvt Ltd, 1989.

[20] M. S. Ghausi and K. R. Laker, *Modern Filter Design: Active RC and Switched Capacitor*. Prentice-Hall Inc.: Englewood Cliffs, NJ, 1981.

[21] The mathworks. [Online]. Available: http://www.mathworks.com/

[22] L. Shampine and M. Reichelt, "The matlab ode suite," *SIAM Journal on Scientific Computing*, vol. 18, pp. 1–2, 1997.

[23] G. C. Temes and J. W. LaPatra, *Introduction to Circuit Synthesis and Design*. McGraw Hill Book Company, 1977.

[24] W. Gander and W. Gautschi, "Adaptive quadrature - revisited," *BIT*, vol. 40, pp. 84–101, 2000. [Online]. Available: http://www.inf.ethz.ch/personal/gander

[25] W. B. Gragg and W. J. Harrod, "The numerically stable reconstruction of jacobi matrices from spectral data," *Numerische Mathematik*, vol. 44, pp. 317–336, 1984.

[26] H. Dym and H. McKean, *Fourier Series and Integrals*. Academic Press, 2005.

Appendices